Creep and fatigue interactions in glass reinforced plastics

Crowther, M. F.

Award date:
1987

Awarding institution:
University of Bath

Creep and Fatigue Interactions in Glass Reinforced Plastics

submitted by M.F. Crowther

for the degree of PhD

of the University of Bath

1987

ProQuest LLC
789 East Eisenhower Parkway
P.O. Box 1346
Ann Arbor, MI 48106-1346

Abstract

Design of glass reinforced plastic (GRP) pipework in the cooling water (CW) systems of power stations is based on the guidelines of BS4994. Concerns had been voiced as to the reliability of the BS4994 approach for service situations where static and low frequency cyclic loading are combined. This study set out to clarify the effect of combined loading on GRP. Static and low frequency cyclic tests were conducted in water at 40°C on coupons of glass reinforced polyester resin presaturated with water. For tests incorporating periodic unload cycles at frequencies of 0.03/min to 15/min failure was determined by time at load below a boundary frequency and cycles above it. This frequency lay in the range 0.12 to 1 cycle/min. For service conditions in CW systems spike overloads are thought to be more damaging and periodic unloads less damaging than normal service loading.

A load normalisation technique based on the strength-life equal rank assumption was developed which removed much of the scatter found on stress-rupture plots. Microscopy during immersed tests and on failed specimens highlighted differences between statically and cyclically-loaded coupons. Dynamic fatigue failures showed large areas of matrix and interfacial cracking, whilst static failures showed more matrix creep and fibre weakening. Evidence was found of enhancement of fibre stress corrosion in some fatigue regimes. A model was developed of the extension of curved warp rovings in the woven roving reinforcement and showed why warp rovings were found to fail predominantly in the centre of warp-weft crossovers.

Acknowledgements

I am grateful to the Science and Engineering Research Council and the Central Electricity Generating Board for their financial support. I am also indebted to my supervisors Mike Phillips of Bath University and Ron Wyatt of the CEGB for their help and advice during the course of the project. I would like to thank everyone at CEGB Bedminster Down for their help and support especially Howard Parsons for his assistance moulding and cutting specimens and aligning the low frequency fatigue rig. I would also like to thank GKN Technology personnel who have helped during the writing-up phase; in particular, Roy Wakeman for his drawings, Angela Lawcock and the photographic department and especially Irene Entwistle who did all the typing.

Contents

Contents (cont'd)

Contents (cont'd)

1. INTRODUCTION AND BACKGROUND

1.1 GRP in the Power Industry

The most promising use for glass reinforced plastic (GRP) in Power Stations is the cooling water (CW) system. Currently most pipework, valves and water boxes are made from cast iron or mild steel. Corrosion presents a major problem especially for coastal stations where sea water is used as the coolant exacerbating the corrosion problems. The effects of corrosion of metal components are two-fold, firstly the structures are weakened due to loss of thickness and secondly, corrosion debris may find its way into the condenser tubing where it can cause costly damage. The situation can be partially ameliorated by coating the steel surfaces with polymeric coatings but the initial costs can be as much as £80 per m^2 and frequent maintenance is also necessary.[1]

There is obvious scope for using GRP, it is much more resistant to attack by water than steel but it can suffer a reduction in strength due to water uptake. If, as it has been suggested, this is an osmotic process, it is lessened in water containing ions i.e. sea water. The relatively low temperatures (less than 40°C) found in CW systems allow GRP to be used with confidence; given that the heat distortion temperature of the resin is around 100°C.

GRP was introduced into power stations as early as 1964 when a GRP expansion bellows was installed at Poole Power Station.[2] Three

similar bellows have been in service until recently with no significant problems. A condenser return-end waterbox at Portsmouth P.S. gave satisfactory service for 11 years between 1966 and 1977.

Other experience with GRP involves a condenser waterbox at East Yelland Power Station which, although made of GRP, was modelled on the original cast iron design (cast iron has a modulus 10 times that of GRP) consisting of a shallow cylindrical shaped GRP shell backed by steel stiffeners. This box split during its early trials. The box was redesigned using a more domed shape which reduced the bending stress concentrations, and subsequently provided trouble-free service for more than 20 years.[2]

At Pembroke Power Station a GRP door on the main condenser failed due to a water hammer pulse caused by the uncontrolled closure of a failing cast iron valve. The GRP door was found to be under-designed. By re-designing the shape of the door - adopting a domed shape thinning towards the centre with external webs towards the flange and using all woven roving reinforcement, a door of the same weight but six times stronger could be made.[2]

These two instances illustrate that if GRP is to be used successfully on CW systems the design needs to be based on GRP properties and should not be a simple copy of the steel structure being replaced. Clearly, limitations in design are prescribed when the GRP component has to be bolted onto existing steel pipework: the shape of the flanges is predetermined to suit its steel or cast iron predecessor.

In recent years design with GRP has improved considerably, following these early trails. A number of GRP components have been installed e.g. at Fawley P.S. These include water boxes, expansion bellows, pipework and valves. They have been in service now for 5 years without any significant problems.

In very recent years, GRP has been used in several critical applications on major power stations in the South West Region of the CEGB and the problems of designing the material safely but economically have become the subject of major investigation.

1.2 Design Considerations

Primarily, it is necessary to consider the type of loading régime, environment and temperature which the structure is required to withstand; then to match what is known about the response of candidate materials to the conditions and select the most suitable. A large safety factor is currently employed for GRP, typically 10 - 16.

The loading sustained by a CW system can be broken down into a background static load, F, over which are superimposed various dynamic loads. At coastal stations, the pressure of the cooling (sea) water varies sinusoidally according to the height of the tide, reaching a maximum twice a day. This means the load the structure sustains varies in the same way, the variation being typically $\pm$

0.2F. The whole system will be periodically depressurised during periods of maintenance, say every few months, so that the load F decreases to zero. Finally, on top of all this the system could be subjected to sudden raising or lowering of pressure, in the form of shock waves or water hammer pulses at random intervals and of varying magnitude during operation. The overall loading picture is quite complex. Added to this is the fact that one side of the structure is immersed in water at up to 40°C.

It is difficult to quantify the operating conditions accurately and there are still many unknowns on the materials side. Safety factors are currently incorporated to surmount these problems. According to BS.4994[3] the safety factor K to be adopted is given by:

$$K = 3 \times k_1 \times k_2 \times k_3 \times k_4 \times k_5$$

k_1 relates to the method of manufacture and is equal to 1.6 for handwork.

k_2 relates to long-term behaviour. A maximum value of 2 can be assumed since long-term tests suggested a high loss of strength.

k_3 relates to temperature. Unity can be asumed if the Heat Distortion Temperature of the resin is sufficiently above the service temperature.

k_4 relates to cyclic loading. For 10^4 cycles, i.e. the twice daily tidal cycle over 25 years at 60% load factor, $k_4 = 1.4$.

k_5 relates to curing procedure. 1.1 is adopted for postcuring for a short period at elevated temperature and at least a month at room temperature.

For a cooling water application,

$$\therefore \quad K = 3 \times 1.6 \times 2 \times 1 \times 1.41 \times 1.1 = 14.8$$

A number of assumptions have been made in deriving the above safety factors. Namely, that the long-term behaviour (25 years) of GRP can be predicted from short-term (up to 2 years) data, that no synergistic effects occur when cyclic loading is superimposed on a static load and that fatigue data obtained at high frequencies can be applied to situations where the cyclic loading is of a lower frequency.

The aim of this project was to try to clarify some of the design procedures, and in particular to ascertain the extent of any interaction between static and dynamic loading, how they should be considered together and to try to gain a better understanding of the failure mechanism.

1.3 Survey of the Literature

The literature relevant to this thesis lies in five main areas: stress rupture, fatigue, mechanisms of stress rupture and fatigue, combinations of stress rupture and fatigue and, lastly, the effect of water. Each of these areas is described in turn.

1.3.1 Stress Rupture

The properties of GRP are highly time dependent - if GRP is loaded in an aqueous environment to say 75% of its dry short-term strength it may support that load for about a day; if loaded to 50% of its dry short term strength it may last a month or so. Attempts have been made to quantify this behaviour and produce rules by which the results from short-term tests may be extrapolated to times as long as 20 years, over which it would be impractical to conduct creep tests. Most methods involve extrapolating from a stress-log time plot which is assumed linear,[4-8] although some authors have obtained better results from log stress-log time plots [9-12].

The use of stress-log time plots has a theoretical basis in the Arrhenius relationship.

$$t_R = t_o \exp[(U_o - \gamma \sigma)/kT]$$

where: t_R = time to rupture

σ = applied stress

T = absolute temperature

t_o = constant associated with atomic vibration period

U_o = process activation energy

γ = constant

The Arrhenius relationship was used as a base by Larson and Miller for creep of metals.

$$T(\log t_R - C) = K$$

K = stress dependent constant

C = constant

This has been successfully applied to GRP by Bershtein and Glikman[7] and by Goldfein[13].

The time-temperature superposition principle (TTSP) has been related to GRP by Wright [14], who plotted creep curves at 20, 40, and 60°C and then shifted them along the time axis by varying amounts to give a single master curve. This enables him to pinpoint an endurance stress for 40 years at 40°C of 25% of the short-term dry tensile strength, a value lower than that extrapolated from the 40°C data alone.

Beckwith[15] combines TTSP with Lamina Constitutive Theory to predict the behaviour of laminates as a function of fibre orientation. He also defines two classes of materials - thermorheologically simple materials (TSM) and thermorheologically complex materials (TCM). TSM require shifting only along the time axis to produce a 'master' curve, i.e. a curve of normalised compliance vs logt - log a_T (a_T is the shift factor). TCM require shifting along both axes.

Work done at Bath University under contract for the CEGB[16] suggests that straight line regresssion analysis of load-logt plots is invalid for long term life prediction, since a down-turn in experimental points was noticed at times greater than 10^6 sec at 60°C and 10^7 sec at 40°C (polyester/glass laminate in seawater). So far no theoretical explanation of this knee in the curve has been offered.

1.3.2 Fatigue

In practice most GRP components also undergo cyclic loading in service, and this cyclic load is superimposed over a static load. Most work on fatigue[17-21] has been done at frequencies in the range 1-30Hz, high compared with the frequencies proposed for this project. The results of fatigue tests on GRP are treated in a similar way to those on metals: i.e. a graph is usually plotted of peak, range or mean stress against log (cycles to failure). An alternative approach is to plot peak/range/mean load as a percentage of the ultimate failure load of test coupons.

More recently Dharan[22] and Talreja[23] have advocated the use of strain-life plots for fatigue data, arguing that the strain seen by the fibres and matrix is identical whereas the corresponding stresses can be quite different.

The effect of variations in mean stress and alternating stress on fatigue life can be shown on fatigue master diagrams, an example of which[24] is shown in Fig. 1.1. Stress amplitude is plotted against

mean stress and contour lines are drawn through points of equal fatigue life. A vast amount of testing is necessary to generate sufficient data to plot one of these diagrams. Attempts have been made to generate approximations to the diagrams based on the Goodman law used for metals given below

$$\frac{S_A}{S_E} = 1 - \frac{S_M}{S_U}$$

Where S_A and S_M are the stress amplitude and mean stress respectively, S_E is the fatigue strength at zero mean stress for a given life and S_U is the ultimate strength of the material. Boller[25], on finding that this equation overestimated his experimental results, modified it by substituting S_C, the stress rupture strength for the time corresponding to the cyclic endurance, for S_U. This improved the fit to experimental data. Smith and Owen[18,26] introduce further modifications proposing the following equation (for tensile means stresses only);

$$\frac{S_A}{S_E} = \frac{1 - \frac{S_M}{S_C}}{1 + \frac{S_M}{S_C}}$$

This they put forward as being sufficiently conservative to allow for scatter in lives. The two relationships above are shown in conjunction with one of Smith and Owen's master diagrams in Figure 1.2.

Most of the fatigue testing of GRP has been conducted at frequencies of 1Hz or above. The fatigue performance of composites at very low

frequencies is of interest to the CEGB and there is little published work on this. One notable exception to this is by Sims and Gladman[27]. They cycled GRP using 5 different loading rates and a triangular waveform, covering a frequency range of 0.00247 to 50Hz. They report a difference of a factor of 100 between lives at these two frequencies, the high frequency giving the longer life. The variation of fatigue life over the frequency range could be removed by normalising the applied stress with respect to the ultimate tensile strength measured at the same rate of stress application as in the cyclic tests.

In service fatigue loading is rarely as simple as in a laboratory test. Design rules which try to model the effects of random service fatigue cycling have been developed. These are based on Miner's Law. From two stress level cumulative damage tests, Broutman and Sahu[28], found that for high-low stress tests the damage sum was greater than 1 and for low-high stress tests, less than 1. Similar work has also been done by Howe and Owen [17].

1.3.3 Damage mechanisms in fatigue and stress rupture

Damage mechanisms in composites depend to a large extent on lay-up and also on the strains to failure of matrix and fibre. For unidirectional composites with high modulus fibres (e.g. Type I carbon) the fatigue strength is virtually the same as the static strength. The strain to which the matrix is subjected is very low so it suffers little damage. Failure is dominated by fibre failures which then produce subsequent interfacial debonding. In the early

stages of fatigue, weaker than average fibres will fail. As the load carried by the intact fibres increases more of these will fail until there are too few intact fibres left to support the load. If the modulus of the reinforcing fibres is lower or fibres at an angle to the applied load are incorporated the strain seen by the polymer matrix is higher. The matrix is now susceptible to fatigue damage, for instance, interfacial shearing and matrix cracking. The composites of interest to the CEGB studied in this work contain low-modulus glass fibres, they have a mixture of woven and chopped strand reinforcement i.e. a high proportion of 90° fibres and a relatively low glass volume fraction. In short they differ markedly from advanced composites. Fatigue damage in such materials will be dominated by the matrix. A schematic fatigue life diagram is reproduced from Talreja's work[23] in Fig. 1.3. Failures of high stiffness fibre composites tend to lie within the horizontal band around ε_c, whilst those of lower modulus fibre composites lie within the diagonal band, below ε_c. (ε_c is the mean composite fracture strain and is obviously not the same for the 2 types of composites discussed).

The accumulation of damage in glass-polyester composites has been extensively studied by Owen and co-workers (see for instance 17,18,29). The first form of damage initiated is transverse fibre debonding. These debonds tend to join up and then give rise to resin matrix cracks which can propagate through resin rich areas. Fibre debonding parallel to the load direction usually occurs next. Finally, fibres parallel to the applied stress fracture and complete

separation follows. Howe and Owen [17] claim that damage is similar in nature in fatigue, monotonic tension and stress rupture conditions. They show that the same processes occur in fatigue as in monotonic tension but their quantitative assessment of resin cracking revealed that resin cracks were far more numerous in fatigue than in the tensile test. Examination of the transverse fibre debonds and resin cracks showed those formed under fatigue conditions to contain more debris. Boniface and Bader [30] reached similar conclusions; although the general damage and sequence of damage were the same, they too noted differences in morphology.

If the constant load in a stress rupture test is above about 30% UTS, transverse fibre debonding will be present from first loading. Transverse debonds can grow in number with time [17] especially in a water environment (see 1.3.5), so a similar damage sequence could result. The action of the environment is to weaken the load-bearing glass fibres. This is generally attributed to stress corrosion (the mechanisms of which are given in more detail in Chapter 5). In stress rupture there is a tendency for fibre failure rather than matrix cracking and 0° fibre debonding. Fracture faces, especially in tests in acid solutions are characterised by their smoothness and lack of fibre pull-out.

GRP composites held at constant stress also exhibit creep. The resin is a viscoelastic material and deforms gradually with time under load. The creep rate increases with temperature. The effect of the time dependent properties of the matrix on stress rupture is to

increase the fibre ineffective length in the vicinity of a fibre break.[31] This occurs by the relaxation of shear stresses local to the fibre end. The raising of the ineffective length causes more load to be carried by the surrounding fibres which in turn may break.

1.3.4 Combination of stress rupture and fatigue

There is a limited quantity of literature on combined loading and the degree of synergism is still unknown.

Thebing and Menges[32] apply the Boltzman Superposition Principle to low frequency cyclic loading, using data solely from static creep tests to predict the life. They claim that the loading and deformation ability under low frequency cyclic load is less utilised than under continuous loading at maximum load, implying that material can be loaded to a higher level in fatigue. From their generalised observations that damage due to creep and fatigue were similar, Howe and Owen[17] thought that damage caused by one type of loading might be detrimental to life under the other loading type. Their experiments showed that after pre-cycling specimens in fatigue the subsequent stress-rupture life was markedly reduced. The results of Bax[33] substantiate this effect. Bax cyclically preloaded filament wound pipe specimens and looked at the changes in lifetime. A pronounced drop in life was produced even by as few as 6 pre-cycles, so that Bax inferred that dynamic design should not be based on static data. Sims and Gladman[34] statically preloaded before testing in fatigue, only finding that there was an increase in scatter. This they put

down to further weakening of lower strength specimens by the preloading - the specimens which were thought to be at the upper end of the strength distribution being unaffected by preloading.

Other authors have found no significant differences in life after preloading.[20,35,35A]

Since this work was started Mandell and Meier[36] have published results of square wave fatigue tests and spike loading and spike unloading tests on glass-epoxy composites containing alternate 0° and 90° plies. They explored the effect of frequency on square wave fatigue and found that the life was longer at higher test frequencies (which was consistent with Sims and Gladman). They then took their fatigue data at the 3 frequencies (0.01, 0.1 and 1.0Hz) and replotted them on a stress vs. log (cumulative time to failure) plot together with static fatigue data on the same material. At high stresses the cumulative time at load to failure in the fatigue test tended towards the time to failure in the static tests. The stress at which this would start to happen might be expected to decrease with decreasing frequency. This can be seen from Mandells graph shown in fig. 1.4.

The cycles to failure under spike loading and unloading waveforms are compared with square wave fatigue in fig.1.5. Mandell and Meier's graph shows that the material has a similar life under square wave and spike unloading at high stress whilst at lower stress spike unloading and spike loading give similar lives. Mandell and Meier were not able to explain this behaviour. The results of the tests

given in subsequent chapters may provide an explanation for this. Mandell's findings will therefore be discussed further in Chapter 6.

1.3.5 Water uptake

Water has a profound effect on the creep and fatigue life of GRP, reducing the creep life by as much as 100 times and the fatigue life by about 10 times[8]. The rather severe treatment of boiling for 72 hours has been shown to reduce the retained wet strength of polyester and satin weave cloth to 30% of the original value[37]. Regester[38] and Ishai and Mazor[39] have shown that the drop in mechanical properties is directly related to the amount of water absorbed in the laminate.

Entry of water into a laminate occurs initially by diffusion processes[40]; the rate of entry is controlled by temperature, relative humidity or the concentration of a salt in an aqueous solution and diffusion coefficient. However, damage in the form of transverse fibre debonding and resin cracking, may permit other transport mechanisms to become operative[41,42]. Ingress of water gives rise to weight gain. Swelling, weight and volume changes follow a similar pattern with time[43]. Leaching of low molecular weight constituents has been shown to occur, but this is usually masked by water take-up. There is some evidence to suggest that there is a correlation between loss of residual strength and weight loss[44].

The volume strain which occurs suggests that swelling stresses can be induced and strains in different reinforcement layers may vary. Hahn

and Kim[45] found that compressive stresses induced in the surface layer during the early stages of absorption, by constraints imposed by the dry interior, could retard swelling (and diffusion); a similar converse effect could occur during desorption. The results of experiments by Gillat and Broutman[46] show that diffusion coefficient may alter with time. This could be due to degradation reactions between resin and water and glass and water, e.g. hydrolysis and saponification, which occur primarily at the glass-resin interface, promoting minor damage thus opening up new pathways for the transport of water. Taneja[42] has shown that at long times mechanisms other than diffusion become important.

The preceeding paragraph shows that composites are not truly Fickian but because alternative models are by necessity complex the simple treatment assuming constant diffusion coefficient is generally used.

1.4 Experimental Strategy

The main area of concern, which this work set out to clarify, was how satisfactorily BS4994 defines design stresses for GRP components subject to a combination of static and low frequency cyclic loads. A large quantity of experimental data has been collected in the past, covering the stress rupture of GRP under constant load, and several extrapolation techniques put forward. The behaviour of GRP under constant load therefore can be predicted with reasonable confidence. Fatigue testing of GRPs has largely been done at frequencies of 1Hz and above; indeed it was probably data in this frequency range which

was used to derive the sub-factor k_4 for cyclic loading in BS4994. A limited amount of work has been done on low frequency fatigue, as described in a preceeding section but none of this was directly applicable to the CEGB's case in particular, where cyclic pressure variations in the CW system are of a very low frequency.

Two particular examples of fatigue work give rise to doubts about the BS4994 approach.

i) Sims and Gladman[27] described how the cycles to failure were reduced at low rates of stress application. The frequency ratio between, for instance, a 1Hz test and the twice daily tidal cycling is over 43,000. This means that the rate of stress application is 43,000 times faster in the 1Hz test than the practical situation. So, it might be argued that the cycles to failure in the low frequency case would be substantially lower and therefore the fatigue design factor inadequate.

ii) Work by Bax[33] showed that a pronounced drop in life in a static test occurred, if the static loading were preceded by as few as 6 preload cycles. The serious misgivings arising from this concerned the periodic unloadings due to plant outages. These unloadings would number roughly 15, for planned maintenance outages alone, during the life of a station. Thus, there is the possibility of a shortening of component life as a result.

It was thus decided that it would be valuable to investigate the behaviour of the material under low frequency cyclic loading, as

similar as experimentally viable to the in-service régime.

1.4.1 Low Frequency Cyclic Tests

Two loading régimes were chosen in an attempt to separately duplicate each of the in-service loads described in section 1.2. The frequency selected for both these régimes was 1 cycle per 2 minutes, so that results could be obtained in a reasonable time and yet be sufficiently far away from the 1Hz level (around which most of the previous fatigue testing had been done).

The tidal pressure variations are represented by a sinusoidal régime, given the test code S1. The waveform and the stress amplitude (20% of the mean value) are identical with the situation at Fawley P.S., but of course frequency is higher. The form of this load variation with time is sketched in Fig. 1.6a).

The unloads due to maintenance outages are represented by a rectangular load-time variation, designated as R1. The ratio of time under load to time off load, 20:1, corresponds approximately to a typical maintenance cycle of outages once every 2 years each lasting 1 month. This loading régime is shown in Fig 1.7b).

Cycles and times to failure over a range of load levels were obtained under each of the cyclic regimes S1 and R1 on presaturated specimens in demineralised water at 40°C. Times to failure under static load were also obtained under the same conditions. (Decisions regarding

specimen condition and test environment are decribed in 1.4.3) The lifetime under each régime could in turn be compared to the static life, and the stress logtime plots would facilitate extrapolation to the design life. When the first results from R1 and S1, consisting of 5 specimens at each load level, were compared with the static loading, no significant differences could be detected. This meant that any effect of the low frequency cycling was too small to be detected with that number of specimens. These preliminary findings led in 2 directions. Firstly, more specimens were tested over the range of load levels in S1, R1 and the static tests, in an attempt to detect differences between loading régimes. Secondly, further tests at different frequencies were planned, to investigate the significance of frequency. The extent of such a programme of data acquisition, where there were, for instance, 10 specimens per load level, load régime and frequency was very large. A decision was made to concentrate on one load level and load régime and vary the frequency.

A rectangular loading régime was chosen in preference to a sinusoidal one for the following reasons:

a) There is a clearly defined element of static loading so that the time-at-load to failure (i.e. the time spent at load per cycle summed over the cycles to failure) could be compared to the time to failure in a static test at the maximum load;

b) The maximum load of the rectangular waveform was more directly

comparable with static loading, than in the sine-wave loading case (The concept of time-at-load for a sine-wave loading régime becomes a question of how much time at which load); and

c) it was possible to arrange a constant loading rate for all frequencies.

The last reason, c) is important because of the dependence of cycles to failure on the rate of stress application (as documented by Sims and Gladman[27].) With a sinusoidal waveform the study of the effect of changing frequency would have been complicated by the effects resulting from corresponding loading rate changes.

The load level selected was 4.6kN. At this load level failure times in a static test ranged from one week to about 2 months. This load was thought from practical considerations to be the most suitable. The introduction of more unloads would mean that less time was spent at load during any time period so if, as had been indicated by the initial tests, the incorporation of periodic unloads had no effect on the lifetime, the total duration of the tests would lengthen. The range of frequencies covered by rectangular wave loading and their test codes are given in the following table, and the waveforms of these rectangular tests are sketched in Fig. 1.7.

Code	Frequency /cpm	Period /sec	Time at load per cycle (secs)
RO	.03	2000	1996
R1	.5	120	116
R2	4	15	11
R3	8	7.5	3.5
R4	15	4	0 (saw tooth)

It will be noticed from the preceding table and Fig. 1.7 how as the frequency of the unloads increases, the time at load per cycle becomes commensurately less, until at 15 unload cycles per minute - (R4) the time at load is effectively zero. The rectangular waveform is strictly speaking trapezoidal, which when the time at load is reduced to zero tends to a saw tooth or triangular wave form. However this group of tests will still be referred to collectively as rectangular.

1.4.2. Cyclic Testing at 1Hz

Tests at 1Hz, in the ambient laboratory environment, from zero load to a range of tensile loads with a sinusoidal waveform, were conducted to provide a 1Hz fatigue strength for 2×10^4 cycles, the design fatigue life. This programme of tests was given the code DS2. Fatigue tests at 1Hz were also carried out in which the magnitude of

the alternating stress component was the same as that in the S1 tests i.e. 20% of the mean stress. This second set of tests were coded DS1 and were also conducted over a range of load levels in ambient conditions.

Tests in programmes DS2 and DS1 were planned so that there would be sufficient time on the fatigue machine to test a group of presaturated specimens in water at 40°C at the 4.6kN load level. These tests, S2, used a waveform identical to DS2, with the maximum tensile load set at the peak load of the saw toothed wave tests, R4, of the low frequency fatigue work. Sketches of the load-time variations for the higher frequency sinusoidal tests are shown in Fig. 1.6 b), c) and d).

The whole matrix of the mechanical tests is summarised in 2 tables. Table 1 shows the tests performed over a range of load levels and Table 2 gives those tests, at the one selected load level, examining the effect of varying frequency.

1.4.3. Choice of Specimen Condition and Test Environment

It was felt that specimens to be used for short term tests in water should be saturated with water before the start of the test so that the condition of the specimens was closer to the condition of long term test specimens and to eliminate changes in specimen condition during testing. In some previous experiments[47,48] only a short presoak or none at all has been used. A short series of water uptake

measurements were done to try to ascertain the immersion time necessary to ensure near complete water saturation at the centre of a specimen. These measurements are documented in Section 2.2. Presaturated specimens were used for all the tests in water.

Although the coolant water in the power station CW systems of concern is saline, demineralised water was used for the wet tests at 40°C. The reasons for this were two-fold. In the first instance, due to the possible osmotic mechanism of water uptake into the composite, degradation by water might be expected to be more severe in pure water than a salt solution. The test situation therefore tends towards conservatism. Secondly certain components of the pre-existing static creep rigs were made from mild rather than stainless steel, so corrosion would have been a major problem.

Erring towards pessimism again, specimens were totally immersed in the tests, whereas the pipes etc. in power stations are exposed to the sea water environment on one side only. Also, the test temperature of 40°C is the highest likely under normal service conditions. In both these instances a longer life would be expected if the true conditions had been duplicated.

2. Experimental Details

2.1 Material Choice and Development of Laminate Manufacturing Procedure

It was decided to keep as close as was practicable to the material currently used in power stations. This is typically alternate layers of Chopped Strand Mat (CSM) and Woven Roving (WR) with a gel coat to improve water resistance. The format of the laminates which was used in this project was a single layer of WR sandwiched between 2 layers of CSM with a gel coat 0.3mm thick on both outer surfaces. It was felt important to use a balanced construction to avoid any tendency for warpage at any stage of construction or testing. The CSM was Supermat PB ($300g/m^2$) from Fibreglass Ltd. The WR was ECK25 ($830g/m^2$) by Turner Bros. Ltd. The reinforcement weights in the balanced laminate construction were chosen so as to reproduce the overall CSM:WR weight ratio used in practice. The post-cure treatment used was five hours at 60°C. A temperature greater than or equal to the testing temperature was chosen for the postcure to rule out the possibility of further curing taking place during the testing and changing the character of the specimens. By choosing 60°C the option of conducting tests at 60°C was retained.

The requirements for the laminates were as follows:

i) Flat and parallel surfaces with continuous gel coat of the correct thickness and good surface finish to facilitate microscopy

3ii) A minimum of voids within and between the layers of reinforcement

It was necessary to develop techniques by which such laminates could be obtained. The making of trial laminates was started in early January 1983.

The first board was made by mixing enough resin, catalyst and accelerator for the whole board at once. After degassing, a thin layer was spread over a sheet of Melinex (an ICI product) on a glass plate. The three layers of reinforcement were applied, (one layer of WR with a layer of CSM either side), stippling each layer with a brush to try to remove as much air as possible. A second sheet of Melinex was carefully rolled over the top and trapped air squeezed out before a top glass plate was put in position and the mould compressed. This first laminate had a large void content, uneven gel coat thicknesses and fibre prominence on the lower surface where the layers of reinforcement had sunk or been pushed to the bottom and made contact with the Melinex.

On all subsequent trial laminates a three stage approach was adopted. The quantities of resin needed for the two gel coats and to bind the glass were calculated on the basis of producing a gel coat 0.3mm thick and having a glass:resin ratio of 1:1 in CSM and 2:1 in WR layers. The resin for the first gel coat was accelerated, degassed and then painted evenly over the Melinex. This was allowed to partially cure, i.e. the resin gelled but did not harden fully. At this point the resin for the middle layer was accelerated and degassed before laying up the glass as before. An intermediate

pressing without the final gel coat was done to consolidate the glass layers and give a parallel-sided flat laminate. When this had partially cured the second gel coat was painted on and the finished laminate left overnight under pressure to complete curing. Two sets of spacers of slightly different heights were used for the two pressings. This method produced very good gel coats but laminates still had large voidage particularly in the WR layer. As a last refinement the WR was left for 2 - 3 minutes before stippling to allow resin to penetrate the rovings from underneath, enabling air to escape to atmosphere. A further refinement was the use of a roller on the WR layer. This had advantages over a brush in that it did not spread resin over the reinforcement preventing the escape of air.

The size of the mould and glass plates allowed areas of $0.2m^2$ of board to be made at a time, and owing to the involved methods which had to be used only one board could be made per day. It was calculated that at least $4m^2$ would be needed for all the tests. The viability of making larger boards at CEGB was investigated but it was found that the thickness of the glass plates to maintain a tolerance on laminate thickness of only $\pm$1mm under the load density needed to compress the laminate before gelation would make the glass plates unmanageably heavy. A large press was available at Fothergill Rotorway Composites Ltd. This was used to make 5 boards each $1m^2$ in area.

The large boards were cut into specimen blanks which were then

post-cured, before being routed to the final specimen profile. The same specimens were used in all the mechanical tests. Their profile was such that a parallel-sided gauge area, 150mm long and 25mm wide was produced. Thirty specimens, 6 from each board, were tensile tested.

The strength value quoted is expressed as ultimate tensile unit load, or UTUL. UTUL is the parameter used to define the strength of GRP

$$\text{UTUL} = \frac{\text{Ultimate tensile load}}{\text{specimen width x kg of glass per m}^2}$$

Strength usually has units of stress i.e. load ÷ area, but here thickness is replaced by glass content. It has been established that strength of the GRP depends on the glass content rather than the strength of the resin or the resin content. The resin content can therefore vary the thickness without altering failure load. A mean value of 250.4 Nm/kg was obtained (standard deviation = 23.9 Nm/kg). The volume fraction glass was found by resin burn off to be 19.8%.

2.2 Water take-up measurements

These were made to find the length of time for which specimens would need to be presoaked in order to be certain that saturation was achieved throughout the thickness. The results are given here before the main mechanical test result section comprising Chapter 3.

Two methods were used to measure water take up.

2.2.1 Weight take-up measurements

Weight take-up measurements were done on 18 pieces approximately 10cm x 7cm cut from the experimental laminates. These specimens were weighed dry and sets of 6 were immersed at 60°C, 40°C and ambient temperature. They were reweighed at intervals. Problems were encountered initially because it was found that as surface moisture evaporated the weight decreased with time. The decrease of weight with time is shown in Figure 2.1. Specimens were left for 10 minutes after blotting before being weighed. A graph of weight take-up vs. time for immersion at the 3 temperatures is shown in Figure 2.2.

At all 3 temperatures water is taken up fairly quickly at first, the initial rate being higher at higher temperatures. At the 2 lower temperatures the graphs level out at about 1% weight gain. The 60°C graph, although it shows some signs of levelling out at 1%, rises again to nearly 2%. It would seem from this graph that a different mechanism operates above 40°C. A substantial amount of fibre whitening was observed on the 60°C samples, indicative of the breakdown of the fibre-resin bond. Under such circumstances processes involving the bulk transport of water along the fibre-resin interface would be possible, rather than solely diffusion of water on a molecular scale which is probably what happens at the lower temperatures.

2.2.2 Measurements using the Water Vapour Transmission Rate (WVTR) Meter

A block diagram of this apparatus is shown in Figure 2.3. The laminate is clamped between the two sides of the chamber. On one side the air is kept at 100% RH by means of a dish of water, or at less than 100% RH if a saturated salt solution is used. Dry nitrogen is passed over the other side of the specimen at a known flow rate (100cc/min) and the moisture content of the gas is measured by an electrolytic hygrometer. The electrolytic hygrometer is basically a glass tube containing two platinum wires wound at constant pitch onto a PTFE former. A film of phosphorous V oxide lies over and between the two wires and a potential difference is maintained across them. When the oxide is dry it is virtually non-conducting. When water is absorbed the film conducts as water is electrolysed. The magnitude of the current is directly related to the quantity of water in the gas by Faraday's law. Since current is the rate of charge transfer the meter is measuring rate of water transfer. The meter is calibrated in ppm of water in the nitrogen gas and a reading of 47ppm on the scale corresponds to a WVTR of 1 g/m^2 day.

A specimen is normally "dried down" before water is introduced to determine the background reading. "Drying down" means passing nitrogen over both sides of the laminate with no water in the lower part of the chamber until the reading levels out at around 5ppm. This is the background reading. Water can then be introduced into the lower part of the chamber remotely (without dissembling it). The

ppm reading rises over a period of several days until an equilibrium is reached. The literature supplied with the instrument indicated that a material with a WVTR of 0.05 g/m^2d (the figure given for a glass fibre laminate 2.3mm thick is 0.35 g/m^2) should take only 24 hours to reach equilibrium.

Once equilibrium has been reached the WVTR is given by:-

$$\text{WVTR} = \frac{\text{equilibrium reading - background level}}{47} \qquad (3)$$

Two methods were used for calculating diffusion coefficient.

a) Lagtime Method

Assuming Fickian behaviour for diffusion across a material with constant D, thickness L, concentration of diffusant C_1 on one side, and zero on the other, the quantity of diffusant, Q_t passing through the sheet in time t, Q_t is given by:

$$\frac{Q_t}{LC_1} = \frac{Dt}{L^2} - \frac{1}{6} - \frac{2}{\pi^2}\sum_{n=1}^{\infty}\frac{(-1)^n}{n^2}\exp\left(\frac{-Dn^2\pi^2 t}{L^2}\right) \qquad (4)$$

At the steady state $t \rightarrow \infty$ and

$$Q_t \longrightarrow \frac{DC_1}{L}\left(t - \frac{L^2}{6D}\right)$$

Using this approximation:-

$$\text{at } Q_t = 0 \quad t_{lag} = \frac{L^2}{6D} \qquad (5)$$

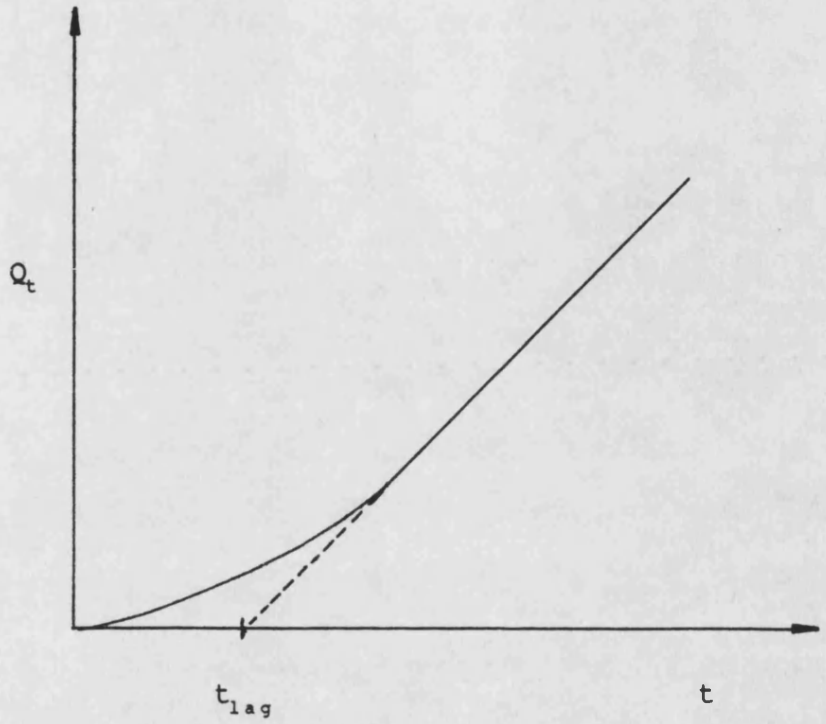

Putting in rough values of D for polymers from Crank [49], a range of lag times is obtained (for a thickness of 2.5mm) from 124 days for Nylon 6 ($D = 0.97 \times 10^{-7}$ mm^2/sec) to 12 hours for polypropylene ($D = 240 \times 10^{-7}$ mm^2/sec). A graph of Q_t vs. time, for a resin sheet (Figure 2.4), was plotted from the graph of WVTR vs. time, (Figure 2.5), by an approximate integration technique. The value of lag time found from this graph was 42 hours, giving a D value of 2.48×10^{-6} mm^2/sec. (L = 1.5mm). This figure is in line with typical figures from Crank[49].

b) 2 Value Method

An alternative method for D does not involve waiting for the system to reach equilibrium but uses two values of transmission rate, J, at two short times. D is calculated from the following equation:-

$$\frac{J_{t1}}{J_{t2}} = \left(\frac{t_2}{t_1}\right)^{1/2} \exp\left[-L^2/4D\left(\frac{1}{t_1} - \frac{1}{t_2}\right)\right]$$

For a resin sheet D was found using this method to be 10.4×10^{-6} mm^2/sec. D was calculated by both methods for a GRP specimen and the values were 1.33×10^{-6} mm^2/sec by the lag time method and 6.04×10^{-6} mm^2/sec by the two-value method. These results (for 40°C) compare reasonably with those of Apicella et al[50] for glass fibre reinforced polyester at 40°C of 7.8×10^{-6} mm^2/sec.

Armed with a value for D it is possible to calculate from theory the time to saturation at the centre of a plate of a certain thickness. The solution for the relevant boundary conditions appears in Carslaw and Jaeger's book on Conduction of Heat in solids and can be transposed to apply a diffusion of water rather than heat[51]. From this solution a graph of concentration at the centre of a plane sheet (as a percentage of the saturated concentration) vs. $Dt \div l^2$ (where l = half sheet thickness) can be plotted, see Figure 2.6. Times to 95%, 99% and 99.9% saturation are shown in the table below for l = 1.125mm at 40°C.

Material	D mm^2/sec	Method	Time to Saturation/Days		
			95%	99%	99.9%
Resin	2.48×10^{-6}	Lagtime	7.5	8.9	9.6
Resin	10.4×10^{-6}	2 value	1.8	2.1	2.3
GRP	1.33×10^{-6}	Lagtime	14.0	16.5	17.8
GRP	6.04×10^{-6}	2 value	3.1	3.6	3.9

Comparing the time to 99.9% saturation for GRP of about 18 days with the water uptake curve (Figure 2.2) for 40°C it can be seen that this time is in approximate agreement. However since the material is not truly Fickian the results can give only an indication of the water uptake behaviour. In view of this it was felt that a presoak of 28 days at 40°C would be adequate to ensure almost total saturation at the centre of the specimens.

2.3 Design and Commissioning of the Fatigue Rig

Two static stress rupture rigs were already in existence. Each was a tank with a number of lever arms mounted on the sides. Test coupons are attached between brackets in the base of the tank and the ends of the lever arms, and the constant loads are applied by hanging weights on the other ends of the lever arms. These were designed and built by the CEGB in 1978 but had been very little used since. One of the rigs was left as built, using its 22 loading points to do the static stress rupture work. The other tank was modified to enable tests with a cyclic load variation to be done. The modified tank had essentially the same features as the original but instead of using weights the load was generated by rolling rubber diaphragm pneumatic cylinders, see Figure 2.7. The pressure in the cylinders and

therefore the load was governed by pressure controllers which could accept a digital signal.

This enabled the system of 20 cylinders in all to be controlled by a computer. The easiest way of arranging the system was to have one pressure cycle and vary the lever arm ratios and the size of the cylinder to achieve different load levels. The lever arm ratios were decided on the basis of getting a sensible distribution of load levels from 20% to 112% of specimen failure load using two sizes of cylinder and three different lever arm ratios. The eventual arrangement adopted was to use either a $26cm^2$ or $38cm^2$ cylinder at lever arm ratios of 7:1, 6:1 and 3:1. The number of lever arms of a particular length and the size of cylinder on each lever arm were arranged so that the number of load points working at high load levels was less than the number at low load levels. This was thought necessary because low load tests take longer to complete. The loads obtainable in the six cases, with the system pressurised to its maximum (0.414 MPa) are shown in the table below:

LEVER ARM RATIO	NO. OF LEVER ARMS AT THIS RATIO	LOAD KN	LOAD % MEAN FAILURE LOAD	NO. OF $39cm^2$ CYLINDERS	NO. OF $26cm^2$ CYLINDERS
7	3	10.0	112.5	1	-
		6.7	75	-	2
6	3	8.5	96	1	-
		5.7	64.5	-	2
3	4	4.3	48	2	-
		2.8	31.5	-	2

The construction of the tension strings which connect the cylinders to the ends of the lever arms is shown in Figure 2.8. It was felt that the alignment of the tension strings would be quite critical, especially in the direction parallel to the side of the tank. The effect of misalignment on the load on the specimen was calculated (ignoring friction in the cylinder bearing, see Figure 2.7) and found not to be too serious. (The load decreased by .002% for a .5mm misalignment of the anchor plate.) However misalignment parallel to the tank wall would be detrimental to the rod bearing inside the cylinder so it was extremely important that the tension strings be installed as close as possible to vertical. Alignment could be checked by undoing the four studs holding the base of the cylinder clevis bracket to the anchor plate allowing the tension string to hang under its own weight. The position of the tension string in the direction parallel to the side of the tank could be adjusted by sliding the rod end bearing at the top of the tension string along the silver steel pin and holding it in position with packing pieces. In addition to this there was a slotted hole in the anchor plate. Final alignment was achieved by placing rubber washers under each of the 4 studs and tightening the studs by varying amounts so as to minimise the hysteresis in the load-unload cycle. It was possible to get the cylinders so well aligned that the deviation from a perfect straight line (of load applied vs. cylinder pressure) amounted to 0.5% to 1% depending on cylinder size and lever arm length, calculated at 2/3 maximum pressure. Calculation of the proportion of the applied load used to overcome friction at the three pivoting points showed that it would be advantageous to use bearings in these

three positions with low coefficients of friction (μ) to reduce frictional losses in the system. The use of a rod-end bearing (μ = .09) at the top of the tension string seemed a convenient way of allowing movement in two directions and keeping friction down.

It was necessary to provide a means of adjusting the length of the tension string since the two sizes of cylinder are of different lengths - this done by means of the threaded barrel and stud arrangement above the cylinder.

The shutting off of the air supply to a load point when the specimen failed was done using the existing microswitch system and 20 solenoid valves. These were wired so that when a specimen failed the contact was broken and the air supply to that load point was shut off. In the event of 240V power failure all load points would be shut down. (The PET computer would also stop under these circumstances.) The pressure in the cylinders was controlled by pressure controllers, of which there were four, mounted in a case together with the regulating valves for the incoming air, which enable the equipment to switch over automatically to an emergency supply should the main compressed air supply fail. The control box was designed and built by John Watson and Smith Ltd. of Leeds who also wrote the software for the Commodore PET computer. Each individual pressure controller could accept an 8 bit digital signal from the PET which it converted to an analogue signal and used this to regulate the pressure. The PET updated the controllers sequentially at a rate of 1 per sec. for each. The system resolution was 0.002MPa. The software allowed the

user to select such variables as fequency, rate of pressure application and maximum pressure, and it was possible to have a different cycle running on each controller. The plumbing system, flexible nylon pipe and push fit connectors, made it possible to run any cylinder from any controller very easily, up to a maximum of 10 cylinders per controller. It was not possible to use the PET to record any data as there was insufficient spare capacity. The rig was fully operational by November 1983 and the first tests were started in December.

2.4 Fatigue Tests at 1Hz

The 2 regimes of dry, room temperature tests could be carried out using a conventional fatigue testing machine. An Instron model 8033 was used. The one programme of tests on presoaked, wet specimens necessitated the design of a test cell which would fit around the Instron's grips. This cell around the specimen consisted of a large diameter perspex tube through which water at 40°C could be circulated. The top of the tube was open and its base could be clamped to a sub-assembly resting on the lower grip. The water was contained in the cell by a disc of rubber sheeting. The rubber discs were slit to allow the specimen to pass through and be sealed in position with a silicon rubber sealing compound. The edge of the disc could then be clamped between the perspex tube and the sub-assembly. The water was heated in a thermostatic bath and circulated around the cell by a small pump. A photograph of the cell is shown in Fig. 2.9.

Chapter 3 Mechanical Test Results

3.1 Statistical Treatment of Mechanical Test Data from programmes St, S1 and R1

Tests with codes St, S1 and R1 were done over a range of load levels, in water at 40°C on presaturated specimens. Restating the information in Table 1; St = Static loading, R1 = rectangular loading with unloads every 2 minutes and S1 = sinusoidal loading about a mean load with the alternating component at 20% of the mean load. The mean load of S1 corresponds to the static load in St and the constant tensile load between unloads in R1. Results were obtained for these 3 loading régimes at 6 load levels, 7.3, 6.3, 5.5, 4.6, 4.1 and 3.1kN. (The mean tensile failure load was 8.9kN).

3.1.1 Preliminary Evaluation

The conventional approach with data of this kind over a range of load levels, at least for stress rupture, is to plot a graph of load vs. log time. In the approach to the statistical analysis of the data the load vs. logtime convention will be broken and scatter diagrams will be shown plotting logtime vs. load. This is because changes in time to failure as a result of alterations in load régime are sought, so time to failure is therefore the dependent variable and load is the independent variable. The cyclic tests are also plotted as log seconds vs. load for purposes of comparison with the static. Scatter

diagrams are shown in Figs. 3.1, 3.2 and 3.3. In each of these graphs one set of fatigue data has been compared separately with the static data for the sake of clarity, since the points lie so close together. In Fig. 3.1 the R1 results are compared with the static ones. For these rectangular tests the "time at load", (time spent at load per cycle multiplied by the cycles to failure), is compared to the static time to failure. If the periodic unloads are having no effect, then damage to the specimen should only occur while it is held at the test load. From this plot it is impossible to tell whether unloading once every 2 minutes during the test makes any difference to the failure time at all. The same can be said of the scatter plots in figures 3.2 and 3.3. Here for the sinusoidal loading, the load values have been plotted taking the mean load as the test load in figure 3.2, whereas the load value used in fig. 3.3 is the maximum of the sine wave, (120% of the mean). The questions being asked here are really

1) does overloading sinusoidally in this manner have a different effect from static loading at the mean level? and
2) does underloading sinusoidally from the maximum load have a different effect from static loading at the maximum load?

A method is needed of ascertaining whether any statistically significant difference does exist between any of these pairs of data sets. First, the ways in which the 2 data sets might differ will be outlined and then a statistical method will be described by which these differences may be detected.

With 2 sets of data on a scatter plot (such as Figs, 3.1, 3.2 or 3.3) the first step when trying to compare the 2 sets of results would be to draw a regression line through each set of data. Three possible situations exist, and these are shown diagramatically in Fig. 3.4.

Case 1 - 2 regression lines of different slopes (Fig.3.4a)

If it can be shown that the 2 slopes are significantly different the data in the 2 sets is best represented by drawing separate regression lines each with its own slope.

Case 2 - 2 regression lines of approximately the same slope but displaced in the y-direction (Fig. 3.4b)

If it cannot be shown that the 2 slopes are significantly different the 2 slopes may be pooled to give a better estimate of the slope of both lines. The new slope is called the pooled slope. If it can also be shown that the data is significantly separated in the y-direction a line with slope equal to the pooled slope is drawn through each set of data. Each of these lines passes through the point $(\bar{x},\bar{y})$ for its own data. ($\bar{x}$ denotes the mean of the x values.)

Case 3 - 2 regression lines of approximately the same slope but lying close together (Fig, 3.4c)

As in case 2 because the slopes cannot be shown to be significantly different the best estimate for each slope is given by the pooled slope. But here for Case 3 where the displacement in the y-direction

is insignificant, 2 separate lines cannot be shown. The data in the 2 sets is to all intents and purposes part of the same population, until further data can disprove this hypothesis and as such should be represented by one line drawn through the combined data from both sets.

A statistical test for significant differences in slope and intercept was carried out on the pairs of data sets shown as scatter diagrams in Figs. 3.1, 3.2 and 3.3. Before giving the results of the comparisons between static loading and a) the rectangular loading, b) sinewave loading plotting mean load, or c) sinewave loading plotting maximum load it is necessary to set up the 3 null hypotheses which it is sought to disprove by the statistical analysis.

a) for R1 and static:- the time to failure under static loading is indistinguishable from the aggregate time at load in a test where periodic unloads to almost zero load are incorported once every 2 minutes.

b) for S1 mean and static:- the time to failure under static loading is indistinguishable from the time to failure under a sinusoidal load which oscillates above and below the static load level by 20% once per 2 minutes.

c) for S1 max and static:- the time to failure under a static load P is indistinguishable from the time to failure under a sinusoidal load with mean value 5/6P and peak value P.

The statistical analysis involves calculating the variances of the data points from the various regression lines and then comparing the variances using an F-test. The method is detailed in the Appendix. The results, expressed as significance levels where a difference was detected are shown in the following table. Percentages shown on this table are the probabilities of obtaining the data in the scatter plots given that the null hypotheses hold. A low percentage indicates that the outcome is improbable and the null hypothesis is unlikely to be true. A percentage greater than 5% means that this outcome is more likely so the null hypothesis probably holds - in this situation there is no significant difference - NSD.

Data sets	Difference in slopes	Difference in y-displacement	Conforms to which case? (see Fig.3.4)
R1 - St	NSD	NSD	3
S1 mean - St	NSD	yes - at 1% level highly significant	2
S1 max - St	yes at 5% level significant		1

This preliminary analysis in conjunction with the scatter plots, shows that 1) there is no difference in time to failure at any of the test loads for R1 compared to static, i.e. case 3 in Fig. 3.4, 2) for S1 mean and static, overloading above the static load sinusoidally shortens lifetime significantly by an amount which is the same over the range of test loads, i.e. case 2 in fig. 3.4, and 3) compared to constant static loading at the maximum load, the

lifetime is longer under régime S1 at high load and this difference is not apparent at low load, i.e. case 1 in Fig. 3.4.

Referring to the scatter diagrams again momentarily (Figs. 3.1 - 3.3), the amount of scatter in times to failure at some of the load levels is quite large - up to 4 orders of magnitude. It is possible that this large degree of scatter might be masking other differences between cyclic and static loading, particularly as some of the test statistics in the preceeding tests bordered on significance. A possible origin of the scatter in times to failure at a constant load level lies in the statistical distribution of failure loads of the test pieces. So, although the load applied to a set of specimens is uniform, the load each one sees, expressed as a percentage of its own failure load may be very different from that seen by others. A method of adjusting the load values which reduces this scatter will now be described.

3.1.2 Correction for variation in innate strength of test pieces

3.1.2.1 Describing the strength distribution

As is the case with other materials, the strengths of GRPs are distributed according to the Weibull distribution. The Weibull survival probability density function, $P_s(V)$ is given below.

$$P_s(V) = \exp[-V(\frac{\sigma-\sigma_u}{\sigma_o})^m]$$

m = Weibull modulus

σ_u = stress below which failure cannot occur

σ = applied stress

σ_o = normalising parameter, called characteristic strength

V = volume term.

This is the equation for a 3-parameter distribution. For a 2 parameter distribution $\sigma_u = 0$.

As a means of testing whether a set of data fits a Weibull distribution, the data may be plotted on Weibull probability paper. (The method is detailed in Johnson's book.[52]) The straight line that could be drawn through the points confirmed that the strengths fitted a Weibull distribution. The parameters m and σ_o and the Weibull mean strength may be found graphically from this straight line. If it is suspected that σ_u is non-zero, from a slight downturn at low strengths, trial values of σ_u have to be subtracted from all the strengths and the graph replotted until the best straight line is obtained. This can get tedious. Also the graphical method becomes more inaccurate for small sample sizes where the intercept and slope of the straight line are uncertain.

A more accurate method exists for the calculation of Weibull parameters, the maximum likelihood estimation (MLE) technique.[53] This is a computerised iterative technique which starts with values

of the parameters, obtained by a method analogous to the graphical method above, and alters them by small increments until the "best fit" is produced. Access to such an MLE programme was available at the CEGB's premises in Bristol, so this was used to calculate the parameters in the subsequent work. The parameters output by the MLE programme were as follows:-

$$m = 9.9 \quad \sigma_o = 217.4 \quad \sigma_\mu = 43.6$$

3.1.2.2 Calculations of failure load using the Weibull Strength Distribution

A large proportion of the data scatter in the logtime-load plots of Figs. 3.1 to 3.3 is directly attributable to the variation of tensile strengths. In the plotting of these scatter diagrams the applied unit load was divided by the average tensile failure unit load to obtain %UTUL. It is very possible that, owing to the scatter in failure loads, the actual strength of a particular specimen would differ from the mean strength. The Weibull distribution of the strength values is used to estimate the actual strength of a particular specimen, giving a better estimate of the %UTUL. This technique is based on work by Hahn [54], but has been adapted by the author to produce a novel method by which scatter in lifetimes may be reduced and information from tests which failed before maximum load had been reached for the first time (load-up failures) and from run-outs may still be incorporated into plots and statistical

analysis. The description of this load adjustment method will begin with the basic technique and then give details of the refinements.

Hahn assumes that a specimen that is statistically strong in a tensile strength test would be very strong under stress rupture conditions, so that its time to failure under constant stress would be longer than average. This is often referred to as the "strength-life equal rank assumption".

For simplicity a 2 parameter Weibull strength distribution will be used to illustrate the method. Probability of survival, P_s, at stress x is given by

$$P_s = \exp\left(\frac{-x}{x_o}\right)^m \quad (x_o \text{ is a normalising paramter, related to } \sigma_o)$$

In order to derive strength estimates for stress rupture specimens, a Weibull distribution of this type must be fitted to experimentally measured strength data. The strength values are ranked in order of increasing strength and median ranks assigned to each one. Median ranks are effectively the cumulative probability of failure up to the ith strength value of a total of N ranked measurements. Median ranks may be found in tables[52] or calculated using

$$\text{Median rank, } R = \frac{i-0.3}{N+0.4}$$

A graph is then plotted of log(-log[1-R]) against log x. It should be possible to draw a straight line through these points whose slope is the Weibull modulus, m, and which cuts the line

$y = \log(-\log[1-0.623])$ at $x=x_o$. The parameters of the Weibull distribution of times to failure in a stress rupture test could be found in exactly the same manner. If the number of test results, N, were the same in the cases of strength and time to failure, the same median rank would be assigned to the ith failure in each, which implies that cumulative failure probabilities are equal. The assumption of equal rank provides a method of estimating the strength of the ith specimen to fail in a stress rupture test. This estimated ultimate strength was used instead of the mean strength in the plotting of normalised load (as %UTUL). In his justification of the technique Hahn states that the ultimate strength of the kevlar-epoxy composite and its stress rupture performance are both dependent on fibre strength. This is also likely to be the case for the glass-polyester composites in this study.

The effect that this procedure has on the stress rupture plot will now be demonstrated with reference to Fig. 3.5. If 6 failures were obtained in a stress rupture test at one particular applied load level, the 6 results would be plotted conventionally at one single load level expressed as a percentage of the mean UTUL. According to the strength-life equal rank assumption the first coupon to fail in the stress rupture test would have a much below average strength. The applied load is therefore a much higher percentage of its estimated strength. The data point is therefore plotted at a higher normalised failure load. A similar situation applies for the specimen with the longest life. Its strength is assumed to be higher initially, so the applied load is a smaller fraction of its UTUL.

The effect of applying this correction to the load values is to push the plotted points closer to any regression line through multi-load level stress rupture data. The consequent reduction in scatter enables statistical significance testing to be made more sensitive, as will be demonstrated later.

3.1.2.3 Load-up failure and run out refinements

The extension to the treatment is as follows:
Suppose at a high load level 6 specimens are put on test and that 3 of these fail on loading. These are ranked in order of failure.

Failure no.	1	2	3	4	5	6
	0	0	0	X	X	X
	load-up failures			failures under static load		

If the load-up failures were completely ignored, UTUL's of the failures under static load would be found from the Weibull graph, assigning to each failure the median rank of the 1st, 2nd or 3rd failure of a total of 3 failures, as appropriate. The strength of what is in reality the 4th specimen to fail would be assumed, wrongly, to be a long way below the mean, whereas it is probably above the mean strength, being the 4th failure of 6. The strengths of the static load failures are therefore found by assigning to them median ranks consistent with their true position in the distribution

of strengths i.e. those for the 4th, 5th or 6th failures of a set of 6. In this way their higher than average strength may be reflected in the scatter plot and any subsequent statistical testing. The load-up failures need not be plotted at all. The procedure for run-outs is analogous to that for the load-up failures. If 6 specimens were put on test, and to date only 3 have broken, these 3 are assigned the median ranks of the 1st, 2nd and 3rd failures of 6. The remaining median ranks will be used for the 4th, 5th and 6th failures as they occur.

Figure 3.6 shows how the regression line is rotated if the refinement is not applied to the %UTUL adjustments. In part a) where the refinement is applied all the data points will be shifted so that they fall on, or close to, the solid regression line. In diagram b) where no refinement is used, the points from the load levels where there were load-up failures will be shifted so that they still lie above the solid line. At the lowest load level where there are run-outs the points lie below the "true" line. The regression line that will be drawn through these wrongly shifted points is rotated clockwise. This is shown as the dotted line in Fig. 3.6b. The larger the proportion of data points from load levels containing load-up failures or run-outs, the more the regression line through the points will be rotated from its true position. This rotation of the regression line would still be expected even when unadjusted data is being plotted.

It is instructive to examine the equations of the regression lines

i) through the raw data and ii) through the adjusted data with the refinement applied.

	i) line through raw data	ii) line through adjusted data
Static	logsec = -.1364 load+12.66	logsec = -.1376 load+12.78
R1	logsec = -.1369 load+12.45	logsec = -.1415 load+12.74
S1 max load	logsec = -.0963 load+10.33	logsec = -.1110 load+11.25
S1 mean load	logsec = -.1156 load+10.33	logsec = -.1331 load+11.24

For the static test which contained a single run-out the regression line has altered very little. About half the failures were load-up failures at the highest load level for sine wave loading. Here the change in the slope of the regression line has been most noticeable. In all cases the slope (Δ logsec $\div$ Δ load) is larger for adjusted data and the intercept is further up the logsec axis. These changes are equivalent to the direction of rotation of the regression line shown in Fig. 3.6b).

The effects of applying this method and the refinement to it should in theory be twofold. Firstly, the amount of scatter is reduced and secondly, when there are many load-up failures, the slope of the regression line should be nearer to that obtained if there were a full set of failures at every load level. In practice a dramatic reduction in scatter is seen when the scatter plots before and after adjustment in Figs. 3.7 and 3.8 are compared. The scatter in the

logtime direction has been reduced from as much as 3 orders of magnitude to only one. The substantial improvement in scatter due to plotting adjusted failure loads is further evidenced by the higher correlation coefficients of regression lines through the sets of data

Data Set	Correlation Coefficient	
	UTUL	Adjusted UTUL
St	-.8737	-.9586
R1	-.8846	-.9798
S1 (mean) S1 (max)	-.8198	-.9543

3.1.3 Re-evaluation of the data using adjusted failure loads

The high degree of scatter in lifetime makes differentiating between 2 sets of data when unadjusted load is plotted almost impossible unless the difference in lifetime is large. When the analysis of variance technique was used to look for differences between lifetimes under static and rectangular wave loading, for instance, no significant difference could be found when the raw data was used. (see 3.1.1) If the same treatment is carried out on the adjusted data there is a different outcome. This is shown in the following table.

Table showing Analysis of Variance Results using Adjusted failure load.

	Difference in Slopes?	Difference in y-displacement?
R1-St	NSD	Yes - at 5% level significant
S1 mean-St	NSD	Yes - at 1% level highly significant
S1 max-St	Yes - at 1% level highly significant	-

NSD = no significant difference

The difference which was found between the slopes of S1 (plotting maximum load) and St data has been made more significant. A significant difference has emerged between R1 and St régimes where there was none before. Further calculations in section 6.1 will show that a difference in lifetime should be expected between static and rectangular wave loading at a frequency of 1 per 2 mins. The observed difference between R1 and St régimes is therefore assumed to be genuine, and not an artifact produced by the treatment of the results. Plotting adjusted load and using this in the statistical analysis of results enables real changes to be detected which would otherwise be masked by the scatter in times to failure.

Having removed most of the data scatter by this technique it is

possible to re-examine the plots comparing R1 and S1 loading with the static in turn.

3.1.3.1 S1 (maximum load) with St (Fig. 3.9)

At high load lifetime under the S1 fatigue régime is longer than when held statically at the maximum load. This shows that the effect of holding the specimen at a high load is worse than the effect of fatigue cycles up to that load. This is consistent with the work of Menges and Thebing. At low load the behaviour is reversed. Static specimens outlive cyclically loaded ones, indicating that cycling is worse than holding at the lower maximum load level. In the sinusoidal tests here the specimen is being under-loaded compared to the static tests at maximum load. Since lifetime is shorted in these sinusoidal tests a dynamic fatigue effect must be occurring.

3.1.3.2 S1 (mean load) with St (Fig. 3.10)

Plotting the mean load of the sinewave régime instead of the maximum load has shifted the whole curve down the load axis by varying amounts. The slope of the line through this data is not significantly different to the slope of the static regression line, but over this range of loads the lifetime under S1 loading is about an order of magnitude shorter than that under static loading at the mean load. In this case the shorter failure time of sinusoidal wave testing could be said to be a result of over-loading above the mean (static) load level for half a cycle so it is not possible to tell from this comparison whether a fatigue effect is occurring.

3.1.3.3 R1(time at load) with St. (Fig. 3.11)

This is by far the most informative comparison possible, since R1 contains an element of static loading. At low load the time at load to failure under rectangular loading is less than that under continuous static load. This shows that the cyclic unloads do have an effect on life, but at this stage it is not apparent precisely what is happening. Results in the next section (3.2) clarify the degree of synergism.

3.2 Results of Tests with Varying Frequency

It was not possible to obtain a multi-load level data set for a succession of different loading frequencies, so, a single load level was chosen. This load level was 4.6kN, about 50% of the mean UTUL for all laminates. The different frequencies and sketches of the waveforms of load variations with time are shown in Fig. 1.7 and Table 2.

Rectangular waveform loading was carried out at 5 unloading frequencies; 0.03, 0.5, 4, 8 and 15 cycles per minute. The duration of each unload was 4 seconds, so that the rate of change of load was constant with time. The time at load varied between 33 minutes and effectively zero. The saw-tooth waveform, R4, has been included in the rectangular waveform tests as it represents the limiting situation with zero at time at maximum load.

The results of these tests are given in Table 3. The variables tabulated are log (total time),log (time at load) and log (cycles) as appropriate, (so for static loading only log (total time) is given). Times and cycles to failure will fit a Weibull distribution and a log normal distribution equally well and it is convenient to perform statistical comparisons using the lognormal in this instance. The results shown in Table 3 are therefore the mean and standard deviation of the logarithms of the times or cycles to failure.

The statistical test which can be applied to these results is the 2 sample t-test. Of the data given in Table 3 the most worthwhile comparisons are a) between the times at load to failure under static and rectangular loading, (St,RO,R1,R2 and R3) and b) between the cycles to failure under the different rectangular loading regimes, (RO,R1,R2,R3 and R4).

The first step is to set up the null hypotheses. They are as follows:

For a), The logarithm of the time under load to failure is identical under each loading régime.
For b), The logarithm of the cycles to failure is identical under each frequency.

The alternative hypothesis is, in each case, that there is a difference in log (time-under load) (or logcycles) to failure. The test statistics were compared with critical values taken from a 2 sided t-table to determine the level of significance.

Test statistics are tabulated for each test in Table 4. For Test a), comparing logs of times under load, no differences were found between any pair of the 3 sets St, RO and R1. These 3 were in all combinations significantly different from the 3 higher frequencies and the 3 higher frequencies were all significantly different from each other. Moving to the comparisons on the basis of log cycles, RO was significantly different from all the other rectangular loading tests whereas R1 is indistinguishable from them. There are also no significant differences between the log (cycles to failure) of any 2 of these higher frequency tests.

There seem to be 2 failure criteria on the basis of these results. At high frequencies the failure occurs after a specific number of cycles, irrespective of the time under load. At low frequencies, the material is held at load for a substantially longer amount of time per cycle, so the time at load criterion is satisfied before the number of cycles required for failure is reached. The boundary frequency is probably around the frequency of R1 - (1 cycle per 2 minutes) since these tests were no different from the low frequency tests in terms of time at load and at the same time no different from the high frequency tests in terms of cycles to failure. The concept of boundary frequency will be expanded further and an actual value calculated in Chapter 6.

3.3 Results of high frequency (1Hz) fatigue tests

Three fatigue regimes had a test frequency of 1Hz, they were DS1, DS2

and S2. The effect of raising mean stress and the effect of the aqueous environment will be examined in turn. Finally failure under high and low frequency fatigue will be compared.

3.3.1 The effect of raising mean stress

If the results in regime DS2 (dry, sinusoidal O-tension) are plotted together with those from regime DS1 (dry, sinusoidal, with alternating load at 20% of the mean load) the effect of raised mean stress may be seen. Such a plot of log(cycles) vs. load is shown in Figure 3.12 where the maximum load for each regime is plotted on the load axis. Raising mean stress from 50% to 83% of maximum load has increased the fatigue life by approximately a factor of 7. Evidently the accompanying decrease in the alternating load has had a greater effect than the raising of the average load since the lifetime has been lengthened.

3.3.2 The effect of an aqueous environment

The scatter plot comparing the fatigue lives under regime DS2 (dry, 0-tension) and S2, (wet, 0-tension) is shown in Figure 3.13. Even though the S2 tests were only conducted at one load level they appear to lie over several loads because of load adjustment. Without resorting to the slopes comparison test it is possible to see that presoaking and testing the specimens wet has shortened life significantly.

3.3.3 Comparing high and low frequency wet fatigue tests

It would be interesting to compare the fatigue lives in a water environment of specimens tested under the same regime but with different frequencies. No actual experimental data are available but using the factor difference highlighted in 3.3.1 it is possible to estimate the life in a low frequency 0-tension test from the S1 figure. This could be compared to the cycles to failure under regime S2. The cycles to failure for S1 and S2 at 4.6kN maximum load are as follows:

	S1	S2
log N	3.710	4.664
N	~5,000	~46,000

The estimate of low frequency, 0-tension life is only 700 cycles. (Reducing the S1 figure by a factor of 7). This estimated lifetime is many times shorter than the lifetime of 46,000 cycles at high frequency. This shows that basing design on high frequency fatigue tests as in BS4994 is potentially dangerous as had been feared.

3.4 Summary of results of mechanical testing

1. A technique is presented whereby in fatigue or stress-rupture tests some of the apparent variability in life at a given load level may be attributed to variations in the inherent strength of the testpieces.

2. When the correction technique is applied to low frequency rectangular wave test results (régime R1) it is possible to observe a shortening of the time to failure due to the imposition of unloading cycles.

3. When the lifetime under low frequency sinusoidal fatigue is compared with static testing at the same maximum load it is possible to discern a fatigue effect which shortens life at low loads. This is apparent from examination of uncorrected data.

4. Comparing high frequency fatigue life with an estimate of the life under a similar regime but at a low frequency, showed the low frequency regime to be much more damaging. This adds weight to anxieties over the use of high frequency data in design for low frequency service.

5. In high frequency tension/tension tests, raising mean stress at constant peak stress causes an increase in the number of cycles to failure.

6. Testing at high frequency in water reduces lifetime by comparison with dry tests.

7. From rectangular wave tets of varying frequency it was possible to observe 2 distinct failure criteria:

   a) At high frequencies failure is determined by the number of cycles;

   b) At low frequencies failure is determined by the time at load.

4. Damage Studies

In order to gain information about the failure processes under stress rupture, fatigue and combined conditions, intest and post-failure examination of specimens was conducted. Slight differences in, for instance, the form of the fracture were noted from one régime to another but before any real trends could be identified systematic observations on as many specimens as possible were needed. The results of these observations are collected in tabular form and example microstructures are shown where appropriate. These studies of damage development are divided into 4 sections: 1) optical microscopy during tests, 2) debonded area measurements, 3) optical examination of failed specimens and 4) SEM observations of fracture surfaces.

4.1 Optical microscopy during tests

A large amount of information could be gained from actually watching how damage accumulated during different tests. It was possible to observe the processes contributing to failure, at what stage in coupon life they were most active and isolate differences and similarities between static and cyclic loading. Observations of fatigue tests in dry conditions were relatively easy and other researchers have reported how fatigue damage accumulates. Information on damage processes during fully immersed tests is scarcer and the following series of photographs of specimens under load in the actual water-filled stress rupture tank are quite novel.

4.1.1 In-tank tests (St, S1 and R1)

Photographs of the specimens while they were on test i.e. in water at 40°C and under load, were taken using an endoscope. A record of the accumulation of damage during the tests could be kept without interrupting them. The photographic apparatus consisted of the endoscope itself, an Olympus OM2 35mm camera and an adaptor, which fitted between the endoscope's eyepiece and the body of the camera. This assembly was held steady and at a constant position relative to the specimen by means of an arm which could be clamped to the side of the tank. Illumination was provided by a light box and a length of 8mm diameter fibre optic cable. The specimen was lit from behind with the light incident at a glancing angle. The arrangement is sketched in Fig. 4.1. Photographs were taken at intervals during each test. Series of pictures were obtained from 5 tests at one load level under each of the 3 régimes (St, R1 and S1). The load level selected was 5.5kN, 62% average UTUL. Photographs from the 2 most informative sequences (one from a static test and one from an R1 test) have been reproduced in the thesis.

4.1.1.1 Static Test Sequence

Seven pictures during a static test are shown in Fig. 4.2. A crack is clearly visible from 20 minutes onwards, and even at 5 minutes there is a suggestion of a crack in the same location.

The middle 5 pictures, those taken with load applied, appear much

whiter in their gauge lengths, than those under zero load. This is due to transverse fibre debonding in the weft rovings. The debonds are opened up under load, and reflection occurs at the interfaces allowing the debonding to become visible. The darkened area beneath the crack visible at 20, 31 and 41 minutes is thought to be an effect of the shallow illumination angle, rather than an absence of debonding. The situation is as follows; after 20 minutes the crack has grown such that it stretches across the width of the outermost warp roving and has penetrated into the thickness of the specimen probably as far as the warp roving, i.e. through the CSM and the weft roving. The faces of the crack are composite-water interfaces at which reflection can occur. Light is reflected upwards where fractured fibre-resin interfaces can further scatter the light - the upper areas appear brighter. The lower half of this transverse roving is effectively in the shadow of the large crack, so appears dark. The dark and light zones in the vicinity of large cracks highlighted their presence in areas where there was extensive debonding.

4.1.1.2 Rectangular régime R1 test sequence

Eight micrographs from a rectangular wave test are shown in Fig. 4.3. the crack which led to the eventual failure is visible as early as the 9th cycle. Its development may be traced throughout specimen life, marked by i) lengthening of the white "streak" accompanying large-scale weft debonding and ii) growth of warp roving-resin debonding. On visual examination of the failed specimen the

debonding was found to be occurring between the WR and CSM layers at the interface. The incidence of this was much higher in R1 tests than St.

Irrespective of load régime, in the final stages before failure - often in the last seconds - the extent of the warp roving debonding increases dramatically. A crack in the outer CSM layers extends across the whole width of the specimen and warp roving bundles fracture, beginning from the side of the specimen where the first damage initiated.

4.1.1.3 Identification of Failure Initiation Sites

It can be noticed that, on both R1 and St, the extent of roving bundle debonding is far less in the initiation region than at the side of the specimen which was last to break. In almost all the tests where in-situ microscopy was carried out, there was a difference in the extent of roving debonding from one side of the specimen to the other at failure, and where a clear resin crack was discernible during testing, the side where less roving debonding was found at fracture coincided with this crack. This observation was important as it enabled the initiation region to be located on other failures. A very high proportion of failures of specimens presoaked and tested in water showed a variation in the extent of this debonding across the specimen width.

4.1.1.4 Comparisons of Static and Cyclic Failures

It was not feasible to reproduce all 15 sequences of pictures. Instead the salient points have been summarised in Table 5. The occurence of 3 features has been tabulated for each of the 15 specimens photographed; the 3 features being i) a difference in the extent of WR debonding across the width of the specimen at failure, ii) a clear crack in the outer layer visible in the position of the final failure and iii) other additional sites of damage which could have led to failure. All 15 tests showed some variation in WR debonding across the specimen width, and in most cases this was pronounced. The incidence of cracking in the outer CSM was higher in both cyclic régimes than the static. For rectangular especially, there were more secondary CSM cracks which did not lead to failure, and the one crack leading to failure was more clearly defined. There was no real evidence that the locus of the final failure coincided with any of the voids present at the start of a test, at least not with those resolvable by the endoscope.

The differences between static and cyclic régimes are as follows: i) a clear crack prior to failure was more clearly visible in cyclic than in static tests; ii) the existence of other possible failure sites is more likely in cyclic than in static tests. These differences are most marked betwen St and R1. The S1 tests showed more intermediate behaviour.

4.1.2 1Hz tests:- (DS1, DS2) Dry in air

No specialised inspection equipment was necessary to observe these specimens under test on the Instron 8033. Photographs were taken periodically, as before, but with a Pentax MX camera, fitted with a close-up lens supported in front of the specimen on a tripod with light provided by a cold light source. One series of micrographs is shown for each. Both are of tests where the maximum load level was 7.2kN (80% Avg. UTUL). Fig. 4.4 is the series for the 0-tension (DS2) test. Transverse cracking, which, from its position must be fibre-resin debonding in the weft rovings, was present from the very first loading cycle. Areas of intense whitening, again debonding along the warp roving resin interface, are visible quite early on and extend as the number of cycles increases. It can be noticed that a greater area of debonding between WR and the outer CSM accumulates prior to failure than in the R1 example, where this type of debonding was previously referred to. Debonding extends both across the width of the sample and along the length of the warp rovings. At failure the whitening, characteristic of this roving debonding, extends over almost the whole of the gauge length. At 50% elapsed life there are 3 possible whitened sites that could lead to failure. In subsequent micrographs it can be seen that one of these extends with time preferrentially while the others remain static, it is this one location which is the failure site. A growing crack in the centre of this white area is visible from 70% elapsed life onwards.

This series of pictures can be compared with those for one of the DS1

tests (mean load ±20%) shown in Fig. 4.5. The scale of roving debonding is much less, both at the final failure and leading up to it. (The area debonded at 88% life in DS1, is approximately the same as the area at 51% life in DS2.)

In both these dry fatigue series, transverse cracking appears with greater contrast than in the St or R1. The higher mean load level in DS1 and DS2 may increase the amount of transverse cracking damage. However, it must be pointed out that the resolution using the endoscope is poor and in addition to this, if water penetrates any cracks, the smaller refractive index difference between water and glass than air/vacuum and glass will reduce scattering.

Observations from the 2 dry fatigue tests are summarised in Table 6. A fourth category has been added since it was possible to differentiate between "other possible failure sites" which had cracks and those which did not. The only large cracks in non-failure locations were found in 0-tension. The same trend of a difference in extent of debonding across the specimen width at the failure was found in 1Hz dry fatigue as in the in-tank tests, however, the difference was less on some of the 0-tension, DS2 specimens. A clear resin crack developed at the failure site after usually, 60-70% life, whereas on one of the static tests, no crack was visible after 97% life. Areas of whitening which could have led to failure were produced, as they had been in S1 and R1, but more frequently.

4.1.3 1 Hz test, S2, presoaked and tested in water

The series of micrographs from this test is shown in Fig. 4.6. Damage tends to develop in one site, there being only small areas of whitening elsewhere. A clear crack is visible from 80% life onwards, and lengthwise roving debonding can be seen growing in the 2 later photographs.

A summary of observations as before is given in Table 7. The behaviour is akin to that of the dry 0-tension tests, even though the load level is lower and the test is in water. Both show other possible sites for failure, some with resin cracks.

4.1.4 Summary of the results of in-test microscopy

A spectrum of different modes of failure between static and the various cyclic tests is emerging. At one end static failures are characterised by a single damage zone which causes eventual failure and little or no prior cracking of the outer material. Failures under low frequency fatigue show some prefailure resin and CSM cracks and alternative failure sites start to appear. The S2 tests (wet tests at 1Hz), ressembling the in-tank fatigue tests but having greatly increased frequency, are similar in failure mode to R1 but there is an increased incidence of secondary damage sites and crack formation. Cracks and secondary damage sites would seem to be a result of a high stress range fatigue at high frequency, since these were visible in DS2 and S2 tests, both of which were 0-tension 1Hz tests. DS2 is the régime incorporating the highest fatigue element

and the failure pattern is the most dissimilar from the static tests. This régime therefore lies at the opposite end of the failure mode spectrum to static tests. The tests could be arranged as below in order of increasing fatigue character:-

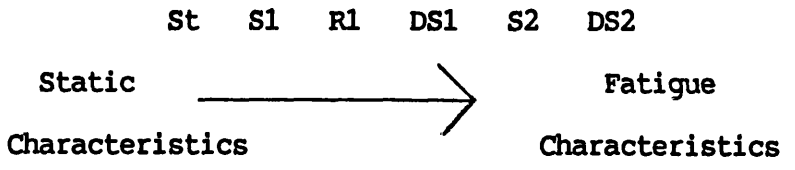

This idea is expanded in a later section where more data is presented.

4.2 Debonded Area (DBA) Measurements

It had been noticed that the size of the whitened area near fracture varied both with load level and from one régime to another. The whitened area is a result of debonding between the WR and CSM layers (i.e. strictly speaking delamination). The outer layers of the composite (gel coat and CSM) were observed to fail before the central WR layer. Once a crack exists in this outer material the woven reinforcement can separate from it by delamination. Once this situation is reached the warp (0°) fibres of the WR are holding all the applied load local to the crack. Delamination can grow provided the warp rovings are strong enough to support the applied load. In general strong fibres would tend to have a large area of delamination associated with them. Small areas could therefore be assumed to show areas where the reinforcement had undergone a large loss of strength. Debonded areas were measured systematically for all specimens to quantify any dependence on load level and verify any changes with loading regime. This was done using a MOP Videoplan Image Analyser

from photographs of failed specimens. The area measured was that directly associated with the final fracture, secondary whitened area were not included.

Comparisons of the DBAs between each loading régime (for St, R1, R2, R3 and R4) were done analogously to comparisons of the times to failure (see 3.2). The average DBA in each of tests R1 R2, R3 and R4 was compared with the average DBA for static tests at the corresponding load level by means of 2-sample t-tests. The statistical distribution of the data in each set, i.e. from a test at a particular load level and load régime,) was ascertained by plotting the ranked areas and their logarithms on normal probability paper. A slightly better straight line was formed by the logarithms of the areas, so the statistical calculations were performed assuming a lognormal distribution. The average areas calculated were therefore the means of the logarithms of the measured areas.

Where multi-load-level testing had been done (e.g. St,S1,DS1 and DS2) the logarithms of measured DBAs are presented graphically versus load. Plotting adjusted failure load gave as before a much higher correlation coefficient. There is no theoretical basis for plotting either area or log(area) on the y-axis. Log(area) was chosen for the graphs shown here purely on statistical grounds.

4.2.1 Effect on DBA of varying time at load per cycle for Static and Rectangular Wave Tests St, R1, R2, R3 and R4

It was possible to compare the DBA at failure of the specimens tested in rectangular wave tests (R1, R2, R3 and R4) with the DBA resulting from the static tests at the 4.6kN level. The following table gives the means and standard deviations of each group of log (areas).

Load Regime Code	St	R1	R2	R3	R4
Mean	2.675	2.811	2.891	2.868	2.975
SD	.1351	.1525	.1074	.0863	.1718

The 3 régimes which incorporate elements of both static and cyclic loading, R1, R2 and R3, all have quite similar mean log(areas) and are grouped between St and R4, (the sawtooth waveform). Three 2-sided 2-sample t-tests revealed that the null hypothesis, that no difference existed between any pair (R1-R2, R2-R3, R3-R1) could not be rejected. These three sets of data were therefore pooled and the new mean and S.D. calculated.

Code	St	R1 R2 R3 pooled R_p	R4
Mean	2.675	2.860	2.974
SD	.1351	.1177	.1718

Two further tests established that the static areas were significantly smaller than the pooled sets, which in turn were significantly smaller than R4. The sets R1, R2 and R3 could be considered to lie in the transition region between static and fatigue failure.

4.2.2 Confirmation of a DBA-applied load relationship and comparison of static (St) and low frequency sinewave (S1) tests

A qualitative difference in DBA had been observed between static specimens tested at high loads and those tested at low loads. Large DBAs at high loads were found to be a general trend for St and S1. Log(areas) were plotted against load, and gave a significant linear correlation. Fig. 4.7a) shows the graph for static specimens, and the increase in DBA with load is evident. This implies that in low load level tests fibres are more severely degraded.

The log(areas) from the low-frequency sine-wave test, plotted against the maximum load, are superimposed over the static log(area) graph in Fig. 4.7b). The debonded area in the S1 test is larger than the DBA resulting from static testing at the mean load, for all load values. This difference was shown to be significant at the 1% level by the comparison of slopes and displacements test, described in section 3.1.1 (see also the Appendix). This implies that more damage to the fibre-matrix bond in the form of roving debonding, is introduced by the S1 loading than by static loading at a load equivalent to the mean load of the cyclic test. Referring to the mechanical test results for the 2 regimes it has been shown in Fig. 3.10 that the time to failure under regime S1 is shorter than that under static loading. The larger DBA in S1 may be contributory factor.

4.2.3 1 Hz Tests : DS1, DS2 and S2

The effect on DBA of altering 2 variables: size of alternating load and environment, could be investigated from the measurements made on the specimens tested at 1Hz. These will be described in turn.

i) Size of alternating load

Log(areas) from tests DS1 and DS2 were compared to ascertain if there was a significant variation in DBA between the mean load $\pm$20% cycling of DS1 and the 0-tension cycling of DS2. The values of log(area), for each of the tests, vs. adjusted load were plotted on the same

graph, Fig 4.8. The 0-tension points can be seen to be displaced towards higher areas than the $\pm$20% points, however there is a degree of overlap. The comparison of slope and displacement test was performed to check if there was a significant separation between the sets of points. It emerged that the displacement was very highly significant, despite the overlap.

Higher alternating loads therefore cause larger amounts of roving debonding.

ii) Environment

Results from tests DS2 and S2 were compared to show the effect of water on the DBA in 0-tension 1Hz tests. The wet fatigue tests, S2, were done at only one load level so a statistical analysis of the type in i) above was not possible. Also, that load level was lower than any of the levels in DS2 - so a t-test was not possible either. The results for both sets are presented graphically in Fig. 4.9, as before, but the regression line and 95% prediction interval for the DS2 data have been added. Seven out of the eight points comprising the S2 data lie inside the 95% prediction interval and 4 of those 7 are above the regression line through the DS2 points. It therefore seems likely that the 'wet' DBA is the same as that which would be expected in a dry test at the same load level. This would imply that environment does not have an influence on DBA in these high frequency, 0-tension cyclic tests. Although DBA is the same for wet tests their lifetime was shown in Chapter 3 to be shorter.

4.2.4 DBA measurements during tests coded DS1

DBA measurements were made on each of the micrographs taken during the lower alternating load fatigue tests at 1Hz, DS1, shown earlier as Fig. 4.5. This enabled graphs of area against cycles to be plotted. The graph in Fig. 4.10 for one specimen tested up to the maximum load of 7.2kN, best shows the general shape. After the initial rapid growth of white area up to about 10% life, the growth rate slows and remains practically constant between 10% and 90% life. During the last few seconds of life DBA grows very rapidly. It was not possible to do in-test DBA measurements on any series of pictures from tests under other load régimes, since for the DS2 tests there was poor constrast between debonded and non-debonded areas, and for the wet tests there was a very indistinct whitened area prior to failure.

4.2.5 Summary and additional comments on results of DBA measurements

The qualitative variation of DBA with applied load was able to be substantiated graphically. The driving force for debonding must be applied load and one would expect the rate of growth of debonding to be dependent on applied load. The slope of the linear portion of Fig 4.10 would therefore be steeper for higher applied loads. Debonding would continue to grow at the same rate until all the available interface had been consumed or, as in the situation here, the warp rovings became too weak to support the load. The small areas of debonding measured on specimens tested at low applied loads are a

result of a low rate of interfacial damage growth and a large reduction in the strength of the warp rovings. The situation is further complicated by the imposition of fatigue cycles. In all cases examined the higher the fatigue content of the regime, the more extensive was the debonding. ("Higher fatigue content" can be taken to mean a greater alternating stress, higher frequency or shorter time between unload cycles.) Cyclic loading is thought to raise the rate of delamination. Whether it also influnces the way in which fibres fail will be examined later.

4.3 Optical Examination of Failed Specimens

4.3.1 Static and rectangular wave loading St,R1,R2,R3 and R4

Failed specimens from the 4.63kN load level were examined with the naked eye and through a low power microscope. The frequency of observation of particular features was noted and the results are summarised in tabular form in Table 8. The column headings are clarified as follows:

i) Secondary damage sites are areas away from the final failure location showing damage in the form of intense whitening which may be the early stages of roving debonding. There were usually accompanying gel coat cracks. Three secondary damage sites was used as an arbitrary divide between small numbers of sites and more widespread secondary damage.

ii) Gelcoat resin cracks are cracks in the outer layers of the specimen, probably in both CSM and resin gel coat. They occur invariably at the edges of the specimen always at the point where a weft roving crosses a warp roving.

iii) Dimpling refers to the permanent deformation of the composite surface as a result of the straightening of the warp rovings under the applied tensile load. With time the warp roving crimp disappears, the weft rovings are pushed outwards and small surface mounds result in the position of the weft rovings. An example of permanent dimpling in a failed specimen is shown in Fig 4.11. The dimpling effect was also observed during the 0-tension dry fatigue tests but only during the loaded portion of each cycle.

iv) Whitening due to water refers to debonding at CSM-resin interfaces, similar to the type observed on water uptake specimens immersed under zero-load, i.e. general whitening around CSM strands irrespective of their direction with respect to applied load. Some WR whitening was observed but only on specimens which had spent the longest lengths of time at load in the aqueous environment.

v) Position of warp failure with respect to weft roving relates to the position of the break in the warp rovings relative to the weft roving crossing them. Two loci were defined; a) where the failure had occurred in the central third of the length of the warp roving crossed by the weft, b) where the fracture occurred outside the central third. These failure loci are shown in Fig. 4.12. A third

category, c) is shown on the table for those rovings where the failure locus was spread across the whole of the length of warp roving at the cross.

The information in each column will be discussed in turn.

a) Secondary damage sites It can be seen that as more unloading cycles are introduced per unit of time at load, the number of specimens where none of these sites was found decreases, and the number of specimens with 1-3 and >3 damage sites increases. It might be expected that R4 should have a large number of specimens with more than 3 damage sites, following the trend in the preceeding load regimes, however, this is not the case. There are, in addition, two specimens from the R4 set with no secondary sites.

b) Gelcoat resin cracks Resin cracks accompanied the whitened areas and these show a similar trend. There are significant increases in their frequency moving from R1 to R2 and from R2 to R3. The increase from R3 to R4 is less.

c) Dimpling Dimples were only found on half the specimens in groups St and R1, and then only on those whose times at load to failure were in excess of about 10^6 secs. These permanent dimples are evidence that resin creep has occurred. On the static specimens only, dimpling and resin cracking were never found on the same specimen. A situation exists for the static specimens where resin cracking predominates at short times to failure, and resin creep occurs at

long test times. This distinction was not found for R1 and R2 tests.

With respect to secondary damage sites, resin cracks and incidence of dimpling, R1 failures ressembled St failures more closely than failures from other rectangular régimes.

d) Whitening due to water The only variation in the extent of whitening due to water was with test duration - there was more whitening at longer times. Two long-duration static tests showed some attack at the WR-resin interface whereas on the other specimens only the CSM-resin interfaces were affected.

e) Position of fibre failures Failures in the middle third of the crossover length (type a) were consistently most numerous for all loading régimes, (except R1). If failures were random, one would expect the frequency of failures in the outer two thirds to be twice that in the central third. Instead the "type a)" failures are up to 4 times more frequent than the "type b)" The frequency of "type a)" failures for static specimens at 4.6kN was compared to that for static specimens from the 4.1kN load level. The frequency dropped from 67% at 4.6kN to 33% at 4.1kN. The figure at the lower load level is that which would be expected from chance. Clearly there is some mechanism operating at higher loads and under cyclic loading which tends to cause failures preferentially in the centre of the roving cross-over.

4.3.2 Sinusoidal loading regimes

No distinct differences emerged beween the two higher frequency dry tests, DS1 and DS2. Roughly equal proportions of the specimens in each group had 1 - 3 and >3 damage sites per specimen. Neither group had any specimen without secondary damage sites. The numbers of resin cracks were also similar for both, averaging close to 11.5. The 1Hz tests in water, S2, resembled those on the dry specimens in respect of the distribution of secondary damage sites. However there was a slightly higher level of resin cracking than in the dry tests, averaging 19 per specimen.

There is a similarity in the occurrence of secondary damage sites and resin cracks between rectangular regimes R3 and R4 and the higher frequency, S2, tests. Failures at 1Hz must be attributable to fatigue, so these similarities would support the hypothesis that R3 and R4 failures are also due to fatigue.

For high frequency tests the locus of warp roving failure was in the central third (zone a) on between 70 - 80% of all occasions. This is higher than the incidence for static and rectangular load variations. Where there were long WR pull-outs the warp rovings had still broken in the central third of a crossover, but in one lying further away from where the outer layers had separated. An example of such a failure is given in Fig. 4.13.

At the low frequency, S1, the specimens still showed more characteristics of fatigue than static failure. There were, on average, 3 secondary damage sites per specimen and 3 resin cracks per specimen. Warp rovings failed predominantly in the central third of the cross-over again. No dimples were found on any sinusoidally loaded specimen.

4.4 SEM Observations

It was not possible to examine as many specimens in the SEM as had been done optically. Specimens were selected from a few loading régimes - St,R1,R2,R3,R4 and S2 - to try to isolate the features on the fracture surfaces resulting from the individual conditions. The fracture surface of each specimen could be divided into 2 parts - i) that due to the crack in the resin gel coat and CSM layer, and ii) that due to warp roving failure.

4.4.1 Failure of CSM layer and gelcoat

The origin of the crack could be traced from lines on the resin surface. These hackle lines, which indicate that the crack was propagating quickly, fan out from its origin. Near the origin of the crack the hackle lines are no longer visible, since here the crack growth rate was slow. For those specimens where the warp roving fracture occurred in the central third of the cross-over, the outer layer crack appeared to have started from debonding in the weft, (transverse), roving and propagated both outwards and across the

width of the specimen in the CSM layer. It was not possible to pinpoint the origin of the weft debonding within the weft roving. The propagation of the crack through the CSM is evidenced in Fig. 4.14. The crack's progress is deviated and decelerated by the CSM strands. It travels with greatest velocity through resin-rich areas, e.g. the gelcoat, as was shown by the deep corrugations of the hackle there. Once the crack reaches the gel coat it propagates undeviated across the specimen's width. It can then turn back into the CSM layer as can also be seen in Fig. 4.14. The gel coat is obviously detrimental to life of the specimen at high loads since it provides an easy pathway for crack propagation.

Occasionally, on those specimens where warp roving fracture occurred outside the central third of the cross-over, the CSM fracture did not start from the weft rovings but from around a warp roving. Such a failure is shown in Fig. 4.15. The resin crack is initiated from 3 locations, all of which lie on the edge of a part of the warp roving. There are very short fibre pull-outs in this initiation area. Flat fracture surfaces with a small degree of fibre pull-out are usually indicative of fibres weakened by stress corrosion.

No differences in the general form of the fracture of the outer layers were found between static and cyclic tests. The only variations in failure mode between specimens tested under different loading régimes, that could be detected by S.E. microscopy, were in the form of fracture of the individual fibres.

4.4.2 Failures of fibres in warp rovings

In-test microscopy using the endoscope had shown that the area debonded at failure was smallest where the pre-failure damage had been initiated. This observation was used in the SEM work to differentiate between rovings which had failed first, due to accumulation of damage introduced by the type of loading, and those which failed during the final stages of the test, from overloading. Groups of about 50 fibre ends were examined, in different warp rovings across each specimen.

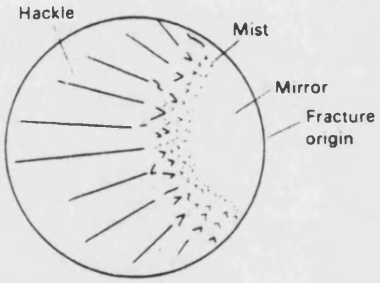

Three fracture zones are usually visible on the fracture surface of a glass rod. They are the mirror, mist and hackle zones. The mirror zone is a smooth, planar area, marking a region of slow, sub-critical crack growth. When the crack reaches a certain length, the remaining material can no longer support the applied load and the rod fails catastrophically. The radius of the mirror zone c, is directly related to the failure stress, σ_b by the following equation

$$\sigma_b^2 c = \text{constant.}$$

This relationship has been shown to apply also to the failure of glass fibres[55].

Those fibres where no mirror and mist regions are visible are those which have failed under a relatively high applied stress, consistent with failure due to overloading in a late stage of specimen life. It was possible to see a gradual decrease in the mirror zone radius on fibres from those at the initiation site across the width of the specimen to those in the final fracture area on some specimens.

4.4.3 Influence of loading regime on fibre fracture appearance

When the fibre fractures in the roving closest to the initiation edge were studied a trend was observed. For static specimens loaded to 4.6kN no mirror zones could be found on any fibre end. A typical fibre is depicted in Fig. 4.16a. As the cyclic content of the régime increased, so did the radius of the mirror zone, until fibre ends like that shown in Fig. 4.16c) were found in large numbers on a specimen from régime R3. Small mirror zones on fibres from static specimens loaded to the lower level of 4.1kN were seen, however. The load supported by the fibres in this more lightly loaded static specimen would be proportionately less than those in the 4.6kN static specimen. Therefore, more slow crack growth due to stress corrosion processes would be possible before the critical crack length was reached. It would be reasonable to assume that fibres from the rectangular régime specimens also failed at a lower load than ones from an equivalent position on the 4.6kN static specimens. It would

appear that the fibre failure load in the initiation region on rectangular régime specimens becomes progressively less as the cyclic content of the régime increases. A possible mechanism will be described in the next chapter.

From the trend described above, it would be expected that fibres in the initiation zone of an R4 specimen would all have completely smooth ends. The fibres whose fracture surfaces were perpendicular to their length did have smooth ends. However, a large number of fibres - over 60% had highly irregular fractures, having facetted appearance. An example is shown in the centre of Fig. 4.17. Some ends had fragmented as shown by another fibre in the same micrograph. Facetted ends are essentially fragmented ends where the chips of glass have been lost from the fracture site. Some fibres on the R3 specimen had failed in this manner but these were relatively few in number. As the frequency of unloads was increased the incidence of secondary fibre breaks increased. Hardly any of these fibre breaks were found on the R1 specimen for instance, whereas they became much more numerous after loading under régime R3. An example from an R3 specimen is shown in Fig. 4.18a. It was very noticeable that when no element of static load was included in the cycling i.e. in regime R4, the form of the fibre breaks away from the fibre end changed dramatically. Instead of the neat fracture with the line of break perpendicular to the sides of the fibre shown in Fig. 4.18a, fractures in régime R4 consisted of as many as 4 breaks locally on the fibre (over a distance of 20μm). The breaks followed an irregular course across the fibre. The form and spacing of these is

shown in Fig. 4.18b. This photograph also shows extensive resin cracking accompanying the break up of the fibres. This form of damage was found only on the R4 specimen.

When the ends of fibres broken in the 1Hz test in water (S2) were examined in the SEM, a very low proportion of the facetted breaks were observed (less than 5%). Just under half the fibres were broken perpendicularly, their fracture surfaces showing, almost exclusively, hackle lines. The largest proportion (about 50%) of the fibres had very unusual fractures, examples of which are shown in Fig. 4.19, the fracture starts perpendicular to the fibre's length but before the crack reaches the opposite side, its path deviates to being almost parallel to the side of the fibre. The crack then returns to running perpendicular, whereafter it soon reaches the edge of the fibre. The two corresponding sides of this type of fracture shown in Fig. 4.19 indicate that no crack branching has occurred. Crack branching would be expected if only form 'a' had been found. This type of lipped fracture was found on the static, R2 and R3 specimens, but very infrequently.

4.5 Summary of Observations on Damage Development

1. A variation in the extent of WR debonding was found across the width of virtually every specimen, irrespective of loading régime. For those specimens photographed during testing, the low debonding side of the specimen at failure corresponded to that side where damage had been observed prior to failure.

2. No coincidence was found between the failure loads and any pre-existent resolvable voids.

3. The debonded area at failure was greater on specimens tested at higher loads and under régimes with a larger cyclic element or with larger alternating stresses.

4. Cracking in the gel coat and CSM layers was more prevalent in those régimes having a larger cyclic element.

5. With respect to secondary damage site occurrence, resin cracks per specimen and the incidence of dimpling, R1 failures show greater resemblance to St failures than other rectangular régime failures; R3 and R4 are more similar to the specimens tested at higher frequencies whilst those from load régime R2 show features of both static and cyclic tests.

6. There was a larger proportion of failures in the central third of the WR crossover in higher frequency régimes. A comparison between 2 sets of static specimens showed that for the lower load level, failures in the central third were found half as often.

7. For static tests, mirror zones were observed on fibre ends in failures at 4.1kN but not in failures at 4.63kN. Mirror zones on fibre ends were larger on specimens from rectangular load régimes with a higher element of cyclic loading. (Except R4 - see 9)

8. For rectangular régimes, the number of secondary fibre breaks increased as the unloading frequency increased.

9. R4 represented an anomaly:- fracture surfaces of individual fibres were not smooth as might have been expected (see 7) but took on a facetted appearance. Secondary fibre fractures were non-planar and often closely spaced.

10. Specimens from S2 tests had a high proportion of lipped fracture fibre ends compared to any other régime.

5 Mechanisms of Failure

In this chapter possible failure mechanisms will be proposed based on the results given in the previous 2 chapters. It is necessary to consider the effect on a WR-containing composite of applying an initially small, but steadily increasing, tensile load in the warp direction before going on to more involved instances.

5.1 Monotonically increasing load and a model of warp roving straightening

Fig. 5.1 shows the initial degree of curvature of the warp rovings, and the relative position of the weft rovings. In Fig. 5.2 a small tensile load has been applied. The effect of this is to straighten the warp rovings, this has two effects on the weft rovings: i) they are pushed outwards and made to kink more markedly; and ii) they are subjected to a higher stress and strain in the load direction than would exist in a 90° lamina of an unwoven 0°/90° laminate. As a result of this higher stress perpendicular to the fibres in the weft roving, transverse fibre debonds are expected at lower applied loads than in a non-woven composite. It is possible to model the straightening of the warp roving and obtain an estimate of the proportion of the load carried by the weft rovings.

The form of the undulating roving in Fig. 5.1 is sinusoidal, however for simplicity it has been modelled as a series of arcs. This is shown diagramatically in Fig. 5.3. The arc AB represents the section

of warp roving between the centre of the warp-weft crossover (at A) and the point between that crossover and the next (at B). The arc AB is divided into small elements each of length δs. To obtain the total vertical deflection at B due to the force P, it is necessary to integrate the expression for the deflection resulting from moment M acting on one element. The expression is:-

$$\text{deflection} = \frac{1}{EI}\int Mx\,ds \qquad (10)$$

from Ref. 56

where E = elastic modulus

I = 2nd. moment of area of the roving cross section

Now, $M = Px$

$x = R(\cos\theta - \cos\phi)$

and $ds = -Rd\theta$

Substituting for M, x and ds in Eq. 10 we arrive at

$$\text{deflection} = \frac{-PR^3}{EI}\int (\cos\theta - \cos\phi)^2\, d\theta \qquad (11)$$

If this integral is evaluated between θ values of ϕ and 0 we obtain an expression for the total deflection at B, which is

$$\text{total deflection, } D = \frac{PR^3}{EI}\left(\phi + \frac{\phi\cos 2\phi}{2} - \frac{3}{4}\sin 2\phi\right) \qquad (12)$$

If values of R, ϕ and I for the test woven roving are inserted in equation 12, the deflection for a given load, $\frac{D}{P} = \frac{8500}{E}$.

The $\frac{D}{P}$ ratio for a straight roving of the same cross sectional area is only $\frac{3300}{E}$. These calculations show that the straight roving is just over 2.5 times stiffer than the kinked one.

A quick calculation using the "rule of mixtures"[57] shows that the transverse rovings in the woven composite are holding twice the load of their counterparts in a non-woven composite. As a consequence, a higher proportion of the load will be supported by the weft rovings transverse to the applied load, as compared to a composite where the fibres in the load direction are straight.

It might be possible to develop a similar expression for the deflection in the horizontal direction and for the force acting along AO to towards O. It is this latter force which pushes the weft rovings outwards. Such calculations are beyond the scope of this thesis, and the effects on warp and weft rovings of the increasing load can only be described in words.

Fig. 5.2 shows schematically the weft roving pushed outwards by the straightening of the warp roving and the resultant transverse fibre debonding. As the applied load increases transverse (weft) fibres become debonded as depicted in Fig. 5.2. until there are enough locally to join up and form a transverse crack. This spreads outwards towards the CSM and gelcoat. There is little opposition to the crack's progress in the CSM layer because its nominal glass volume fraction is half that of the WR layer and the proportion of

fibres in the load direction is low. The crack propagates rapidly to the outside through the unreinforced gel coat resin. Once a crack exists in the gel coat resin, (termed 'resin crack') it can spread widthwise across the specimen and has been found to turn back into the CSM layer, (this was shown in Fig. 4.14).

Once a transverse crack exists the warp roving is able to straighten more. This straightening is almost complete at the edges of the specimen where the end of the weft roving is free. In the interior warp roving straightening is resisted by continuous weft rovings. If the load is further increased gross cracks will spread across the whole width of the specimen on both faces so that the warp fibres of the WR layer are supporting the whole load. Once this situation prevails these warp rovings start to debond quickly. The origin of the shear stresses causing this debonding is shown in Fig. 5.4. Once the debonding has advanced further than the crossover where it first formed, the debonding proceeds between WR and CSM rather than between warp and weft. (The 2 pieces of the cracked weft roving were usually found to be completely detached, so they must at some point debond from the outer CSM layer as well.)

The interfacial debonding continues as long as the ratio of the applied tensile stress, σ_a, to the resulting interfacial shear stress, τ_a, i.e. $\frac{\sigma_a}{\tau_a}$ is less than the ratio of the corresponding strengths, $\frac{\sigma_*}{\tau_*}$. $\frac{\sigma_a}{\tau_a}$ will stay roughly constant as σ_a increases. σ_* will however decrease slightly as the debonded area (DBA)

increases because of the increased probability of failure associated with larger volumes of material. By this stage of the test the load-bearing warp rovings are completely straight and the resin which was transferring load from one fibre to the next is probably too damaged to perform properly so the rovings are essentially bundles of unsupported fibres. A small proportion of these fibres will be unable to support their share of the applied load once a serious flaw along their length has been exposed. The increasing applied load has to be shared between a decreasing number of intact fibres so final failure will rapidly result. An increase in modulus in the final stages is unlikely to be seen in practice because the final failure is thought to begin before the warp rovings have unkinked themselves over the entire length of the test coupon.

5.2 Static Loading

Consider the effect of holding the specimen at an intermediate load level, as is the case in a static stress rupture test. All the static tests were done above the level where transverse fibre debonding occurred on initial load-up. The initial configuration is therefore that depicted in Fig. 5.2 where the warp rovings are partially straightened and the transverse debonds are not sufficiently prevalent to give rise to a crack. There is a large stress in the direction of the applied load on the transverse roving and the constraints on warp roving straightening imposed by the weft rovings will be high.

5.2.1 Response of resin: dimpling or cracking

The formation of the dimpled surface on specimens and the failure of the composite under a static load can now be explained. The resin is a viscoelastic material and is susceptible to creep. With time plastic strain develops, which reduces the constraints imposed by the weft rovings on warp roving straightening. Elastic strain, which is recoverable, is accompanied by stresses acting to oppose the outward movement of the warp rovings. As the elastic strain is turned to plastic strain, which is non-recoverable, the restoring stresses reduce in magnitude. The warp rovings are able to straighten more as the constraints are removed with time. It is possible to reach a situation where, when the applied load is removed after a long period, the resin creep process has reduced the restoring stresses so much that the warp rovings remain straight, and the weft rovings remain pushed outwards, so that the surface of the specimen is distorted locally. This is the origin of dimples seen on the surface of long-life static specimens. Static specimens with lives less than $\sim 10^6$ seconds tended to form cracks before much dimpling had time to occur.

For the static specimens photographed during testing, it was possible in some cases to identify the eventual failure location by observation of a crack early in the test. Even at lower loads it is likely that several adjacent transverse debonds could join to produce a crack through the transverse roving. Water aids this debonding. In the stressed state water diffuses through the composite faster and

the quantity of water that can be held by the composite is greater than in the unstressed state. Water may be contained in the structure particularly in damaged areas e.g. in transverse debonds where a space is created. Glass is strongly hydrophilic and this is a reason why fibre-resin interfaces degrade even in the unstressed state. If bulk water is contained in one transverse debond, the debond could act as a reservoir for water to diffuse on and attack other fibre-resin interfaces further towards the interior of the specimen. A resin crack in the outer layers would result in the same way as previously once transverse debonds had joined, despite constant rather than increasing load.

When a crack exists linking the warp roving to the bulk water of the environment, water has a much easier pathway to reach the stressed glass fibres of the roving than in the case where it has to diffuse through undamaged outer layers. So, where such a crack exists the roving is liable to fail both due to the presence of larger quantities of water and the stress concentration at the tip of the crack. The higher stress and the water both increase the probability that a particular fibre within the roving bundle will fail. When one fibre has failed the likelihood of others failing is increased because the average fibre stress on the remaining fibres capable of supporting the load is raised. The first fibres to fail are those close to the original transverse crack, in the roving which has had maximum exposure to the environment. These proposals follow from observations made of specimens during the tests. Stress corrosion which is generally viewed as the mechanism of fibre failure under these conditions will be discussed later.

The apparent lowering of the strength of an exposed roving might be expected to change the DBA around that roving since $\frac{\sigma_*}{\tau_*}$ would be lower than for other (undamaged) rovings. This is therefore a probable explanation for the smaller DBA around the roving at the initiation site for static and indeed all water-immersed specimens. The absence of a DBA variation in tensile-test specimens adds more weight to this explanation since presumably all the roving strands had approximately the same strength.

5.2.2 Failure of warp rovings

A higher than expected proportion of the warp rovings were noticed to have failed in the central third of the roving cross-overs. One reason for this lies in the geometry of the undulations of the warp rovings. In the model of warp roving straightening developed in a preceeding section the roving was treated as a series of arcs. This is not an accurate representation - the form of the kinked roving is sinusoidal. As such the radius of curvature of small sections of the roving between 2 nodes must vary, reaching a minimum at the antinodes before returning to infinity at the next node. The equation governing the straightening of a curved beam having initial radius of curvature R_o is as follows:

$$\frac{\sigma}{y} = E\left(\frac{1}{R_o} - \frac{1}{R}\right) \qquad (13)$$

Where σ = stress developed parallel to the neutral axis at a distance y from it

E = elastic modulus

R = new radius to which the beam is bent

If $R \rightarrow \infty$ i.e. the beam is straightened, $\sigma = \frac{yE}{R_o}$

If E and y are held constant, σ reaches a maximum at the point on the roving where R_o is minimised, i.e. in the centre of the cross-over. This explains why more rovings were found to have broken in this location.

5.3 Failure Under Cyclic Load

5.3.1 Resin Processes

Of the two components of the composite the resin is the more degraded by fatigue loading. Since glass does not exhibit any significant plastic deformation at ambient temperatures, the possibility of it showing any 'dynamic' fatigue (as opposed to static fatigue) must be extremely slight.

Resin fatigue damage manifests itself in the form of an increase in the number of resin cracks per specimen in those tested in cyclic regimes as compared to static. In the R4 regime, the 'saw tooth' waveform, the resin cracking was most extensive. In the R1 regime, having the slowest cycling rate, the resin cracking was still more extensive than in the static but there was evidence of dimpling, indicative of resin creep, whereas none was found on the R4

specimens. The above generalised observations point to the fact that creep damage and fatigue damage must be developing concurrently in the regimes R1 to R3 where the cycling is interrupted by periods of holding at maximum load. The effect of interrupted static and cyclic loading on the resin will be examined. For this resin creep under static load will have to be treated in a more quantitative manner. The response of the resin component of a composite under static load is modelled in a simplified way below.

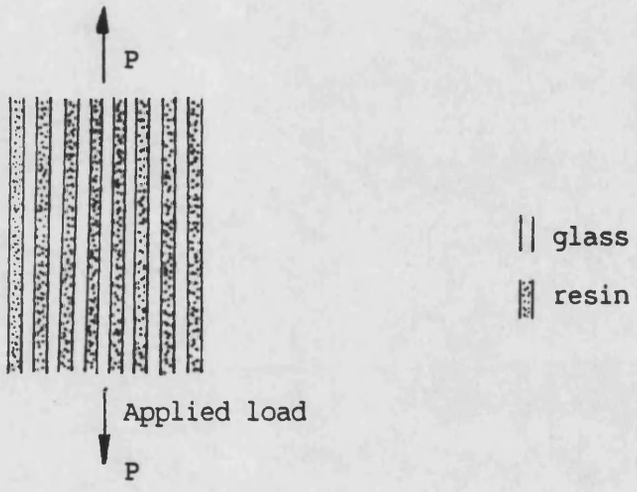

Initial conditions	At time t
t = 0	
Glass stress = σ_{go}	σ_g
" strain = ε_{go}	ε_g
Resin stress = σ_{ro}	σ_r
" strain = ε_{ro}	ε_r

Put $\sigma_{go} = \sigma_g$ so $\varepsilon_{go} = \varepsilon_g$ because we assume that no glass creep or stress relaxation occur at room temperature. Also $\varepsilon_g = \varepsilon_r = \varepsilon_{ro}$. Resin does undergo stress relaxation so $\sigma_{ro} \neq \sigma_r$.

The form of the variation of resin stress with time is

$$\sigma_r(t) = \sigma_{ro} e^{-t/\tau} \qquad (14)$$

where τ is the time constant of the exponential decay

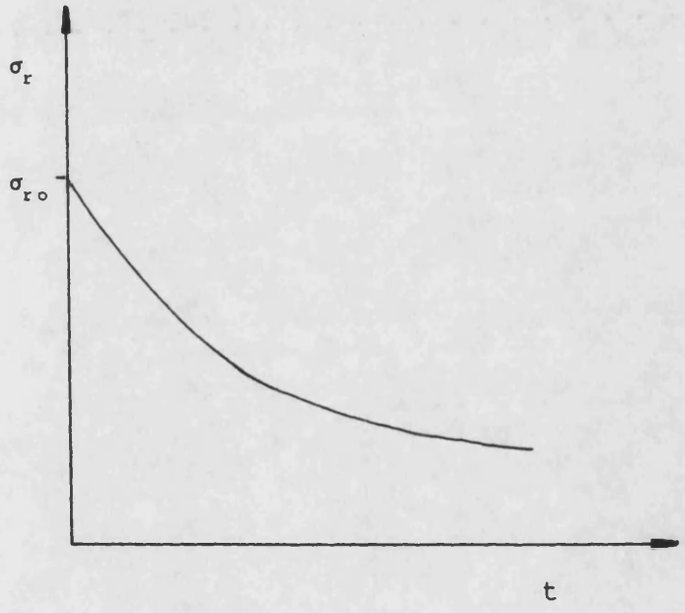

This would be the case if the resin strain were constant. This is approximately so for a unidirectional composite (glass-polyester, with 30% glass by volume) loaded in the fibre direction since (from the rule of mixtures) the fibres are carrying 92% of the load. If all the load carried by the resin were transferred to the glass the load on the fibres would increase by less than 10%. The resultant increase in glass strain would not make much difference to the resins viscoelastic behaviour.

For the woven roving composite examined in section 5.1 it was calculated that the curved warp roving was 2.5 times less stiff than a straight roving. From the rule of mixtures the modulus, E_c of a glass-polyester composite of 30% volume fraction glass, loaded parallel to the fibre direction is

$$E_{11} = E_{glass}V_f + E_{resin}(1-V_f) \qquad (15)$$

$$= 70 \times .3 + 3 \times .7 = 23\text{GPa}$$

The effective modulus of a curved roving of the same composite might be $23 \div 2.5 = 9.2$GPa. The modulus of the weft roving where loading is transverse to the fibre direction,

$$E = \frac{E_{glass}\, E_{resin}}{E_{glass}(1-V_f) + E_{resin}V_f} \qquad (16)$$

$$= \frac{70 \times 3}{70 \times .7 + 3 \times .3} = 4.2\text{GPa}$$

The resulting modulus of the woven composite is calculated using equation 15 to be 6.7GPa (assuming equal proportions of warp and weft). The measured modulus of actual specimens was 5.86 GPa. The figure of 30% volume fraction used in the calculations is believed to be approximately that local to the central WR layer in the specimens. The reasonable agreement is encouraging, despite ignoring any contribution to modulus from outer layers and constraints thought to be imposed on warp straightening by weft rovings. In this instance the 0° fibres of the warp strand are carrying only 62% of the total load, when stress relaxation of the resin cocurs the remaining 37% of

the applied load is transferred to the warp fibres. Their loading increases by a factor of 1.6. The increased load on the curved warp roving will cause it to straighten, thus increasing the strain in the resin by a large amount. The situation for the curved roving cannot be approximated to by the Maxwell model of equation 14 because $\frac{d\varepsilon}{dt} \neq 0$

It is possible to model viscoelastic behaviour where creep and stress relaxation are occurring simultaneously using a 'standard linear solid' approach[58]. The solution of the differential equation which contains $\frac{d\sigma}{dt}$ and $\frac{d\varepsilon}{dt}$ terms is also a decaying exponential of a similar form to that shown previously. It would be difficult to find values to insert into such a solution so any further explanations will make use of a sketch of the likely resin stress decay function. The effect of resin viscoelasticity on the fatigue damage sustained by the resin on each unloading cycle will now be examined.

If unloading cycles are introduced at intervals the resin stress will drop to near zero as the specimen is unloaded, and then return to approximately its original value. The stress range of every unloading cycle will vary according to the amount of stress relaxation that has been allowed to occur between unloading cycles. Fig. 5.5 shows the stress ranges of 10 unloading cycles for 2 frequencies of unloading. It can easily be seen from the 2 diagrams that more high stress range unloadings will occur in a test of frequency 2f than in a test of frequency f. The fatigue life of the resin must be shorter under high stress range fatigue than low. As

a consequence, more fatigue damage, in the form of resin cracks and breakdown of the resin glass interfaces, occurs in 10 cycles at frequency 2f than in 10 cycles at frequency f. The variation in fatigue damage after approximately the same number of fatigue cycles is shown by the relative amounts of cracking on R1, R2 and R3 specimens. In general the more frequently the specimens were unloaded the larger the number of cracks found.

The shorter the time at load during the life of the specimen, the smaller is the scope for resin viscoelastic effects to occur and, consequently, the more lightly stressed individual fibres will be in the moments shortly before the final failure. It might therefore be expected for the size of the mirror zones on the fibre fracture surfaces to be larger as a result.

5.3.2 The Effect of Resin Processes on Fibre Fracture

5.3.2.1 Appearance of the fracture surface

The radii of mirror zones on fibres in the initiation region of the specimens was indeed observed to increase with increasing frequency of unloads. This is thought to be a consequence of resin viscoelasticity, the drop in resin stress with time results in a

simultaneous increase in fibre stress. The more time available for resin stress relaxation before failure, the larger will be the stress on the fibres immediately before their failure i.e. the fibre failure stress, σ_{gf}.

$\sigma_{gf}^2 \propto \frac{1}{a}$ where a is the mirror zone radius[55]. (17)

Fibres having large mirror zones, e.g. those on R3 specimens, failed at a lower stress.

This would suggest that the decrease in mirror zone size was due entirely to the increase in fibre loading as the resin stress relaxes. The difference in mirror zone radius between say R1 and R3 was large - from roughly 1/4 of the fibre diameter for R1, to the whole fibre diameter for R3, which is a change of a factor of 4. To retain the proportionality of equation (17) the fibre stress in regime R1 must be twice that in regime R3. The approximate initial loading of resin and glass was calculated in a preceeding section to be 37% and 63% respectively, allowing the fibre stress, given complete resin relaxation to increase by a factor of only 1.6. In reality the mirror zone size change between static specimens, where total resin stress relaxation might be able to occur, and R3 specimens would be much larger than a factor of 4, because mirror zones on static specimens were too small to be visible in the SEM. This implies that the fibre stress on the R3 specimen must be a very small fraction of that in the initiation zone of a static specimen. Given this and the fact that the time available at load is shortened

progressively as more cycles are introduced and yet the mirror zones have been able to grow progressively larger, the fatigue loading must enhance the growth of the mirror zones in some way.

The absence of substantial plastic deformation in glass rules out any true dynamic fatigue failure of glass fibres. Their failure in an aqueous environment under load is accepted to be by stress corrosion. A possible influence of cyclic loading on stress corrosion will now be outlined. It is first necessary to consider what processes are important for sub-critical crack growth in glass and how such rate-controlling processes might be affected by cyclic loading. These are: transport of the environment to the crack tip; ion exchange at the crack tip and chemical reactions at the crack tip[59]. Transport of the environment - in particular H^+ and OH^- ions - is vital to the stress corrosion process. This can be a limiting factor, and is probably the factor which could be affected most. The rate of stress corrosion and therefore the rate of sub-critical crack growth will rise if transport of the reactive species to the crack tip is enhanced. It is conceivable that the products of the crack tip chemical reactions are forced out of the crack as the load is reduced and fresh liquid is sucked in as the load is reapplied. In fact during visual examination of immersed high frequency (i.e. 1 Hz) tests just such a pumping action was visible. The effect of an increasing quantity of reactive species on the crack velocity has been demonstrated by Wiederhorn. The graph below is reproduced from Ref. 59.

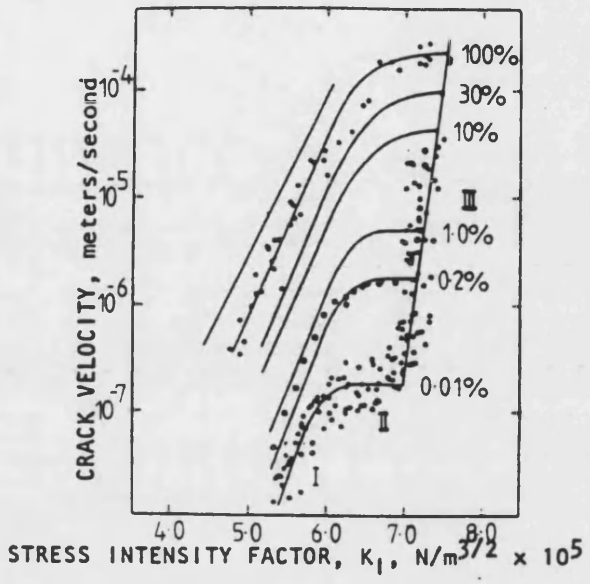

This data was actually obtained from measurements of the crack propagation rate in soda-lime-silicate glass in nitrogen gas with various relative humidities (RH). In regions I and II of the curves crack velocity is higher for higher RH. One theory for the breakage of bonds during stress corrosion involves the formation of activated complexes. The reaction rate for chemical reactions of this type will be higher if the concentration of the products is lowered and that of the reactants raised. If fibre stress corrosion is limited by transport of active species, this idea would explain quite well how a larger mirror zone could grow in a shorter time at a lower fibre stress in a high cyclic content régime.

However, the difference in mirror zone sizes between for instance R3 and static specimens was very large, too large to be accounted for by the calculated variation in fibre stresses. The relationship between mirror zone size and fibre failure stress is given in equation 17. The constant of proportionality in this equation is dependent on the stress intensity factor K_I,

$$\text{since } \sigma = \frac{K_I}{(2\pi a)^{1/2}} \qquad (18)$$

It might be possible that K_I is not constant from one régime to the next. There are 3 possible reasons why this could be so.

a) Wiederhorn shows that there is viscous drag between the walls of the crack and the entrant liquid when the crack tip is advancing quickly ($>10^{-1}$ m/s). This he suggests causes cavitation at the crack tip, a drop in pressure and a reduction in the stress intensity factor at the crack tip. The opening of the crack during the loading part of the cycle might cause a similar cavitation even though the actual growth rate might be orders of magnitude slower. For the régimes with larger elements of time at load it is thought that there would be ample time for the pressure to be equalised and K_I return to its higher value. For higher frequency loading where the loading rate is higher and time at the maximum load is very short this would become a more viable explanation.

b) For lower applied stresses the Charles-Hillig[60] theory shows that dissolution by stress corrosion changes the aspect ratio of the crack

tip such that K_I is lowered. The increased transport of water to and products from the crack tip area could lead to increased general dissolution close to and at the crack tip.

c) There is some evidence to suggest that limited crack tip plasticity can occur in glass[59]. This flow would also act to blunt the crack tip and thus lower K_I.
None of these ideas is particularly plausible however, and it is not certain whether K_I does vary or not at this stage.

5.3.2.2 Probability of Fracture

The behaviour of the resin under the fatigue load also affects the volume of fibres exposed to the environment and therefore their apparent strength. Two contrasting cases will be examined in what follows; failure under static load, and failure under a regime with a high cyclic element, e.g. R3.

In the static case the tendency is for resin creep to occur rather than resin cracking but a small crack can develop at the specimen's edge near the change of section where there is a slight stress concentration. In R3 large resin cracks will occur at several locations on the specimen. After a certain time (at load) into each test the situation is shown schematically in Fig. 5.6. Stress corrosion cracks are believed to start from 'type C' flaws on the surface of glass fibres[61]. The number of such flaws exposed to the water environment will be much greater in the high cyclic element

régime than the static one, because the area of interfacial damage in R3 is greater. The rovings in the damaged areas of R3 are less well supported by resin and the resin connecting individual fibres in the rovings may have been damaged by the fatigue cycles. This means that these areas are inherently weaker because load transfer from one fibre to another, the source of strength of composites, is prevented. Consequently the probability of fibre failure in R3 specimens where more matrix damage has been sustained is expected to be higher.

5.4 Control of life by cycles criterion above the boundary frequency

In Chapter 3, (section 3.2), the notion of the existence of 2 failure criteria, one based on time at load and the other based on cycles, was put forward. Low frequency rectangular wave tests were found to fail after a particular time under load, whereas high frequency tests failed when a certain number of cycles had been reached. The boundary frequency dividing these failure criteria was thought to be in the region of 1 cycle per 2 mins.

Having noted all the differences in fracture surface, resin cracking etc. which occurs between régimes of varying unloading frequency, it is difficult to account for the fact that specimens tested under régimes with frequencies in excess of the boundary frequency for example R3 and R4, failed after the same number of cycles. Evidence has been produced for the existence of certain processes which must act together to cause the eventual failure. These processes have been laid out in Fig. 5.7 in terms of how they change with the

balance of fatigue and creep elements in the rectangular regimes.

For the higher cyclic element régimes the damage to the matrix is higher so that larger volumes of unsupported fibres are exposed and access by reactive ions from the environment is greater, however the stress on the fibres and K_I are lower. Towards lower cyclic element régimes the smaller area of matrix damage produces a smaller volume of exposed fibres, higher resin creep throws more load onto the fibres and K_I is probably higher, but the reaction rate is limited by slower rates of water transport to the crack tip. A balance is struck between the damaging effects of fatigue on the matrix and beneficial ones (reduced fibre stress and K_I) so that failure is determined by the number of cycles.

5.5 Failures under low cyclic element loading régime, RO

No detailed study of the failed specimens was made, but they appeared, in general, to resemble static failures, as was expected. The cyclic content of this régime was so low that much resin stress relaxation between cycles could occur. There was little opportunity for the damage zone size to be raised above that for a static test, owing to the decreasing stress range of successive resin fatigue cycles. The probability of fibre failure by stress corrosion is effectively the same as in the static test, so failure results after an elapsed time at load. If the cyclic content of a loading régime is kept low enough so that the size of the whitened zone is not increased, the actual number of cycles will not affect the lifetime.

5.6 Failure in the saw-tooth regime, R4

The saw-tooth wave form differed from R1, R2 and R3 in that there was no element of static load. The pure fatigue loading resulted in gross damage to resin and resin-glass interfaces, since there could be little or no resin stress relaxation. The average area debonded at failure was twice that of the specimens tested statically at the maximum load. This would have a profound effect on the fibre failure rate. It is probable that some stress corrossion would occur in the portion of the fatigue cycle where the R4 specimens were highly stressed. However the probability of fibre failure is so great by virtue of the large damage zone, that the short time per cycle available for stress corrosion has no serious consequence.

If R4 did follow the same pattern of failure as R1, R2 and R3, it would be expected to show smooth fibre failures like the ones on R3. A certain number were found, but irregular fractures were far more common. It is difficult to explain these facetted and fragmented fibre ends. One explanation stems from the presence of large amounts of interfacial debonding between fibres and surrounding sheaths of resin. A fibre might be pulled a distance out of its sheath if it had already failed elsewhere in the large damage zone, and be unable to return once the load was removed because of frictional forces exerted by the sheath of resin. The extended fibre might then be subjected to bending and/or compression imposed by elastic recovery of the surrounding material. The ensuing stress state could be responsible for the change in fracture morphology. Multiple fibre

breaks are indicative of such a mechanism operating. These were found on R4 specimens.

5.7 Failures under sinusoidal loading

Sinusoidal loading can be treated in the same way as régimes R1, R2 and R3, except that whereas previously there were distinct elements of static and cyclic loading, the two types are now intimately mixed. The same tenets regarding resin stress relaxation etc. can be applied to explain the observed features of the fractures.

The larger whitened damage zone on failures in régime DS2, (0-tension, dry, 1Hz), compared to those from DS1, (mean $\pm$20% dry, 1Hz, maximum load identical to DS2), reflects the larger alternating component, (producing more matrix fatigue damage), and smaller mean stress, (reducing matrix stress relaxation), in DS2. Frequency will also determine to some extent how damaging the superimposed fatigue cycles are. However, as will be shown later, the effect of frequency is a function of the size of the alternating load and the average rate of load application.

To describe fatigue behaviour, 3 independent variables i.e. mean load, load amplitude and rate of load application, are required. The damage developed by cyclic loads at differing frequencies will probably be determined by the ratio of the load amplitude to the failure load (measured in a tensile test at a loading rate equivalent to the loading rate in fatigue). It is suggested that the principles

derived by Sims and Gladman[27] concerning rate of load application in fatigue, could be extended to cover sinusoidal loading as well as saw tooth. If so, the rate of load application is more important than frequency. At high load application rates the tensile failure load is higher, so that for a given load amplitude each cycle at high rate introduces less damage than a low load application rate cycle. The result is a larger number of cycles to failure under high load application rates. This was shown by results for R4 and S2 where although the load ranges were equal, S2 had a much higher loading rate and consequently its life was an order of magnitude longer. The 3 variables (mean load, load amplitude and average load application rate) will describe any sinusoidal load régime. A method of ascertaining the life under any régime will be set out in Chapter 6.

5.8 Further work on Failure Mechanisms

The phenomena described in the results chapters have been able to be only partially accounted for in the preceeding sections. There remains a vast quantity of work which could be done to provide essential data and more accurate models of the mechanisms of fibre and resin failure in combined creep and fatigue.

In particular, verification of the effects of periodic unloading on the resin alone would be of value, and give better information on how the stress range of the resin would drop after lengths of time at the maximum strain. A more accurate model of roving extension, perhaps

incorporating the sinusoidal geometry of the warp rovings, would be preferable - if rather complicated to develop.

Much of the explanation of microscopical variations in the fracture surfaces of fibres relies on circumstantial adaptation of the available literature to fit the unique situation here. This points further research in the direction of fracture mechanics of glass fibres in a corrosive environment under cyclic loads, to answer such questions as "Does K_I decrease due to viscous drag in fatigue?", or "Is K_I in fact constant after all?" and "Is there any significant crack tip plasticity in glass?"

6. Implications for Future GRP Design

In this chapter the findings of the mechanical tests detailed in chapter 3, are assessed in the light of the proposed mechanism of failure described in chapter 5. In particular, the implications of the existence of a boundary frequency dividing creep-dominated from fatigue-dominated behaviour will be discussed for periodic unloading. New philosophies for design under 3 types of loading régime will be proposed, based on the findings of this work. Finally the results obtained by Mandell and Meier[36] will be interpreted in the light of the existence of a boundary frequency.

6.1 Periodic Unloading (Rectangular Waveforms)

This load form combines static and cyclic loading such that blocks of static and cyclic loading are isolated in time. As the cyclic content of the load régime is increased, failure is determined by the number of unloading cycles and not the time at load. The boundary frequency appeared to lie close to the frequency of régime R1 (1 per 2 min) since at failure the time at load and cycles criteria were fulfilled simultaneously. Above the boundary frequency cyclic loading starts to influence failure.

Examination of failed specimens revealed a gradual increase in prevalence of certain characteristics of fatigue i.e. resin cracking and fibre-resin debonding as the component of cyclic loading increased. However the mechanism of final composite failure was

proposed to be essentially the same as under static conditions, namely stress corrosion of fibres. The effect of the imposed unloading cycles was thought to be a raising of the fibre failure probability coupled with enhancement of stress corrosion processes. In mechanistic terms, the boundary frequency can be defined as the frequency above which the interfacial damage produced by fatigue alters the failure probability of fibres under stress corrosion conditions, and above which fatigue enhanced stress corrosion occurs. The actual boundary frequency can be calculated from the average time at load to failure of specimens from St and R0, and the average cycles to failure of R2,R3 and R4. (R1 has been omitted from these calculations because of its likely proximity to the boundary frequency.) Given that time and cycles to failure are both lognormally distributed:-

Mean time at load to failure = $10^{\log t}$

where logt is the mean of the logarithms of the times at load to failure of all the specimens in régimes R0 and St:

Mean cycles to failure = $10^{\log N}$

where logN is the mean of the logarithms of the cycles to failure of all the specimens in régimes R2,R3 and R4.

By definition the boundary frequency,

$$f_b = \frac{10^{\log N}}{10^{\log t}} = 10^{(\log N - \log t)} \qquad (19)$$

Due to the wide scatter of the experimental results a value of f_b must be an estimate of the true value. It would therefore be more informative to quote, for instance, a band of frequencies where there is a 95% probability of the boundary frequency lying. In equation 19, f_b is expressed as 10 raised to a power. The exponent is the difference between two means. The confidence interval (CI) on the difference between two means can be evaluated from equation 20.

$$CI = |\bar{X}_1 - \bar{X}_2| \pm ts\sqrt{(1/n_1 + 1/n_2)} \qquad (20)$$

where $\bar{x}$ = sample mean

n = sample size

t = Student's t value, with n_1+n_2-2 degrees of freedom

s = combined standard deviation

$$= \sqrt{\frac{(n_1-1)s_1^2+(n_2-1)s_2^2}{(n_1-1)+(n_2-1)}} \qquad (21)$$

Now, the means and standard deviations of logN and logt are as follows:-

	logN	logt
mean	3.5817	5.8002
SD	0.68617	1.15845
n	39	20

and s was calculated to be 0.87248

Hence, the 95% confidence interval on $\log f_b$ is

$$-2.6983 < \log f_b < -1.7385$$

The corresponding limits on f_b are .0020 Hz to 0.0183 Hz i.e. 0.12cpm to 1.04cpm.

The most likely value of f_b is 0.36 cpm, (or approximately 1 cycle per 3 minutes). The frequency of régime R1 lies within the confidence band, but to the higher frequency end. This is the reason why no difference could be detected between R1 and St on a time to failure basis nor between R1 and the higher frequency tests on a cycles to failure basis. It is also expected that the R1 frequency lay close to the boundary frequency at other load levels, since the stress vs log time regression lines for St and R1 were indistinguishable without the adjustment of failure load. Once a great proportion of the scatter about the 2 lines had been removed by adjusting the load values, a shortening of time at load to failure for R1 was detectable. This result is consistent with the frequency of R1 being towards the higher frequencies in the 95% confidence band.

This work has shown that there is a boundary frequency for intermittent cyclic loading to one particular load level, for rectangular wave loading with a specific rate of load application (RLA). If the boundary frequency could be derived for any load level and RLA it would be of great value to the designer. If the rectangular wave load variation in service were at a frequency below f_b, the structure could be designed purely on creep: if the frequency were above f_b, only the number of cycles to failure to be endured would need to be taken into account. This is important since it shows that the BS4994 approach is not correct for periodic unloading.

The necessary data to derive f_b are the time to failure under continuous static load at load level P, and the cycles to failure in saw-toothed loading from zero load to load P at the required RLA. The first piece of data is readily available since substantial information exists regarding the environmental stress rupture performance of composites of interest to the CEGB. Much mechanical testing is required to establish the life-time under saw-tooth wave fatigue with varying loading rates, in an aqueous environment. (It would be possible to conduct such tests in the fatigue tank designed for this project.) The amount of testing needed could be lessened if it could be shown that the normalisation procedure described by Sims and Gladman[27] held at the low loading rates equivalent to the pressure changes within CW systems. In their treatment, the fatigue strength for saw-tooth wave loading is normalised by dividing by the tensile strength measured at the same loading rate. Once a fatigue "master" curve is known, the fatigue life for the relevant RLA can be obtained provided the tensile strength at the RLA of interest is available. If this treatment is possible it will reduce testing time and cost. Given the extremely low frequency of complete unloads in service, (depressurisations of the CW system occur at intervals greater than 2 months), the life of the component is more likely to be controlled by the stress rupture at the static load, rather than the number of fatigue cycles. If this is proven to be the case by future testing periodic unloads could be ignored for design purposes.

6.2 Sinusoidal Loading

The situation for sinusoidal loading is necessarily more complicated since at no time in the cycle is the specimen subjected to pure static loading. The degree of fatigue enhancement will depend on the 3 variables, mean load, load amplitude and average rate of load application, as described at the end of Chapter 5. In the limit, where the alternating load is low, the life, when given as time to failure, will approach that under static loading at the mean load. As the alternating load increases the degree of fatigue enhancement is magnified, and time to failure deviates more and more from the static. Because at no time is the loading purely static, the concept of a boundary frequency does not apply to sinusoidal loading. It would be better to design entirely on a fatigue basis for sinusoidal loading. The most readily interpretable form of presenting such fatigue data is a master diagram. Master diagrams were described in section 1.3.2 and an example reproduced in Fig. 1.1. It might be possible to normalise load in a similar way to that proposed for saw-toothed wave form. Although the RLA varies continuously during the cycle an average rate could be used which corresponded to the slope of a line joining one minimum (load) to the next maximum (load) of the sine wave. The alternating load on the master diagram would be plotted in an analogous manner to the fatigue strength for the sawtooth fatigue master curve. From such a diagram the fatigue life under sinusoidal loading at any RLA with any mean load-alternating load combination could be ascertained. The diagram, with normalised alternating load axis, would be expected to be similar to published

diagrams for tests at a single frequency. A sketch of such a diagram is shown in Fig. 6.1.

The unit alternating load + failure load at the required RLA along the vertical axis is dependent on alternating load and RLA. Both may be varied independently of the other. The effect of altering each will be examined with respect to the position of a point on the 10^4 cycles contour of Fig. 6.1.

Case i) Suppose that the point on the 10^4 cycles contour in Fig. 6.1 represents the lifetime of waveform 1 in Fig. 6.2 a). If load amplitude is increased while maintaining the same RLA the frequency of the new waveform (2) is lowered. Since load amplitude increases and failure load stays constant, the alternating load + failure load ratio is raised. The point on Fig. 6.1 moves upwards towards lower lives.

Case ii) The 10^4 cycles contour point now represents the lifetime under waveform 1 in Fig 6.2b. If load amplitude is kept constant and RLA increased to that in waveform 2, (the frequency is forced up), the alternating load failure load ratio decreases. The failure load is higher for greater RLAs. The point on Fig 6.1 now moves downwards, i.e. towards longer lives.

The quantity of fatigue enhancement depends on the alternating load: failure load ratio. This ratio could prove to be useful in design, to assess the fatigue life of the material under any sinusoidal waveform. However, its applicability to sinusoidal loading has not been fully verified. A lengthy data acquisition exercise is

necessary to establish this and construct such a diagram. This was outside the scope of this work.

6.3 Periodic Spike Overloads

In service GRP structures are often subject to pressure surges, caused by, for instance, valves opening or closing in the system. A generalised form of the load variation with time is shown in Fig. 6.3. The maximum load P_1 is approximately three times P_o, the normal service load. At present structures for CEGB applications are designed as if the structure were required to withstand load P_1 throughout its life. This can give rise to safety factors as large as 60 on normal service loading. A new proposal for design under these conditions will now be put forward, based on the treatment suggested for periodic unloading. (see 6.1)

As was the case in periodic unloading the amalgamation of static and cyclic elements is such that the elements of static and cyclic loading are separable in time. For periodic unloading a boundary frequency, f_b, was found to exist. It is assumed that such a frequency also exists for this load type. The design philosophy is therefore directly analogous to that put forward for periodic unloading.

It is possible to estimate a value for f_b for levels of P_o and P_1 around which tests could be conducted in the future for verification. As before, the information needed is i) the life under static load at

P_o and ii) the cycles to failure under saw tooth loading between Po and P_1. The life under constant load can be found from the stress rupture curve for any load level by extrapolation. In the absence of fatigue information the cycles to failure in régime R4 could be taken as an estimate of the fatigue life in a saw-tooth mode where P_1 = 4.63kN, P_o = 1.54kN (i.e. P_1/P_o = 3) and the period equals that of R4.

So, fatigue life N_f ≅4700 cycles

creep rupture life $t_f = 9 \times 10^9$ seconds at P_o = 1.54kN, i.e. 17% UTUL.

$$f_b = \frac{N_f}{t_f} = 5.3 \times 10^{-7} \text{Hz}$$

i.e. .05 cycles per day or 9 cycles per 4 weeks

In the absence of any other data is is not possible to estimate f_b for service conditions, however it is likely to be of the order of 10 cycles per month. Spike overloads occur more frequently than this in service, so the life is expected to be controlled by the cyclic overloads.

Finally, once design data has been acquired to cover low frequency cyclic loading it may be possible to rank types of cyclic load in order of the damage they produce in the structure.

A possible order is as follows:

Spike overloads are more damaging than normal service loading.

Normal service loading is more damaging than periodic unloading.

It may then be possible that designing for the worst cyclic condition will be adequate to cover the effects of all less destructive régimes.

6.4 Re-examination of the results of Mandell and Meier

Having now established the existence of the boundary frequency, Mandell and Meiers results outlined in section 1.3.4 will now be re-examined. The boundary frequency is by definition where failure due to cyclic and static loading occurs simultaneously. From fig. 1.4 this is estimated to be 0.1Hz at around 340MPa. The 2 diagrams (figs. 1.4 and 1.5) were produced from tests on different batches of material which had different strengths, so information from one may not transfer to the other accurately. Nevertheless at the frequency of 0.1Hz it might be expected that failures start to be controlled by time at stress somewhere near 340MPa. Since some overlap might be expected where both criteria were fulfilled together cyclic failures should become detectable below 200MPa. Turning to fig. 1.5: at the stress level of 310MPa expected to be just within the time at load controlled region, square wave and spike unloading have similar lives but the spike loading gives a longer cyclic life. If the time at load per cycle for square wave and spike unloading were the same (not given by Mandell) the cumulative time at load would also be the same. The spike loading incorporates such a small time at the high load that failure occurs when the cycles criterion is satisfied. At lower

stresses the boundary frequency becomes much lower, so that the frequency of 0.1Hz will always be above it and failure is controlled by cycles. At low stress the cycles to failure of all three waveforms should be the same, no matter what time was spent at load. This convergence is definitely shown to happen for the spike loading and unloading but the square wave is still showing a slightly shorter life. There is insufficient data given to find out whether this life is significantly shorter. If the squarewave life at low stress is not significantly shorter then the existence of a boundary frequency will fully explain Mandell and Meier's results.

7. Overview

This thesis has shown that the BS4994 approach is not applicable to the design of pipework and valves etc. for power station cooling water systems. The multiplication of subfactors for creep and fatigue loading is a simple attempt to allow for combined static and cyclic loading and represents the case where the structure is weakened simultaneously by the 2 forms of loading. Tests where unloading cycles were incorporated into a static test ruled out this form of interaction between static and cyclic loading. No synergistic effects were found and the extent of degradation was no worse than that which would result from the more severe load regime acting alone. The failure criterion was determined by time at load below a boundary unloading frequency and by the number of cycles above it. Where a small number of unloading cycles (fewer than the cycles required for fatigue failure) were introduced this had no detectable effect on the time at load to failure. This is contrary to what had been expected from Bax's work where a small number of pre-loading cycles reduced the subsequent stress rupture life. This means that considering the very low frequency of CW system depressurisations the total number of such unloading cycles would not come near the cycles to failure, and depressurisations could be ignored.

High pressure spikes however might prove more damaging than normal service loading and these would need to be allowed for. High pressure spikes are random in terms of frequency and size so their effect on life would be difficult to quantify even if further tests

confirmed that they were more damaging than normal service loading. The simplest way of allowing for these would still be to apply a safety factor.

It was not possible to perform the large number of tests required to construct a master diagram for this material, besides which such diagrams are already in existence in the literature for similar materials. However combining a master diagram with Sims and Gladmans treatment of the effects of frequency on fatigue will provide a technique of estimating the fatigue life under any combination of alternating stress, mean stress and frequency. This is believed to be the simplest method and a fairly accurate one of allowing for low frequency tidal pressure variations.

During the course of this work other discoveries were made and techniques developed.

1. A large amount of scatter is inherent to fatigue and stress rupture tests on composites. A normalisation technique was developed whereby an estimate of the strength of individual test pieces could be made. This used the strength-life-equal-rank assumption. This made a vast improvement to the correlation coefficients of the regression lines without distorting the data. A refinement was also added so that information from load-up failures and run-outs could be added. The use of this adjustment method made the statistical tests for differences between sets of data more sensitive.

2. Novel observations of specimens during tests under water were possible with the endoscope. These showed the progression of damage

throughout the test, and, more importantly, showed where the first damage had formed so that this area could then be examined in greater detail after failure in the SEM.

3. Large numbers of failed specimens were examined so that any trends would become apparent. Specimens which had been tested in regimes with a larger fatigue content showed larger amounts of damage to the resin. Conversely specimens from regimes with a large element of static loading showed more weakening of fibres due to stress corrosion. More resin creep was also observed to occur in high static content regimes. The amounts of fatigue and static character in any test determined the balance between resin cracking and resin creep. The deformation mode of the resin was also thought to influence how the fibres failed and the probability of them failing.

4. An abnormally high proportion of warp rovings failed in the central third of the roving cross-overs. This follows from the sinusoidal shape of the warp rovings. When the curved roving is straightened, higher stresses are generated where the radius of curvature is smallest. This occurs at the centre of the cross-over. An attempt was made to model mathematically the straightening of the warp rovings. Although this model was not developed very far it did predict approximately the modulus of the material.

The mechanism of failure in low frequency fatigue tests in a water environment is seen as "fatigue-enhanced" stress corrosion. Owen was at least partly correct stating that damage due to stress rupture and fatigue in composites was similar. The work reported here has

highlighted some similarities in the types of damage, but the extent of each type does vary. The precise nature of the fatigue enhancement on a microscopic level is still uncertain, and what really happens at the tip of a crack in a glass fibre will probably remain unknown for a long time.

References

1. Wyatt, R.C., CEGB Report No. SSD/SW/77/N169.

2. Bryan-Brown, M.H. and Walker, D.M., CEGB Report No. SSD/SW/80/R352.

3. British Standard Specification BS.4994:1973, "Vessels and Tanks in Reinforced Plastics"

4. Boller, K.H., Forest Products Lab. Report No. 2039, Nov. 1955.

5. Steel, D.J., Trans.J. Plastics Inst. Oct. 1965, pp. 161-167.

6. Kabelka, J. Brit Plast. Fed. 5th Int. Reinf. Plast. Conf. Nov. 23-25 1966 Paper 17.

7. Bershtein, V.A. and Glikman, L.A., Soviet Physics - Solid State, Vol.5, No. 8. Feb. 1964, 1651-1656.

8. Dixon, R.H. Ramsey, B.W. and Usher, P., Royal Inst. of Naval Architects, Symposium on GRP Ship Construction, Oct. 1973, Paper 1.

9. Schumacher, G., Materialpruefung, vol. 10, no. 7, p.231-7.

10. Schumacher, G., Materialpruefung, vol. 10, no.3, 88-95.

11. Holland, N.H. and Turner, B.F., CEGB South West Region, Report No. RD/SW/R42, Jan. 1966.

12. Cameron, J.B., Plastics Inst. Trans. and J. vol.35, no.19 p681-7.

13. Goldfein, S., J. Appl. Polym. Sci., Vol. 10, 1966 pp.1737-1750.

14. Wright, D.C., RAPRA Confidential Technical Report 1908, Oct. 1975.

15. Beckwith, S.W., SAMPE Qtly, vol. 11, no.2 Jan.1980 pp.8-15.

16. Wyatt R.C., Norwood L.S., Phillips M.G., CEGB Report No. SSD/SW/N161.

17. Howe, R.J. and Owen, M.J., Brit. Plast. Fed., Reinf. Plast Group, 8th Int. Reinf. Plast. Conf. Oct.1972, Paper 21.

18. Smith, T.R. and Owen M.J., Brit. Plast. Fed. 6th Int. Reinf. Plast. Conf. London, 1968 Paper 27.

19. Dew-Hughes, D. and Way, J.L., Composites vol. 4 no. 4 July 1973, p.167-73.

20. Hahn, H.T. and Kim, R.Y., J.Comp. Mat. vol.10 Apr. 1976 pp156-80.

21. Agarwal, B.D. and Dally, J.W., J.Mat.Sci. vol.10 no.2 Feb.1975 pp.193-9.

22. Dharan, C.K.H., J. Mat.Sci., 10, 1975, p.1665-1670.

23. Talreja, R., 3rd. RISØ International Symposium on Metallurgy and Materials Science, 1982, Fatigue and creep in Composite Materials, pp.137-153.

24. Johnson, A.F., Engineering Design Properties of GRP, British Plastics Federation, 1979.

25. Boller, K.H., Modern Plastics, 34, June, 1967, p.163.

26. Smith T.R., and Owen, M.J., Modern Plastics vol. 46 no. 4 1969, p.124-5, 128-32.

27. Sims, G.D. and Gladman, D.G., Plastics and Rubber: Materials and Applications, May 1978, pp.41-48.

28. Broutman, L.J. and Sahu, S., 2nd. ASTM Conf. on Comp. Matls; Testing and Design, April 20-22, 1971, Anaheim, California.

29. Owen, M.J., Short Fibre Reinforced Composite Materials, ASTM STP 772, B.A. Saunders Ed., American Society for Testing and Materials, 1982, pp.64-84.

30. Boniface, L. and Bader, M.G., ECCMI, Bordeaux, 24-27 September 1985.

31. Lifshitz, J.M. and Rotem, A., J. Composite Materials, 4, Jan 1970, p.133.

32. Thebing, U. and Menges, G., SPI Reinf. Plast. Comp. Inst. 33rd Ann. Conf. Washington DC Feb. 1978, Section 20-E ppl.

33. Bax, J., Plastics and Polymers, Feb. 1970, vol.38, no.133, p27.

34. Sims, G.D. and Gladman, D.G., Plastics and Rubber: Materials and Applications, Aug. 1980, p.122-128.

35. Aveston, J., Kelly, A. and Sillwood, J.M., NPL Report No. (DMA(A)18) Oct. 1980.

35A. Lyons, K.B. and Phillips, M.G., Composites vol. 12, no. 4, Oct. 1981 p265-71.

36. Mandell, J.F., and Meier, U., Long Term Behaviour of Composites, ASTM STP 813, T.K. O'Brien Ed., American Society for Testing and Materials, 1983, pp55-77.

37. Rawe, A.W., Trans. J. Plast. Inst. Feb. 1962, pp.27-38.

38. Regester, R.F., SPl 22nd. Ann. Tech. Conf. Proc. Jan 31-Feb 3 1967, paper 16-D.

39. Ishai, O. and Mazor, A. Rheologica Acta vol.13, no.3, 1974 pp.889-902.

40. Regester, R.F., Corrosion-Nace, vol.25 no.4. April 1969.

41. Wyatt, R.C., Ph.D Thesis, University of Bristol, 1968.

42. Pritchard, G. and Taneja, N., Composites vol. 4 no.5, Sept. 1973, p199-202.

43. Chamis, C.C., Lark R.F. and Sinclair, J.H., Advanced Comp. Matls - Environmental Effects, ASTM STP 658, pp160-192.

44. Ishai, O. and Arnon, U., J. Test Eval., vol.5 no.4, pp.320-6.

45. Hahn, H.T. and Kim, R.Y., Advanced Comp. Matls - Environmental Effects ASTM STP 658 pp98-120.

46. Gillat, O. and Broutman, L.J., Adv. Comp. Matls - Environmental Effects, ASTM STP 658, pp61-88.

47. Carswell, W.S. and Roberts, R.C., Composites vol. 11, no.2 Apr. 1980 p.95.

48. Raffel, B.D., SPI, 23rd Ann.Tech. Conf. Feb.6-9 1968 Paper 12-C.

49. Crank, J. and Park, G.S., "Diffusion in Polymers", Academic Press, 1968.

50. Apicella, A et al Composites, Vol.13, no.4 Oct. 1982 pp.406-10.

51. Carslaw and Jaeger

52. Johnson, L.G., The Statistical Treatment of Fatigue Experiments, Elsevier, 1964.

53. Crowder, M.J., Kimber, A.C., Smith, R.L. and Sweeting, T.J., "Statistical Analysis of Reliability - Course Notes", Department of Mathematics, Surrey University, March 1986.

54. Hahn, H.T., "Proof load determination for pressure vessels wound with Aramid Fiber", Lawrence Livermore Laboratory Preprint UCRL 82643, July 3, 1979.

55. Jaras, A.C., Norman, B.J. and Simmens, S.C., J.Mat.Sci. 18(1983) pp2459-2465.

56. Ryder, G.H., Strength of Materials,Macmillan, 1969.

57. Hull, D., An Introduction to Composite Materials, Cambridge University Press, 1981.

58. Young, R.J., Introduction to Polymers, Chapman and Hall, 1983.

59. Wiederhorn, S.M., "Mechanisms of sub-critical crack growth in glass" in Fracture Mechanics of Ceramics, Eds., R.C. Bradt, D.P.H. Hasselman and F.F. Lange, Plenum Press, New York, 1978.

60. Charles, R.J. and Hillig, W.B., Surfaces, stress-dependent suface reactions and strength. chapter 17 of High Strength materials, Ed. V.F. Zackay, Wiley and Sons, 1965.

61. Schmidt, G.K. and Metcalfe, A.G., I & EC Product Research and Development, vol. 5, no.1, pp1-8, March 1966.

Table 1 Matrix of tests over a range of load levels

Load Type	Test code and frequency	
	Dry, Room temperature	40C, wet and presoaked
Static	-	St
Rectangular	-	R1 0.5/min
Sinusoidal	DS1 (P±20%P) 1Hz	S1 (P±20%P) 0.5/min
	DS2 ($\frac{1}{2}$P±$\frac{1}{2}$P) 1Hz	

Table 2 Matrix of tests at a single load level

Load level P = 4.6kN

All testing done on presaturated specimens in water at 40°C.

Load Type	Test Code	Frequency
Static	St	-
Rectangular	RO	0.03/min
	R1	0.5/min
	R2	4/min
	R3	8/min
	R4	15/min
Sinusoidal	S1 (P±20%P)	0.5/min
	S2 ($\frac{1}{2}$P±$\frac{1}{2}$P)	1Hz

Table 3 Tables of mean, standard deviation and sample size for tests at a single load level

		RO	R1	R2	R3	R4	St
a) log(total time)	$\bar{x}$	5.8189	5.5498	4.9078	4.2097	4.2810	5.7814
	s	0.42028	0.68380	0.79464	0.57995	0.65456	1.38733
	N	10	13	14	14	11	13
b) log(cycles)	$\bar{x}$	2.5223	3.4706	3.7317	3.3346	3.6789	-
c) log(time at load)	$\bar{x}$	5.8181	5.5351	4.7731	3.8787	-	5.7814

$\bar{x}$ = mean
s = standard deviation
N = sample size

Table 4 Test statistics for t-tests to determine significant differences for single load level tests

Test a) log(time under load to failure)

	St	RO	R1	R2	R3	R4
St	-	0.081	0.525	2.339**	4.713**	∞**
	RO	-	1.149	3.782**	9.000**	∞**
		R1	-	2.661*	6.816**	∞**
			R2	-	3.402**	∞**
				R3	-	∞**

Test b) log(cycles to failure)

	RO	R1	R2	R3	R4
RO	-	3.853**	4.377**	3.769**	4.761**
	R1	-	0.912	0.560	0.057
		R2	-	1.510	0.178
			R3	-	1.393

** - significant at the 1% level

* - significant at the 5% level

Table 5 Summary of Endoscope Observations

Specimen and Load Type	Difference in Extent of Debonding	Clear Crack in position of Final Failure	Other possible Failure Sites
Static 1	√	x	x
*2	√	√	x
3	√	Possibly	x
4	√	x	x
5	√	√	x
Sine 1	Slight	x	Possibly
2	√	√	√
3	√	√	x
4	√	Possibly	Possibly
5	√	Possibly	√
Rectangular *1	√	√	√
2	√	√	√
3	√	√	x
4	√	√	√
5	√	Possibly	x

*Denotes series of micrographs reproduced for this specimen

Table 6a Summary of Observations During Dry 1Hz Fatigue Tests DS1 and DS2

Specimen Number and Maximum Load of Cycle kN		Difference in Extent of Debonding from One Side to the Other Near the Break	Clear Resin/CSM Crack Visible at Failure Site Prior to Failure	Areas of Whitening Other than at Eventual Failure Site	>5mm Resin and CSM Cracks Other Than at Eventual Failure Site
0-tension - DS2					
	1	√	√	√	√
7.2	2	x	√	√	x
	*3	√	√	√	x
	4	x	√	√	√
6.72	5	x	?	√	x
	6	√	√	√	x
	7	√	√	small	x
	8	√	√	small	x
6.25	9	√	√	√	x
	10	√	√	√	√
	11	x	√	√	x
5.76	12	√	√	small	x
	13	√	√	small	x

* Denotes series of micrographs reproduced for this specimen.

? Specimen not photographed at a time close enough to failure to have developed a crack.

Table 6b Summary of Observations During Dry 1Hz Fatigue Tests DS1 and DS2

Specimen Number and Maximum Load of Cycle kN		Difference in Extent of Debonding from One Side to the Other Near the Break	Clear Resin/CSM Crack Visible at Failure Site Prior to Failure	Areas of Whitening Other than at Eventual Failure Site	>5mm Resin and CSM Cracks Other Than at Eventual Failure Site
mean +20% – DS1					
	*1	√	√	√	x
7.2	2	√	√	small	x
	3	√	?	small	x
6.72	4	√	√	small	x
	5	√	?	√	x
6.25	6	√	?	small	x
5.76	7	√	x	√	x

* Denotes series of micrographs reproduced for this specimen.

? Specimen not photographed at a time close enough to failure to have developed a crack.

Table 7 Summary of Observations During 1 Hz Wet Tests S2

Specimen	Difference in Extent of Debonding	Clear Crack in Position of Final Failure	Secondary Areas of Whitening	Large Secondary Resin Cracks
1	√	√	√	√
*2	Slight	√	Small	x
3	√	√	Small	Small Cracks Only

* Denotes series of micrographs reproduced for this specimen

Table 8 Table Showing the Frequency of Observation of Certain Features on Failed Specimens from Static and Rectangular Regimes

Code and Number of Specimens Examined	Number of Specimens with Indicated Number of Secondary Damage Sites			Gelcoat Resin Cracks (Average No. per Specimen)	Number of Specimens Showing Dimpling	Whitening due to Water	Locus of Warp Failure with Respect to Weft Roving		
	none	1-3	>3				a)	b)	c)
St (11)	9	2	-	0.91	6	Extent of whitening increasing ↑	6	3	2
R1 (11)	6	5	-	1.00	5		4	5	2
R2 (13)	2	6	5	8.00	1		7	6	-
R3 (13)	-	8	6	14.00	-		8	2	2
R4 (12)	2	8	2	16.50	-		6	2	4

Fig. 1.1 Master diagram for E-glass fabric/polyester. (From Ref. 24)

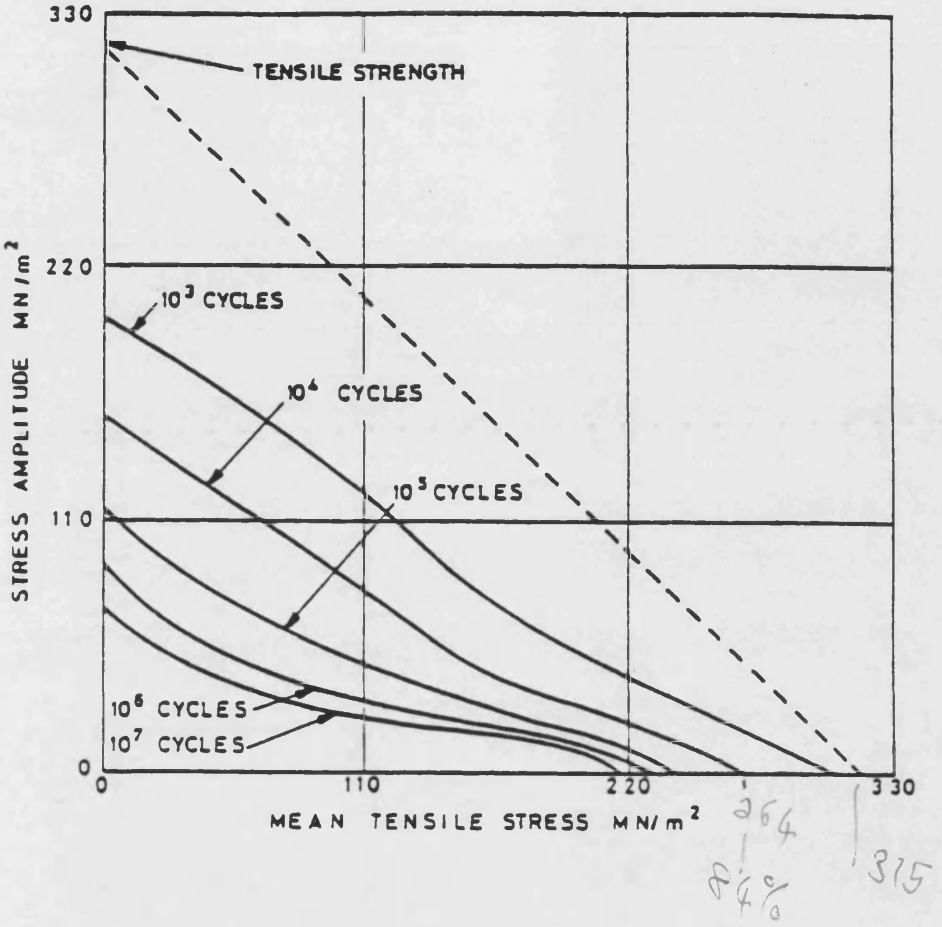

Fig. 1.2 Master diagram for chopped strand mat/low reactivity polyester laminates showing empirical laws. (From Ref.26)

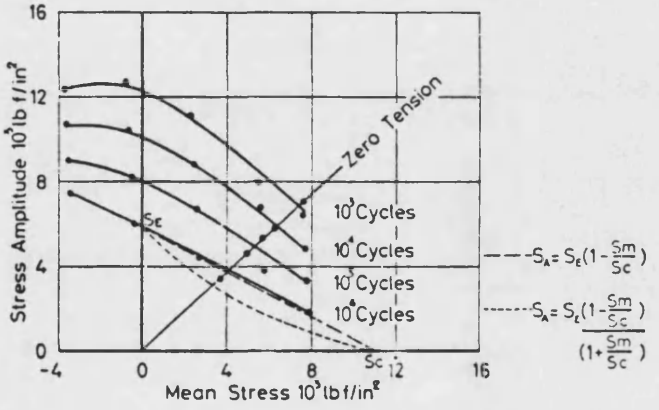

Fig. 2 Master diagram for chopped strand mat/high reactivity polyester resin laminates

Cyclic speed 74c/min; 20°C and 40-42 RH

Fig. 1.3 A schematic fatigue life diagram for tensile fatigue of unidirectional polymer matrix composites. (From Ref. 23)

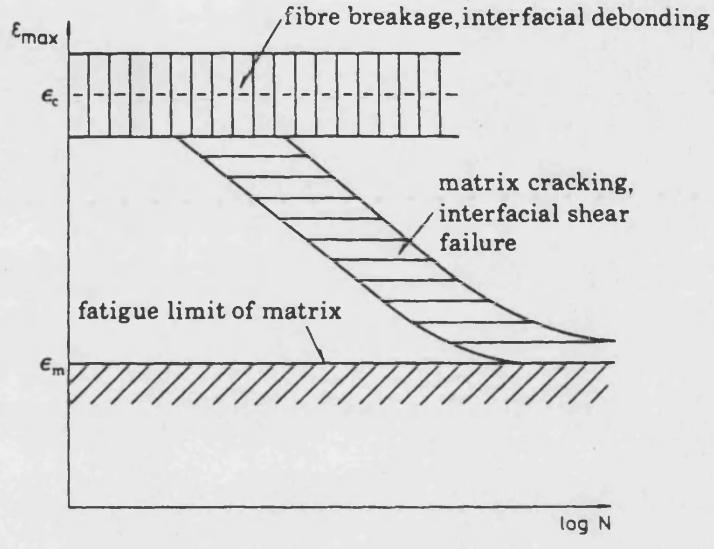

Fig. 1.4 Cyclic and static (constant force) data plotted versus cumulative time at maximum stress to failure. (Mandell and Meier[36])

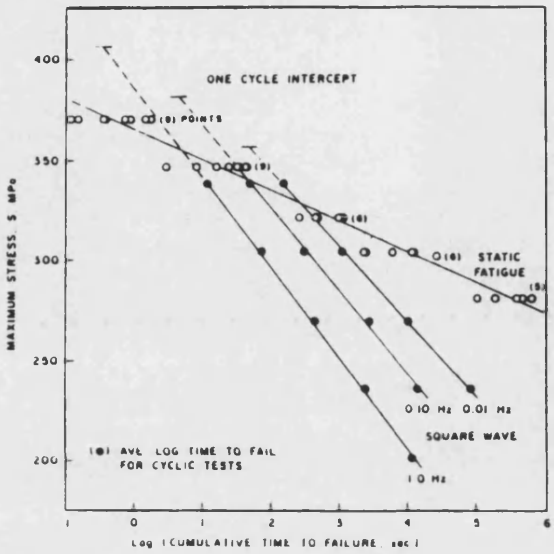

Fig. 1.5 S-N data for spike loading and unloading compared with square wave, minimum stress 17 MPa, 0.10Hz. (Mandell and Meier[36])

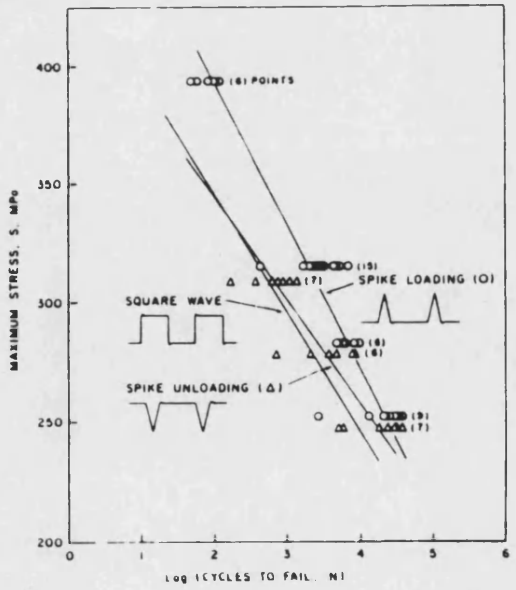

Fig. 1.6 Forms of sinusoidal load variations with time

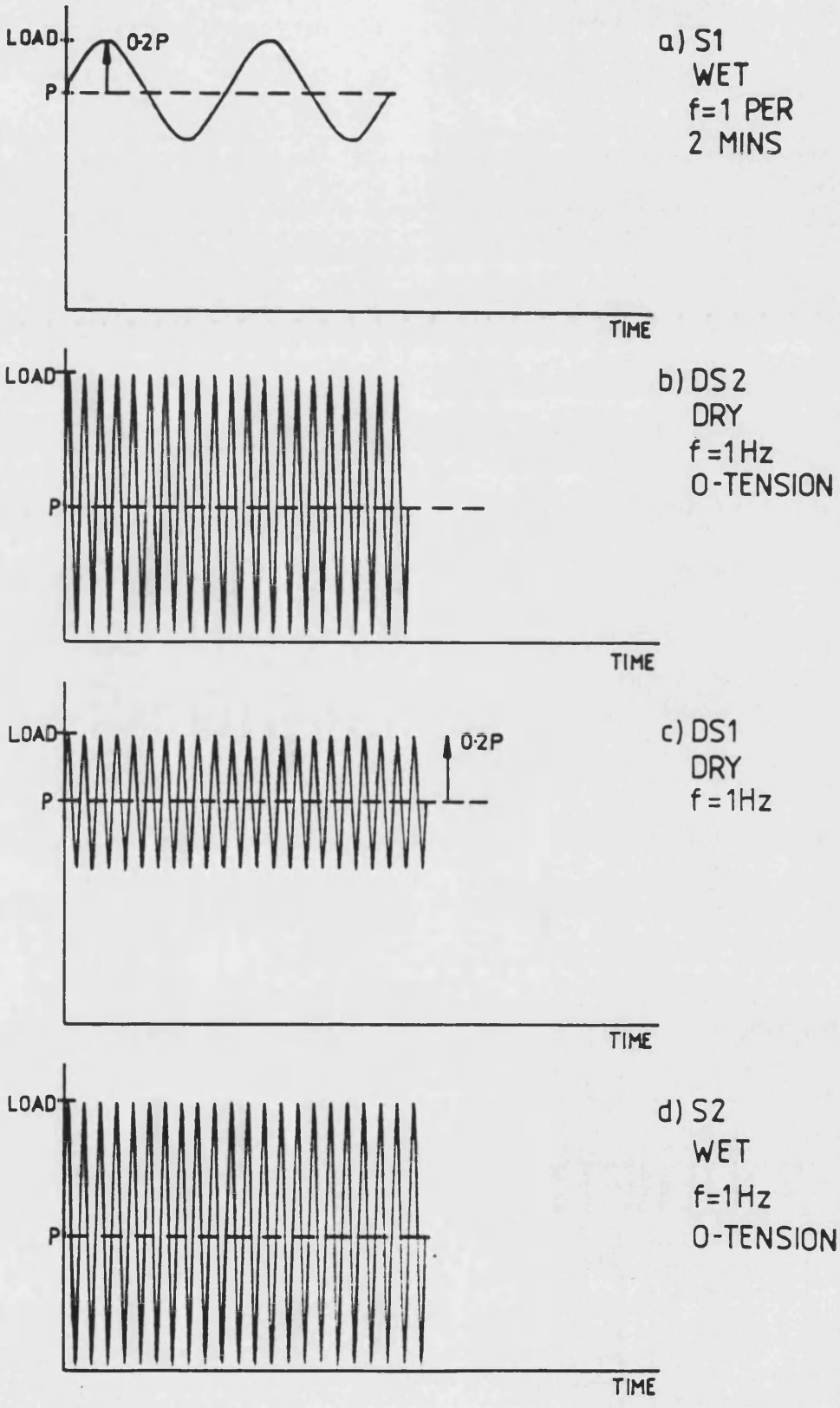

Fig. 1.7 Forms of rectangular wave load variations with time

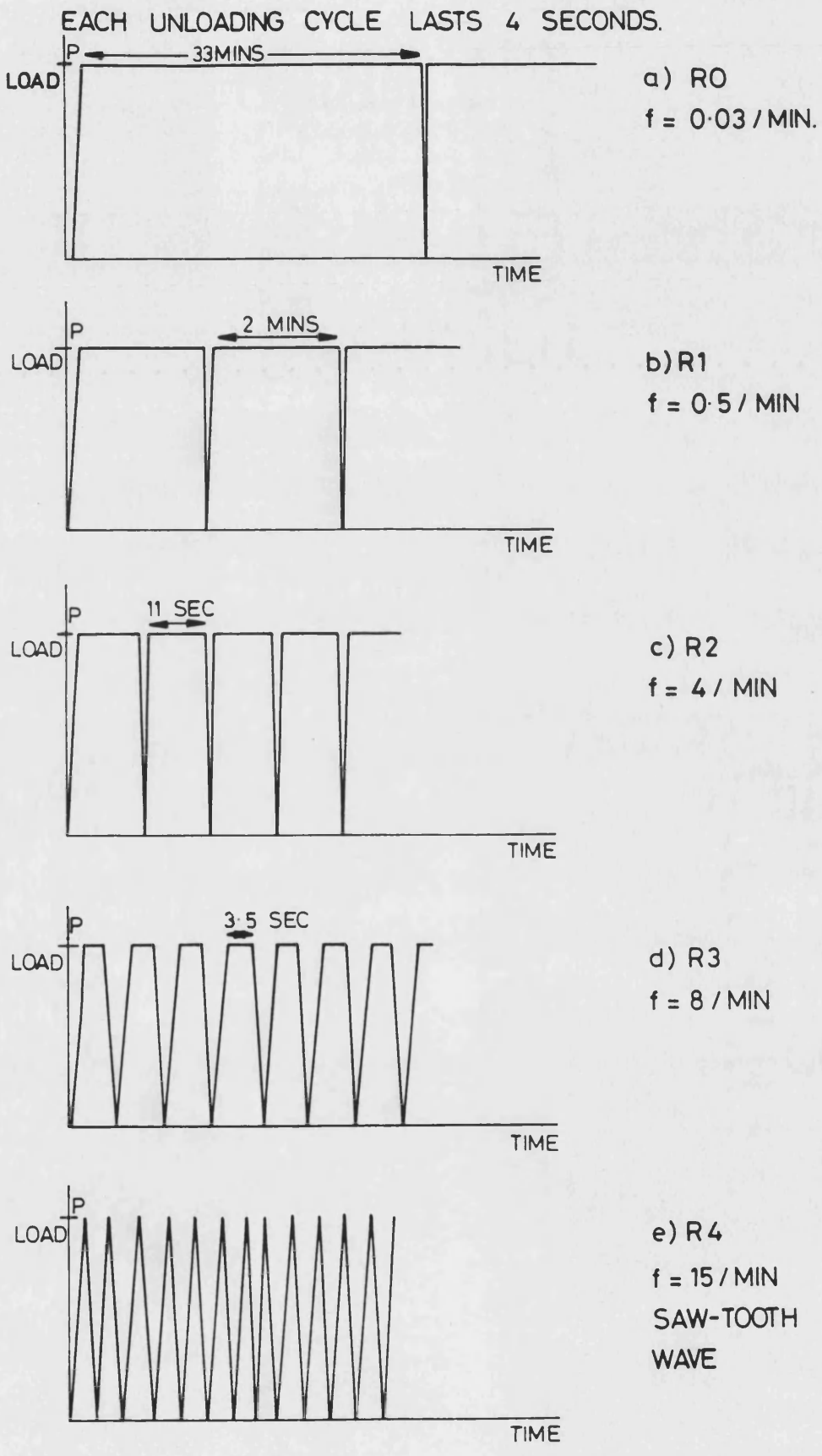

Fig. 2.1 Graph showing specimen weight change with time after removal from water bath

(Measurements made at ambient temperature)

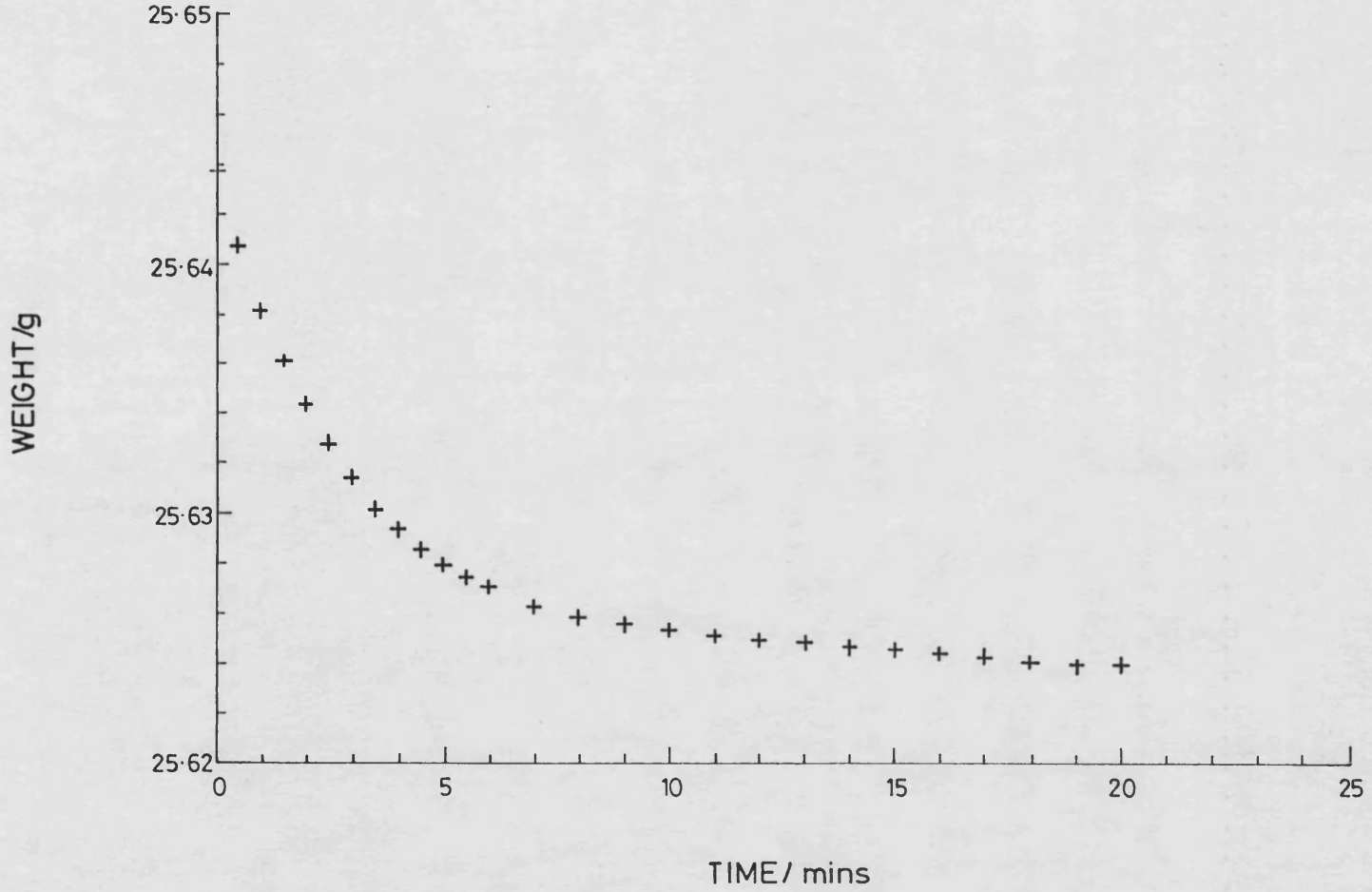

Fig. 2.2 Graph showing weight gain vs. time of immersion

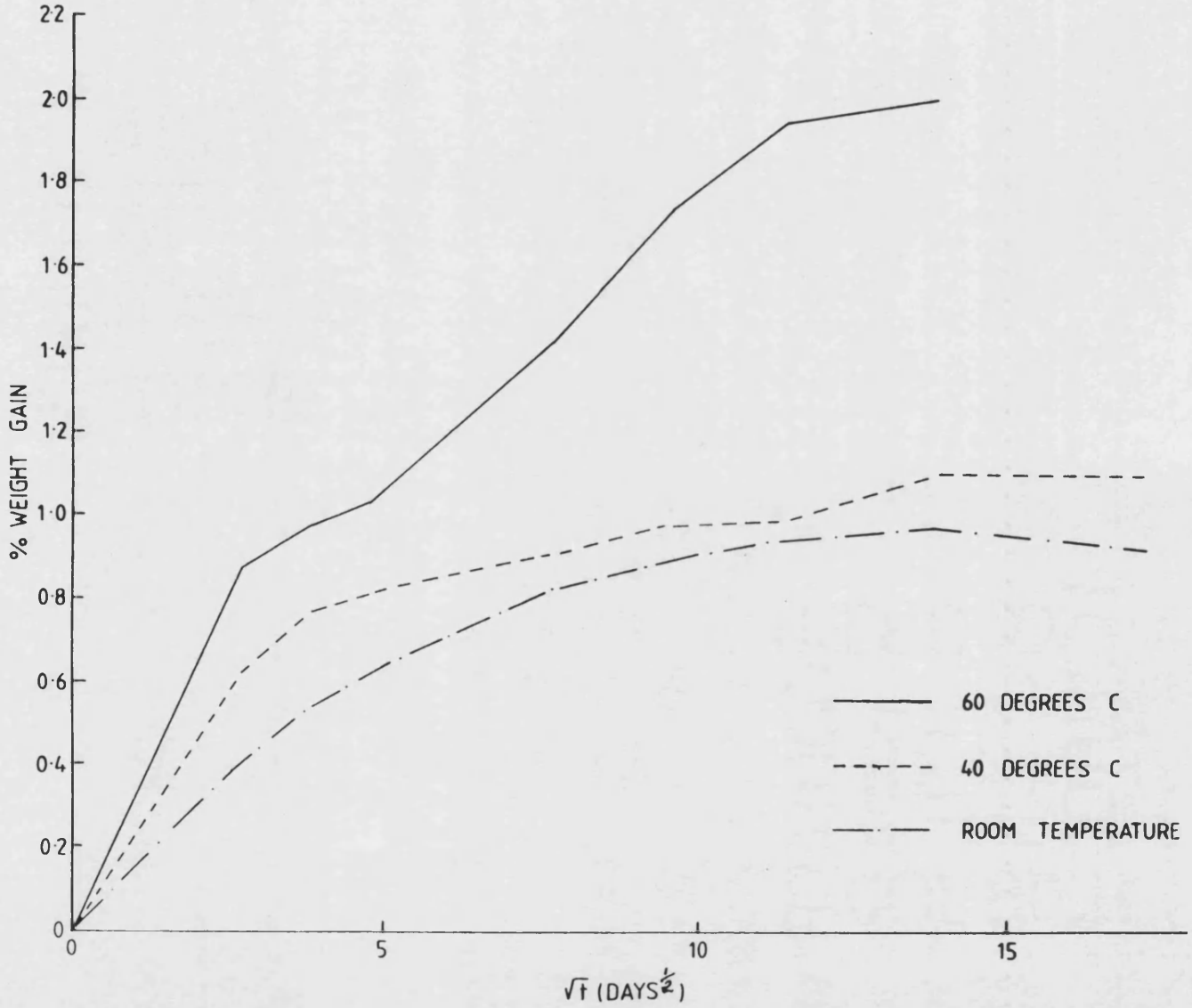

Fig. 2.3 Schematic diagram of WVTR apparatus

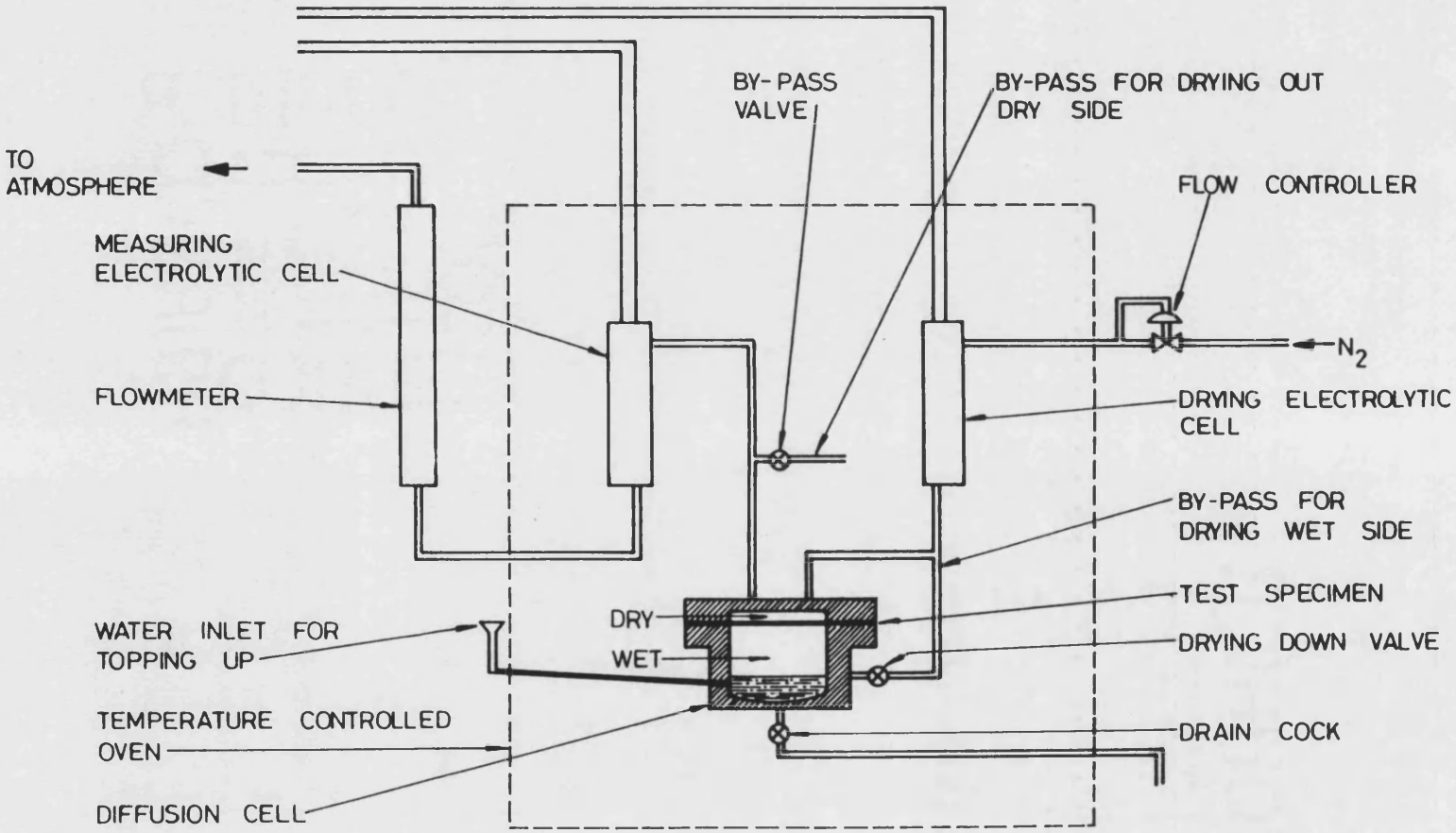

Fig. 2.4 Graph of total quantity of water through the resin plate in time t

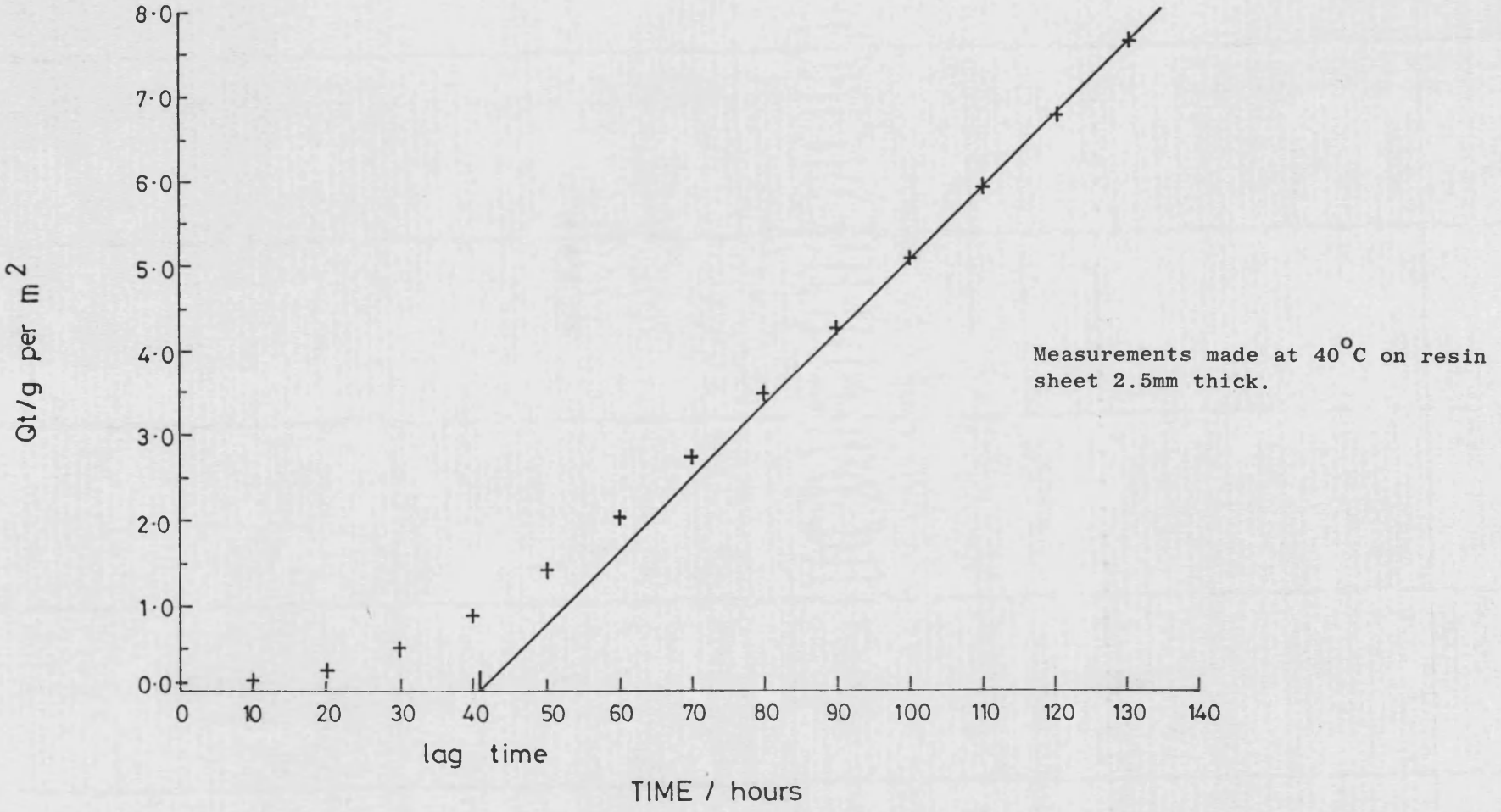

Fig. 2.5 Graph of WVTR against time for resin

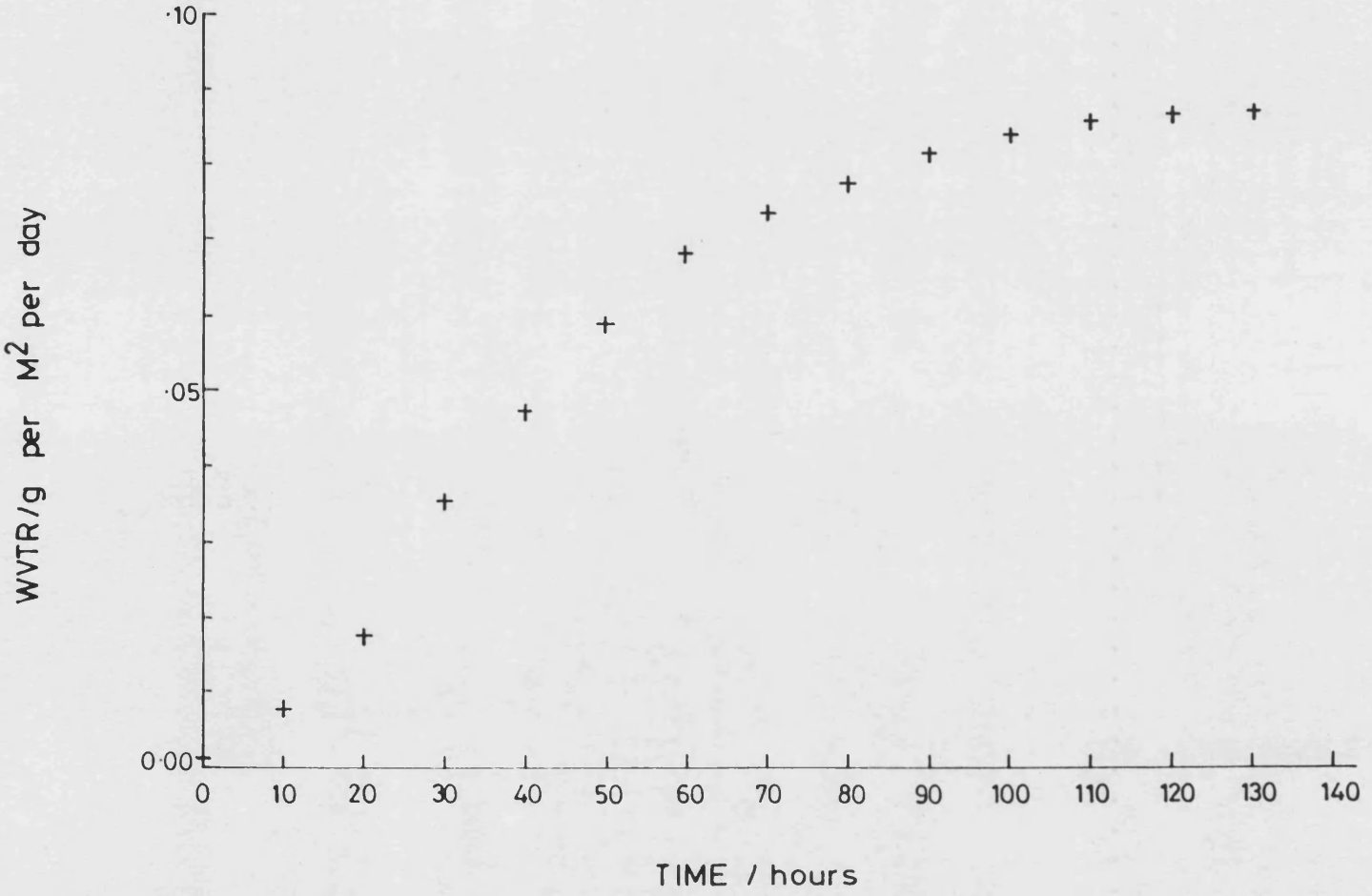

Fig. 2.6 Graph showing percentage saturation at the centre of a sheet of resin

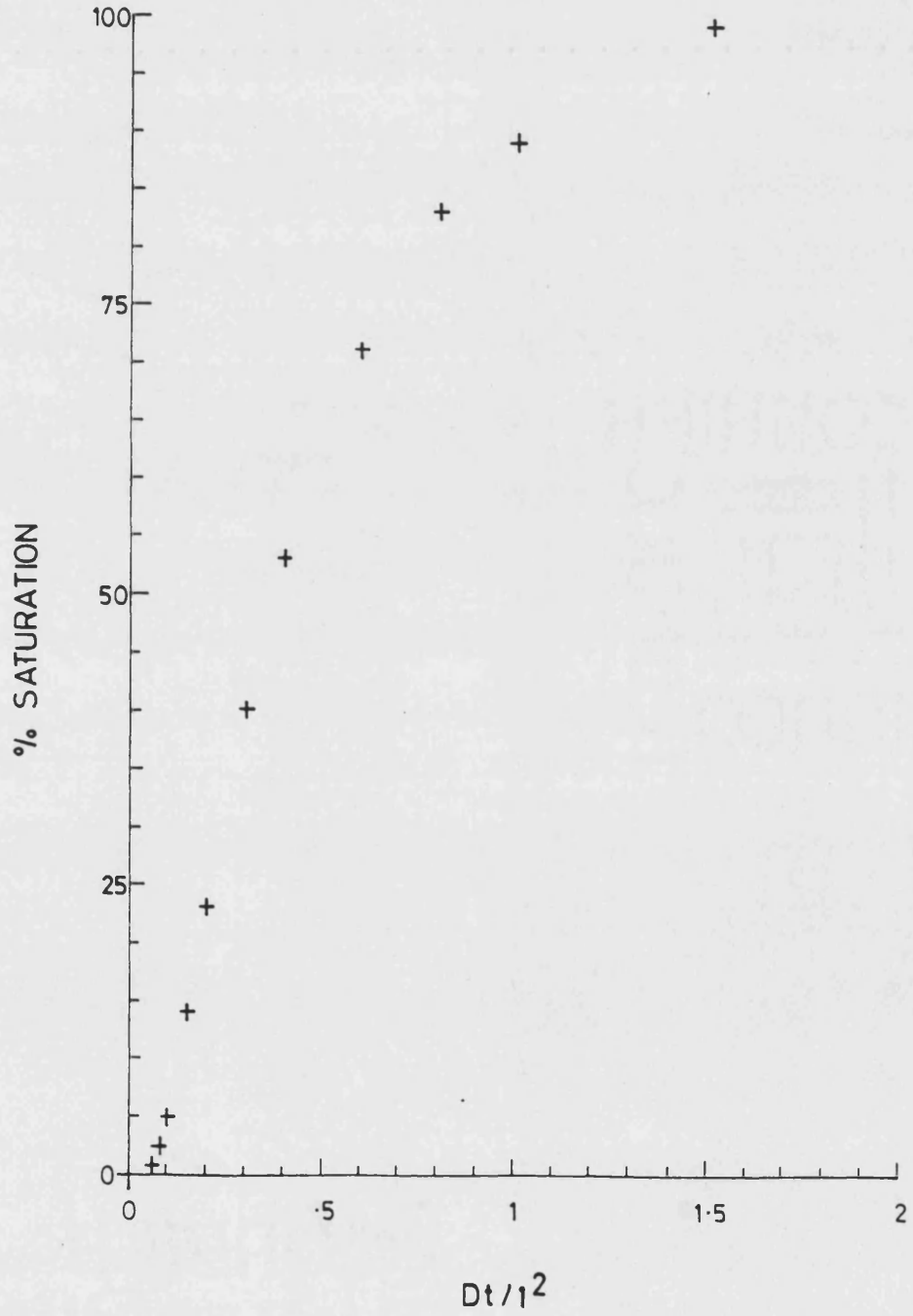

Fig. 2.7 Diagram of cylinder construction

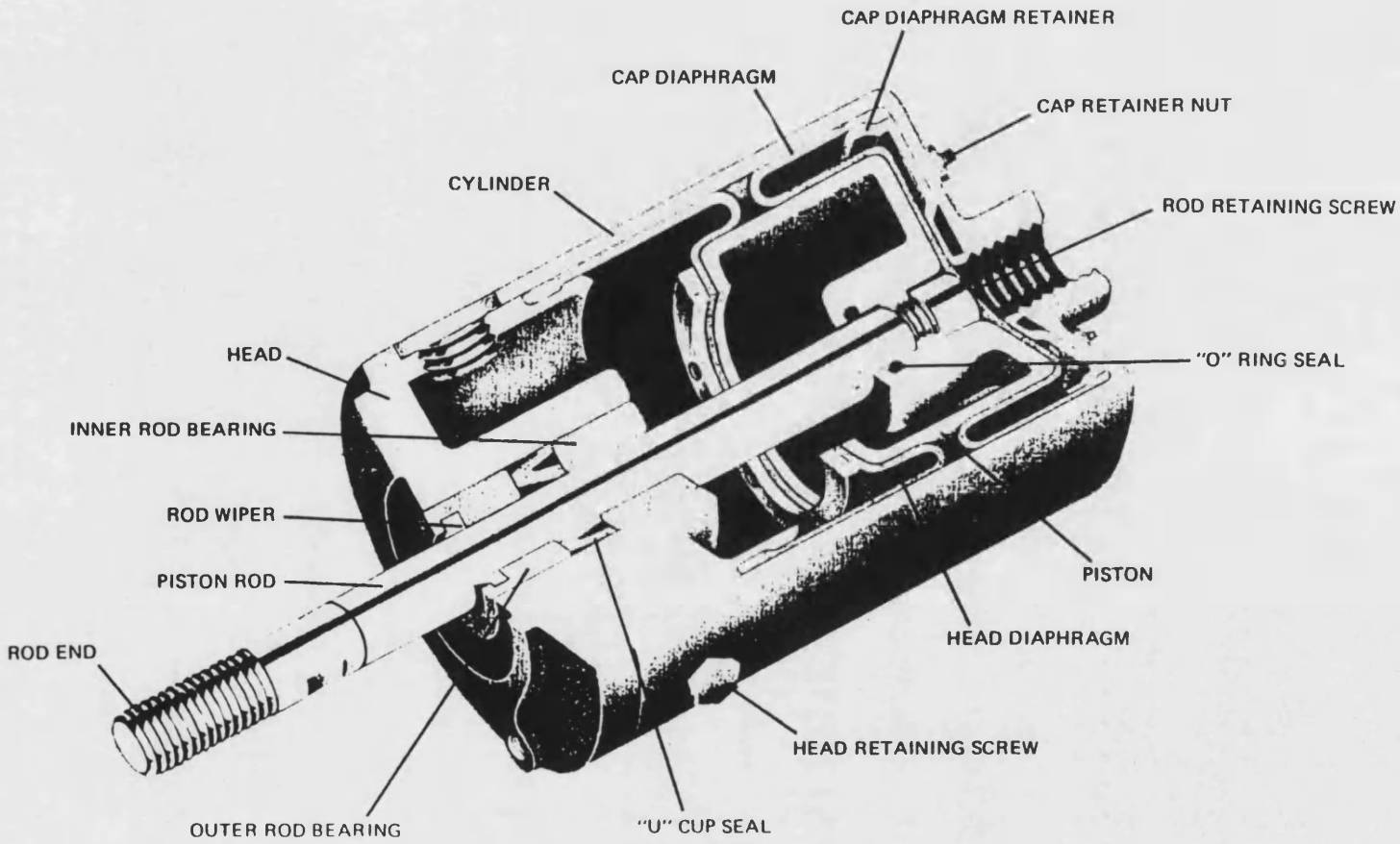

Fig. 2.8 Diagram of tension string construction

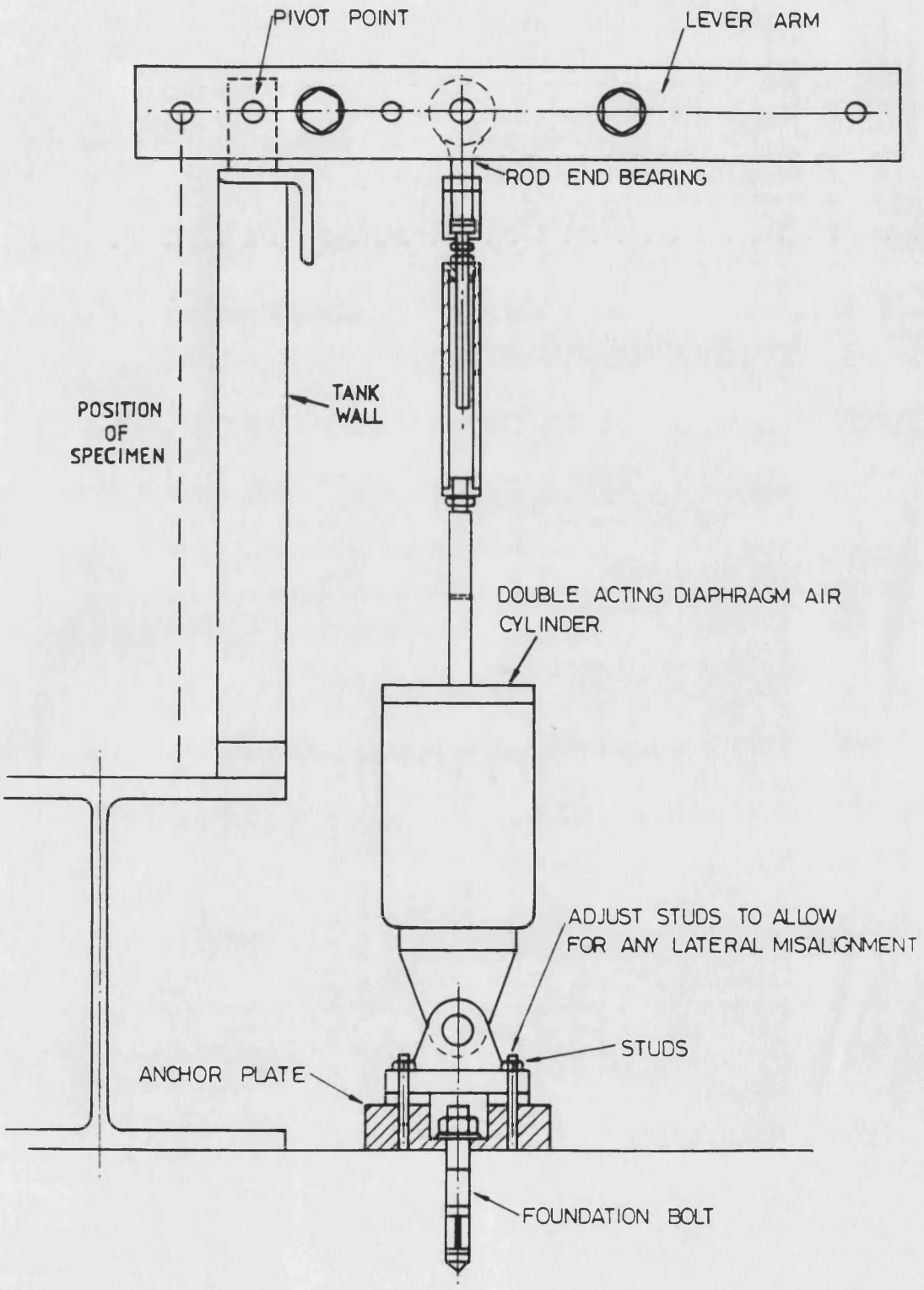

Fig 2.9 The environmental cell for 1Hz fatigue tests in water

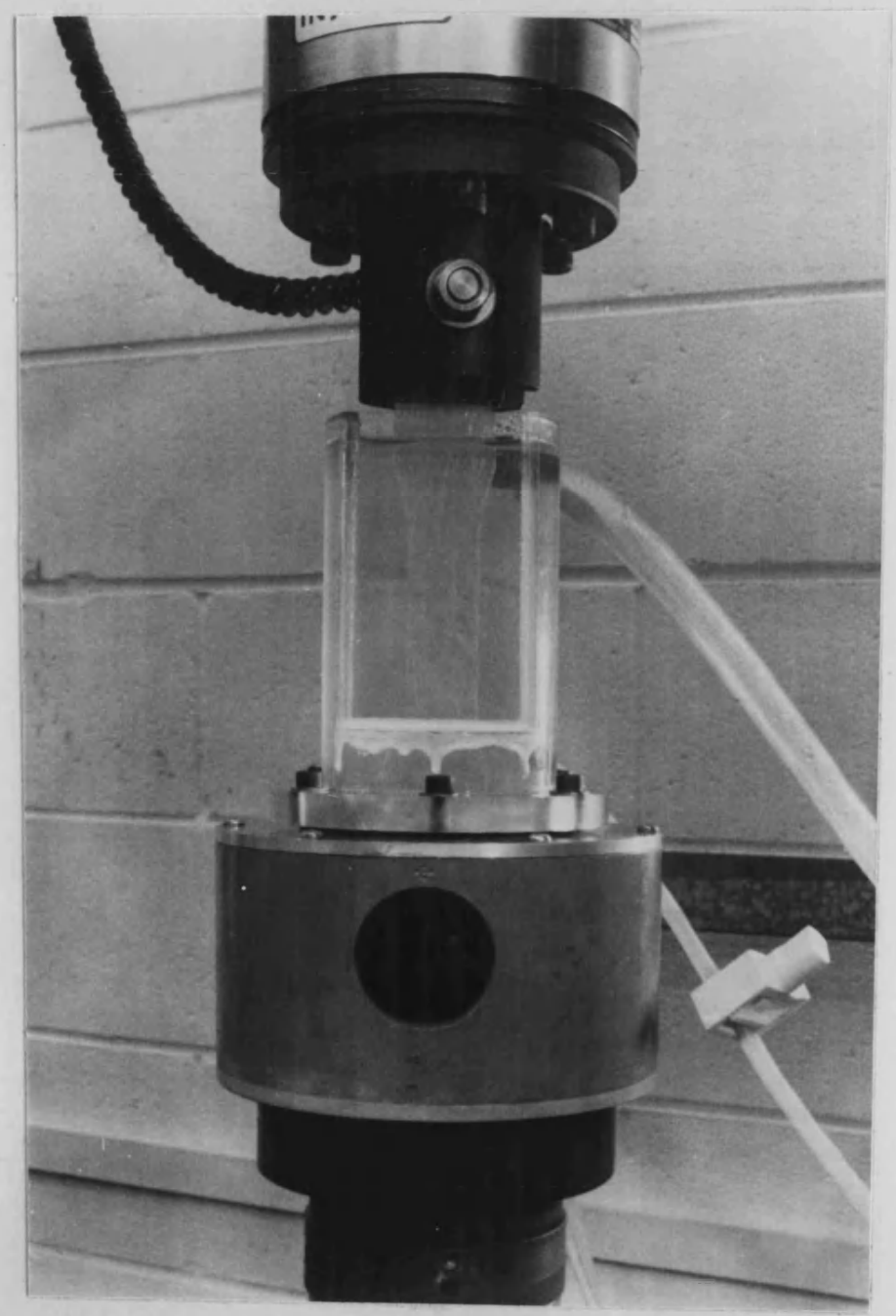

Fig. 3.1 Log(time) vs. load plot comparing R1 and St

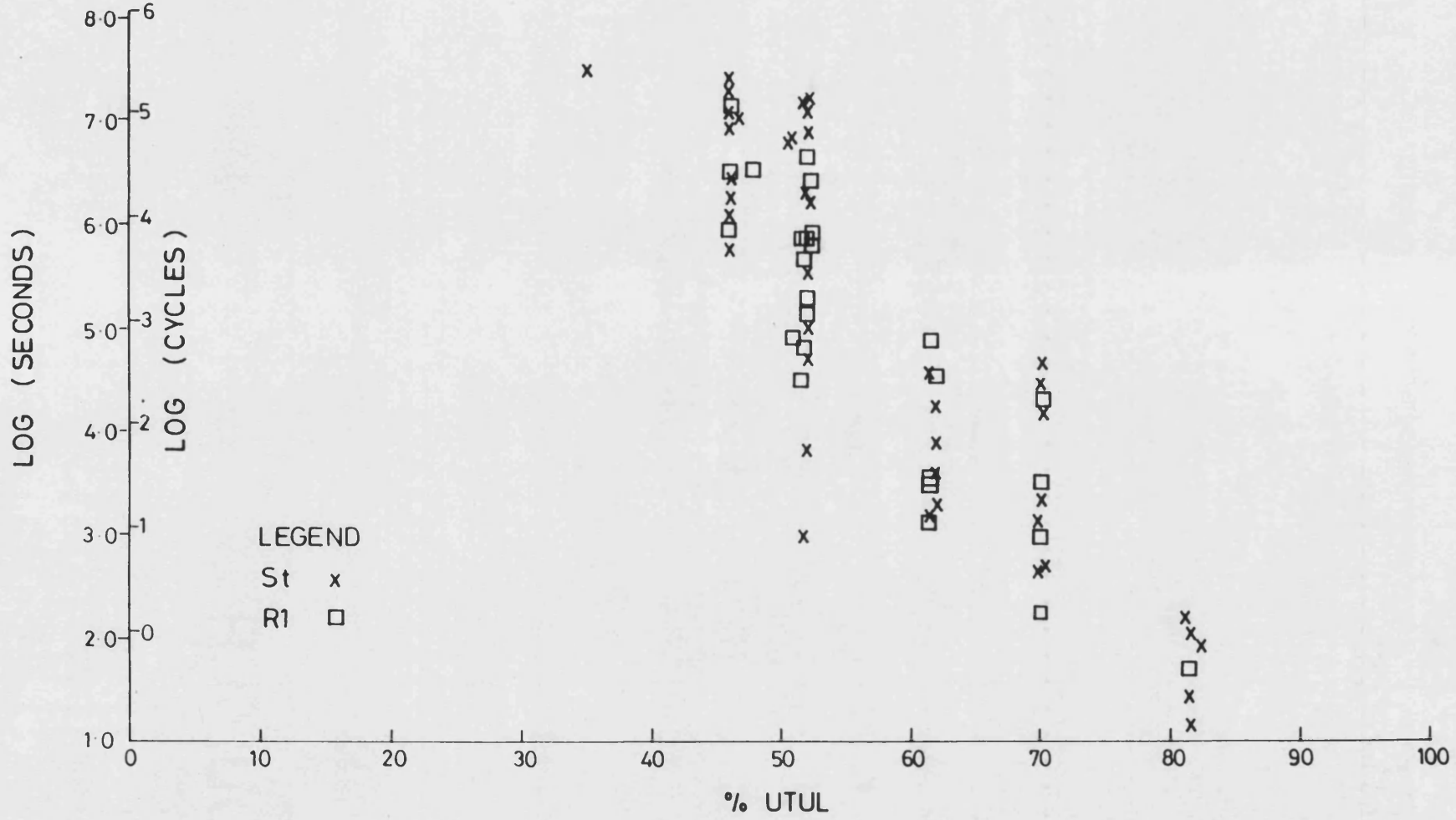

Fig. 3.2 Log(time) vs. load plot comparing S1(mean) and St

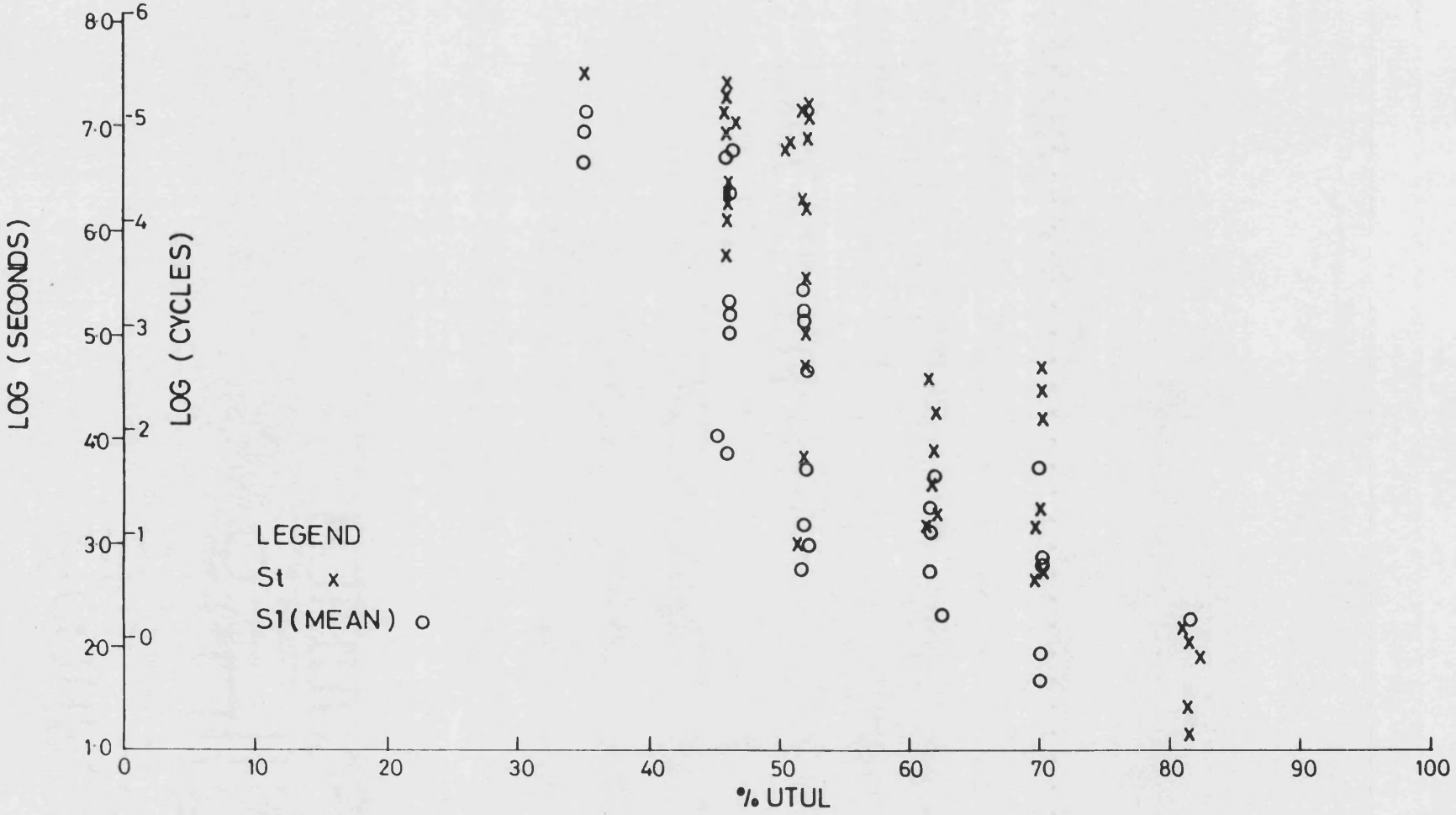

Fig. 3.3 Log(time) vs. load plot comparing S1(max load) and St

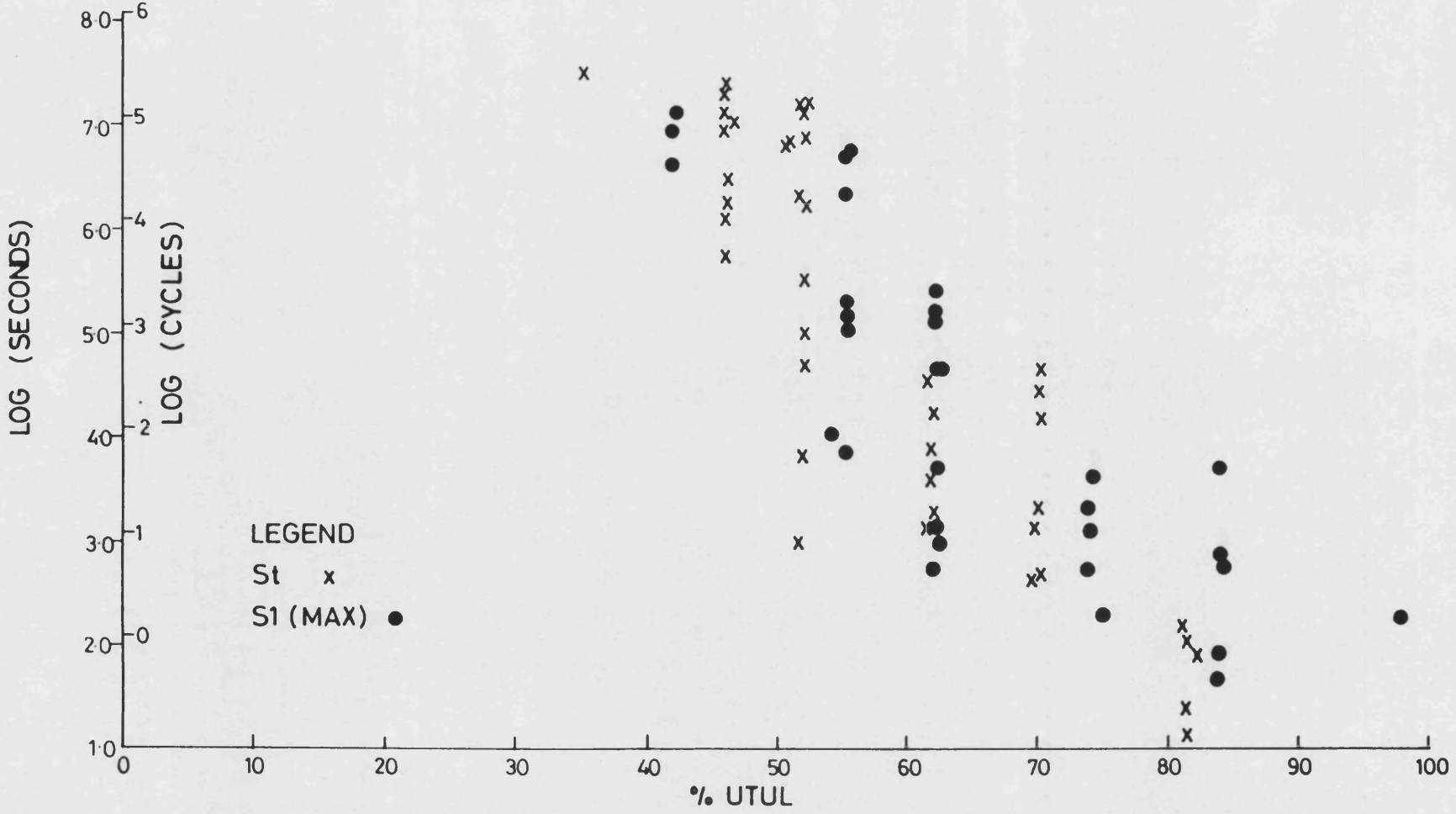

Fig. 3.4 Possible differences between two regression lines

a) CASE 1- LINES OF DIFFERENT SLOPE.

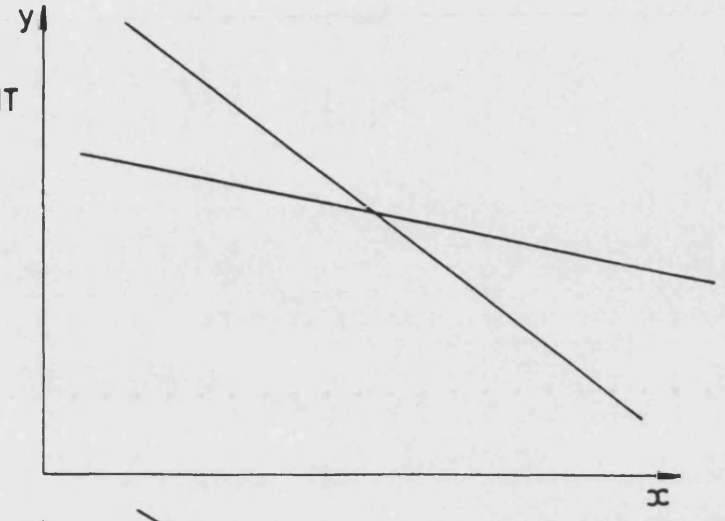

b) CASE 2- LINES OF SIMILAR SLOPE BUT DISPLACED IN THE Y-DIRECTION ie INTERCEPTS ARE DIFFERENT.

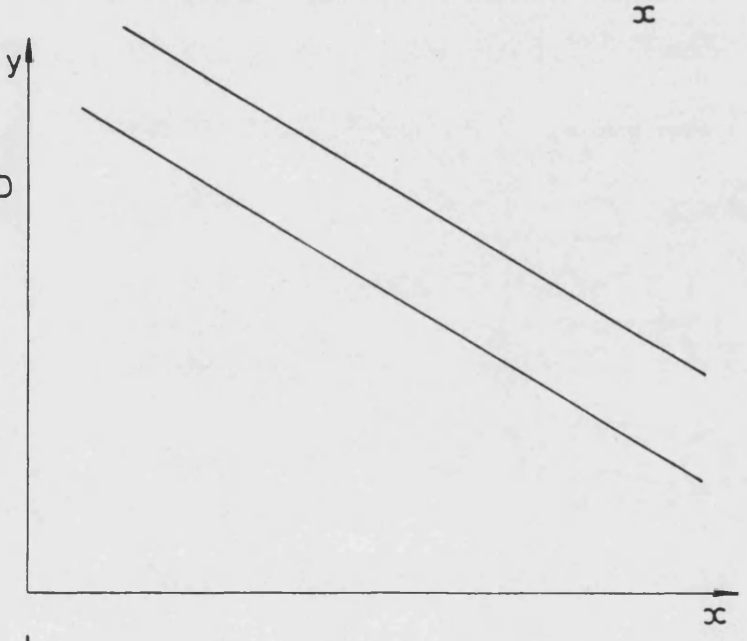

c) CASE 3 - LINES OF SIMILAR SLOPE AND INTERCEPT

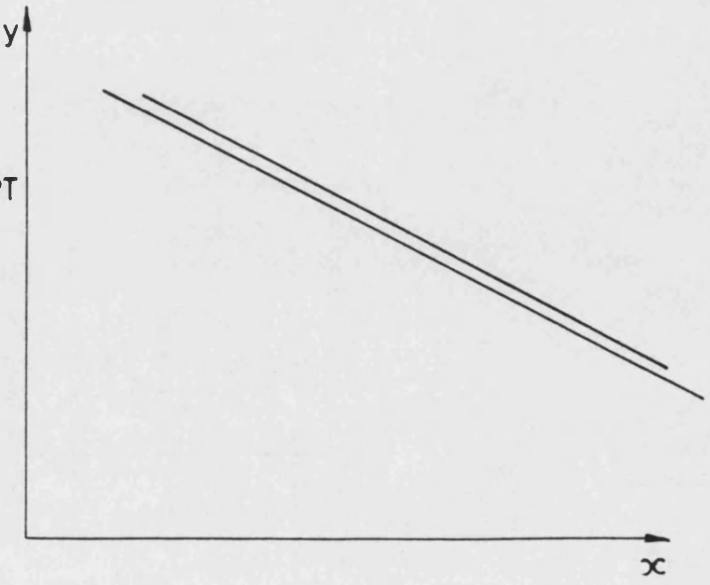

Fig. 3.5 The effect of applying load adjustment to complete data set

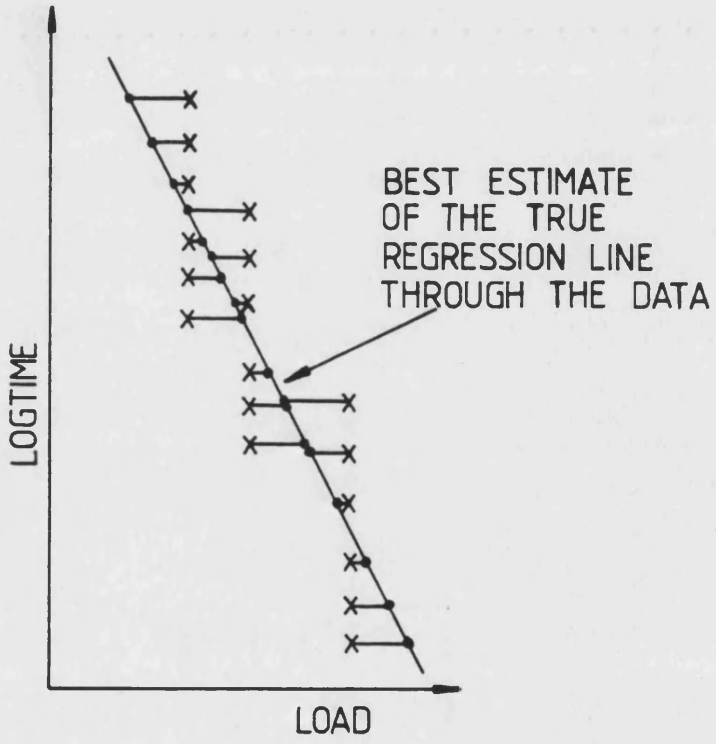

×—FAILURE UNDER STATIC LOAD
•—AND WHERE THE LOAD WOULD BE SHIFTED TO

Fig. 3.6a) The effect of applying load adjustment to data containing load-up failures and run-outs

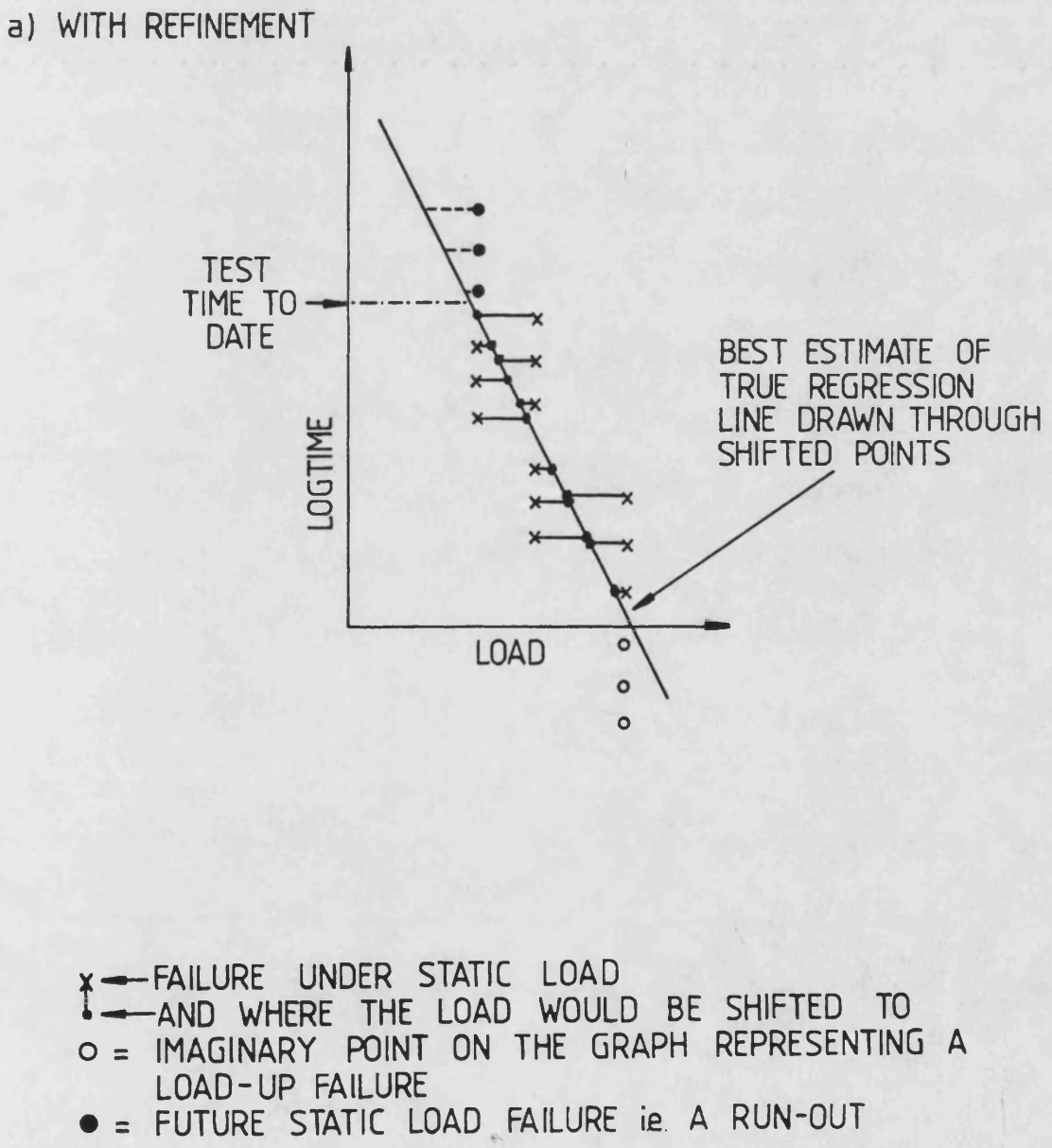

Fig. 3.6b) The effect of applying load adjustment to data containing load-up failures and run-outs

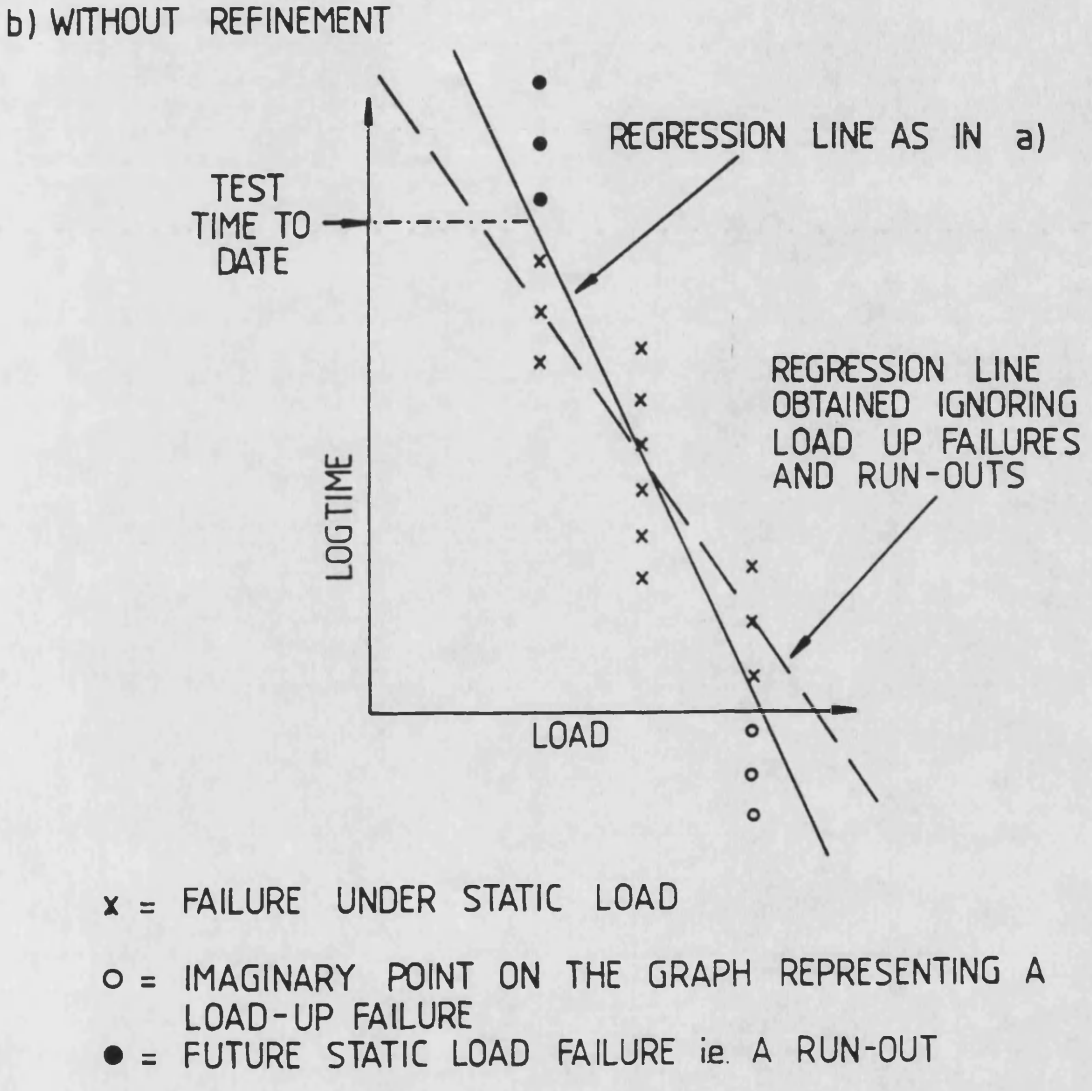

Fig. 3.7 Scatter plots before adjustment.

a) R1-St

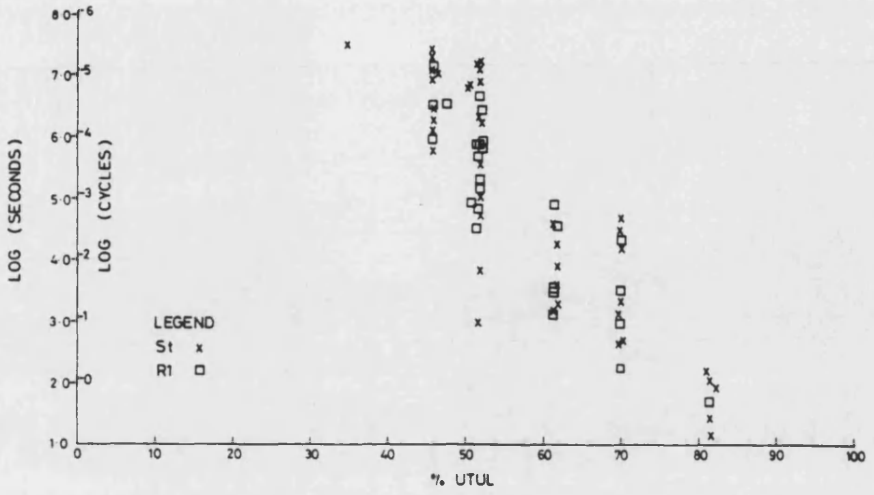

b) S1 MEAN-St

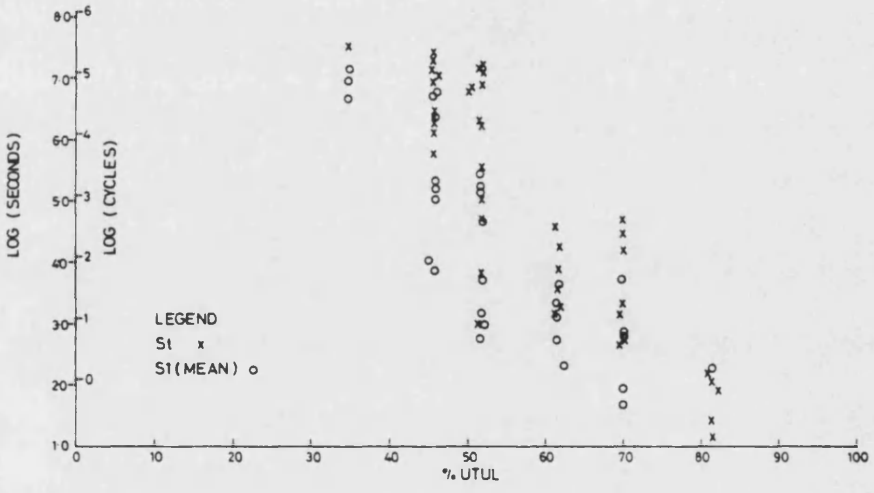

c) S1 MAX-St

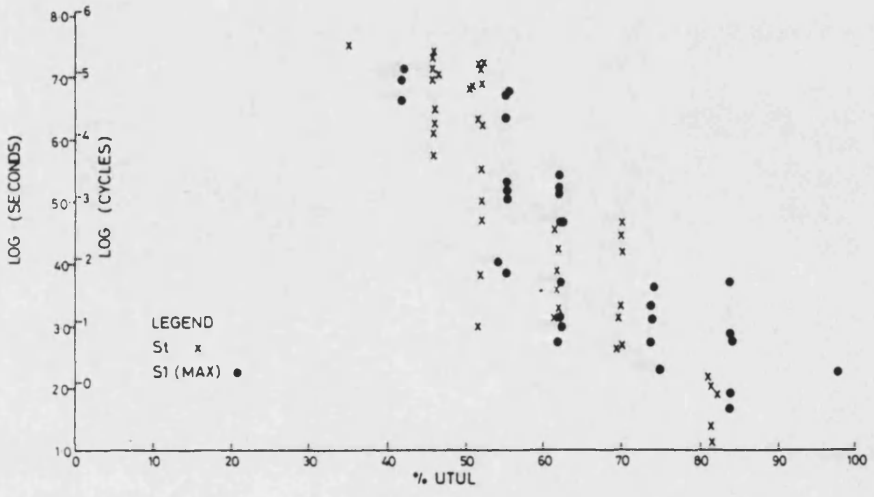

Fig. 3.8 Scatter plots after adjustment.

a) R1-St

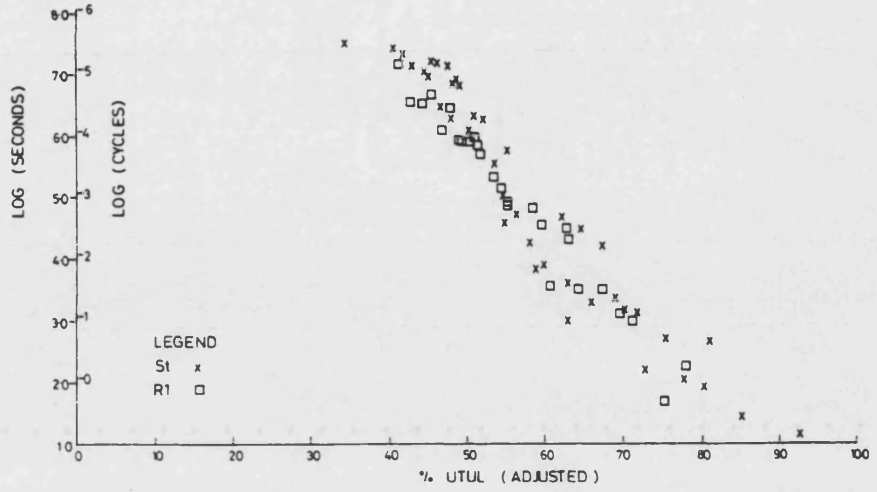

b) S1 MEAN- St

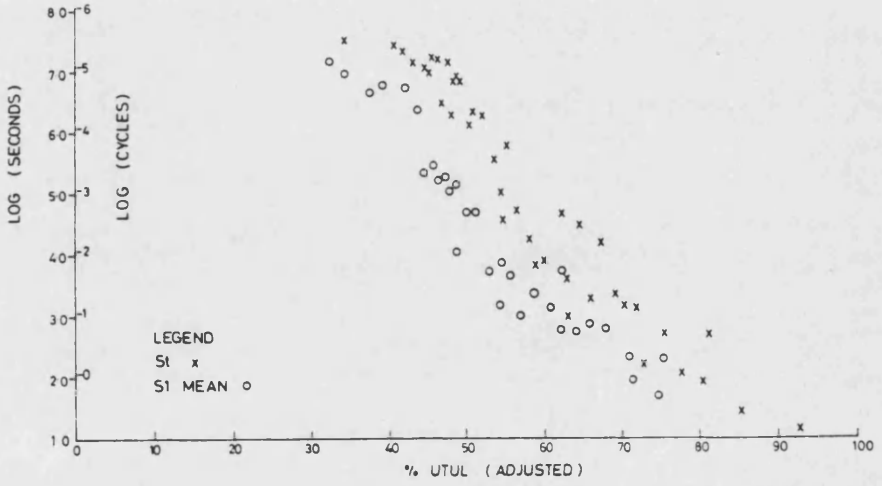

c) S1 MAX-St

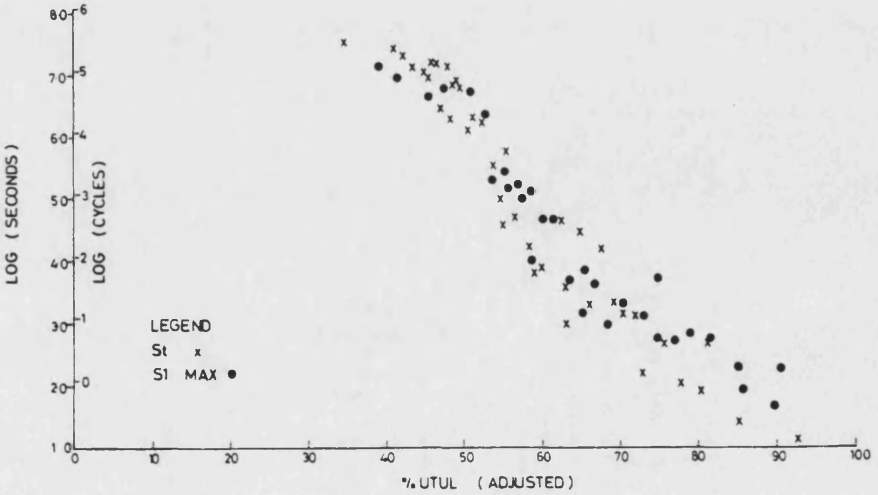

Fig. 3.9 Log(time) vs. adjusted load plot comparing S1(max load) and St

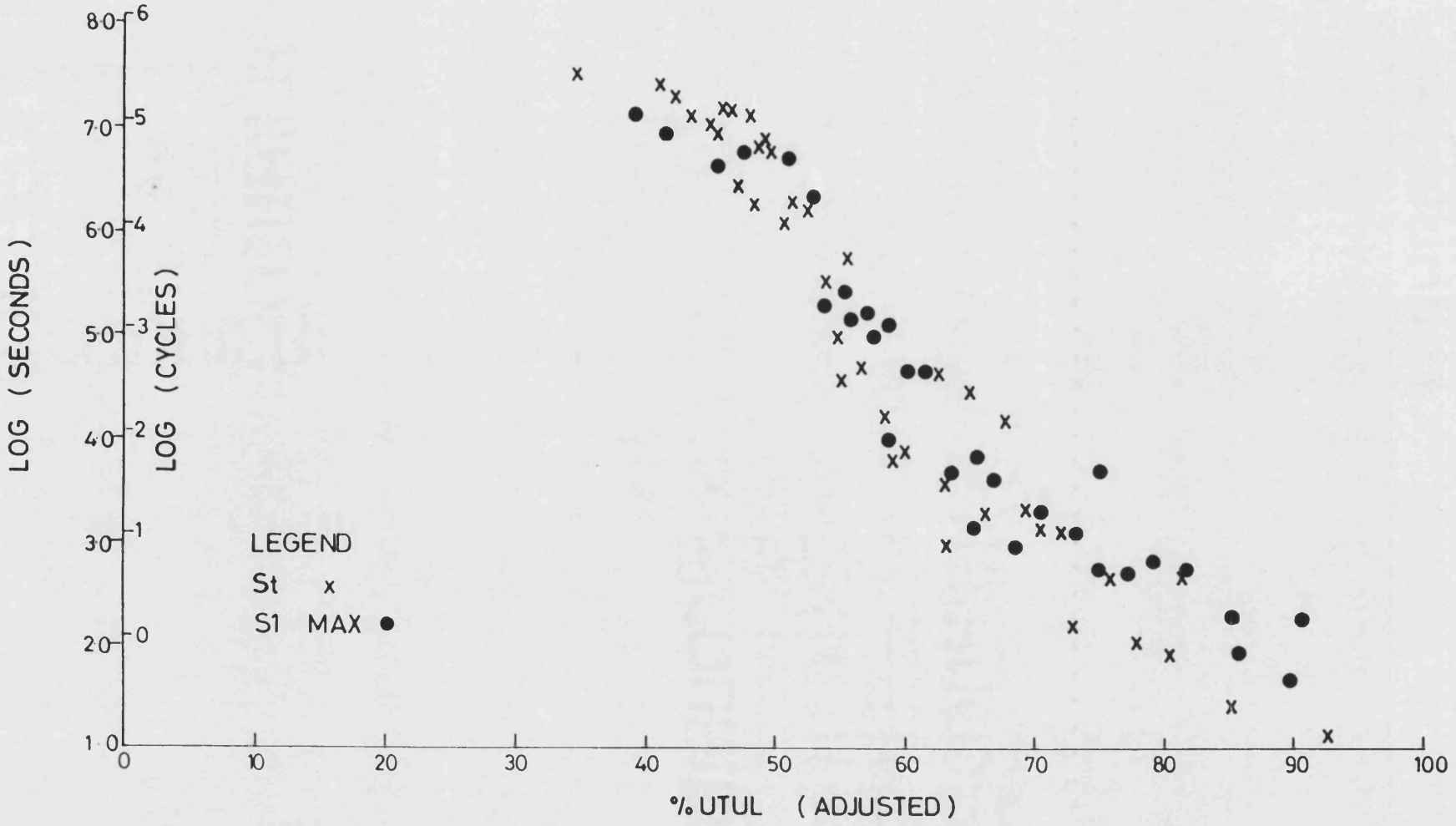

Fig. 3.10 Log(time) vs. adjusted load plot comparing S1(mean load) and St

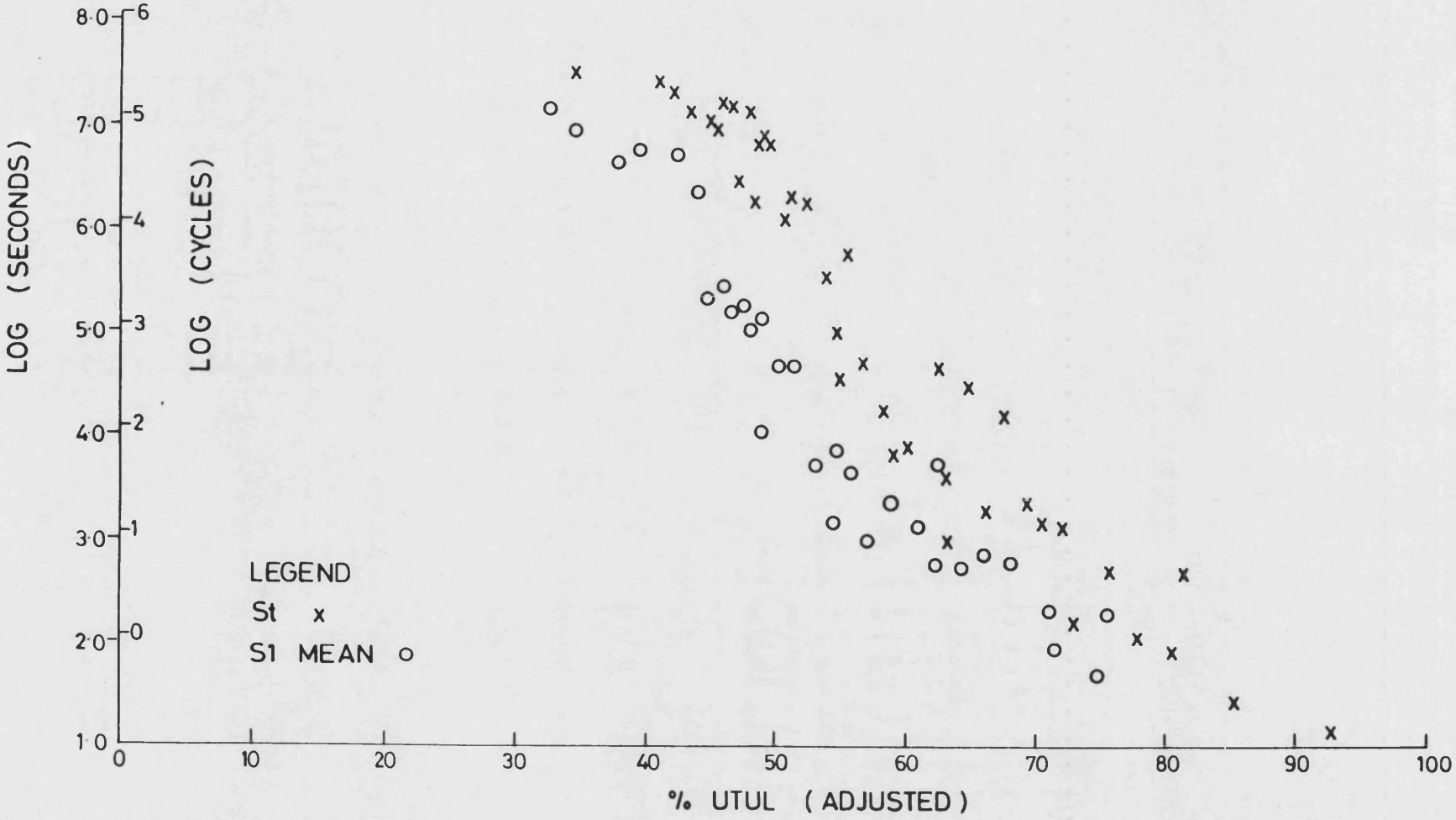

Fig. 3.11 Log(time) vs. adjusted load plot comparing R1 and St

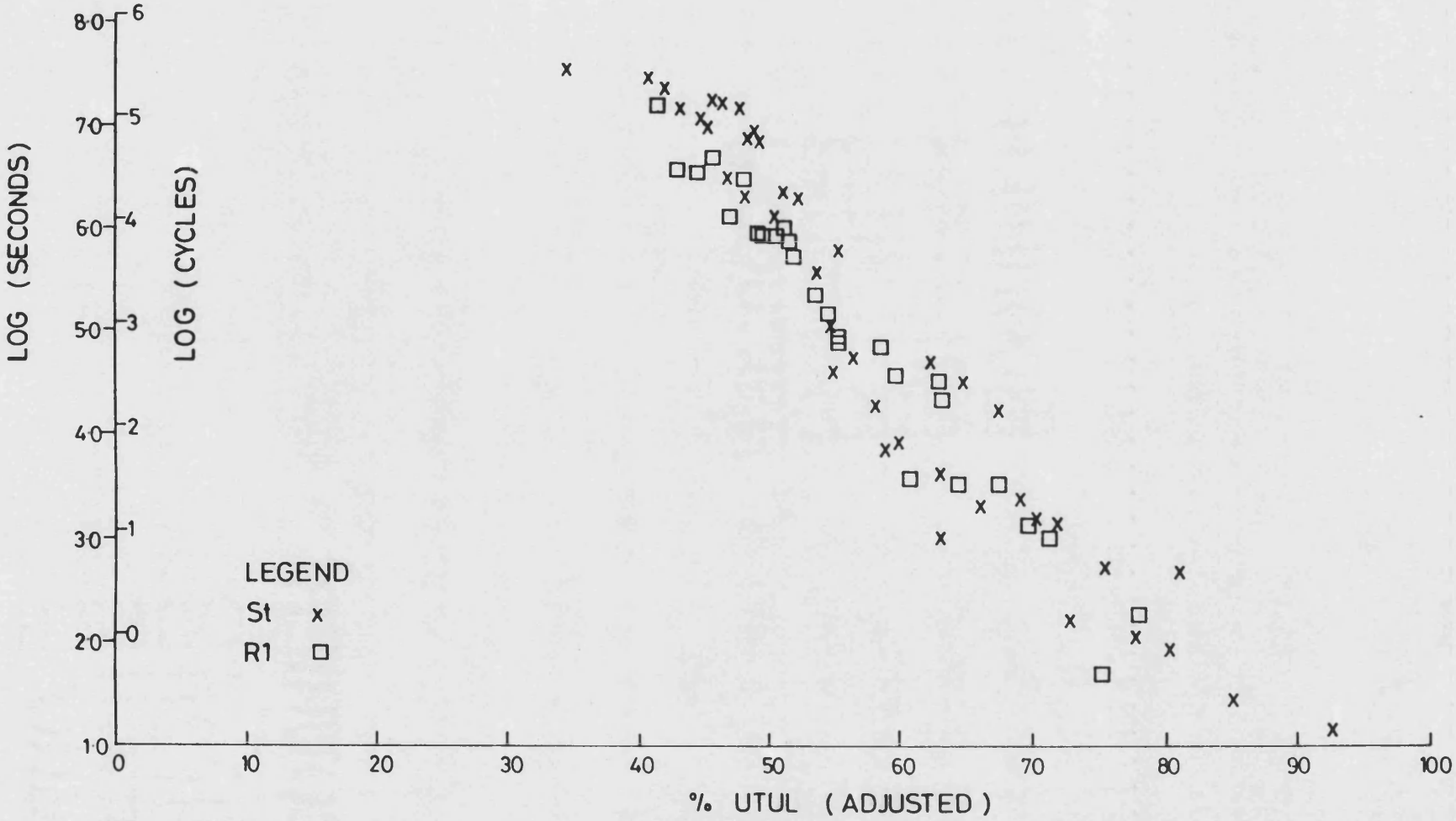

Fig. 3.12 LogN vs. load plot showing effect of raised mean stress

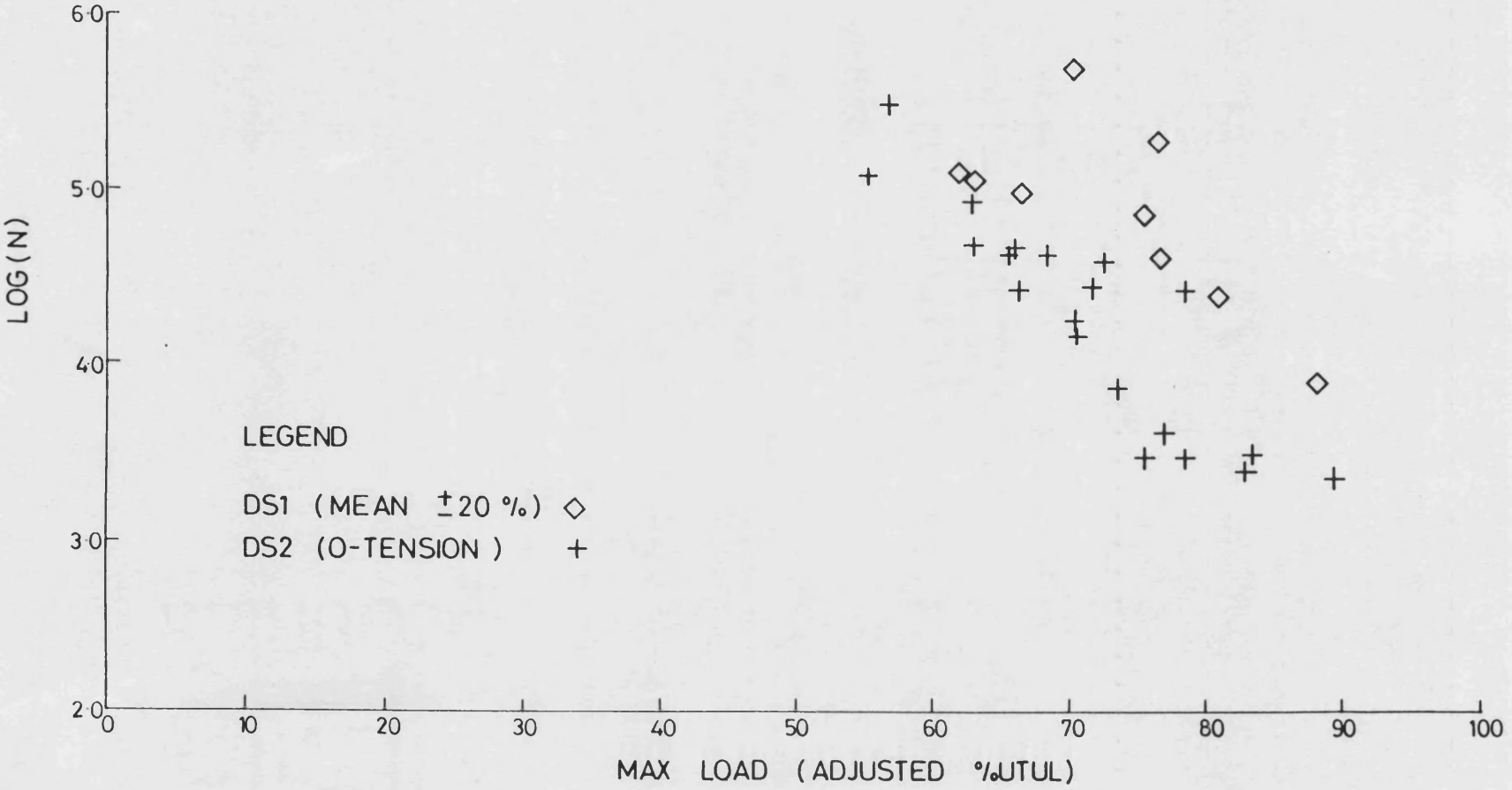

Fig. 3.13 LogN vs. load plot showing effect of environment

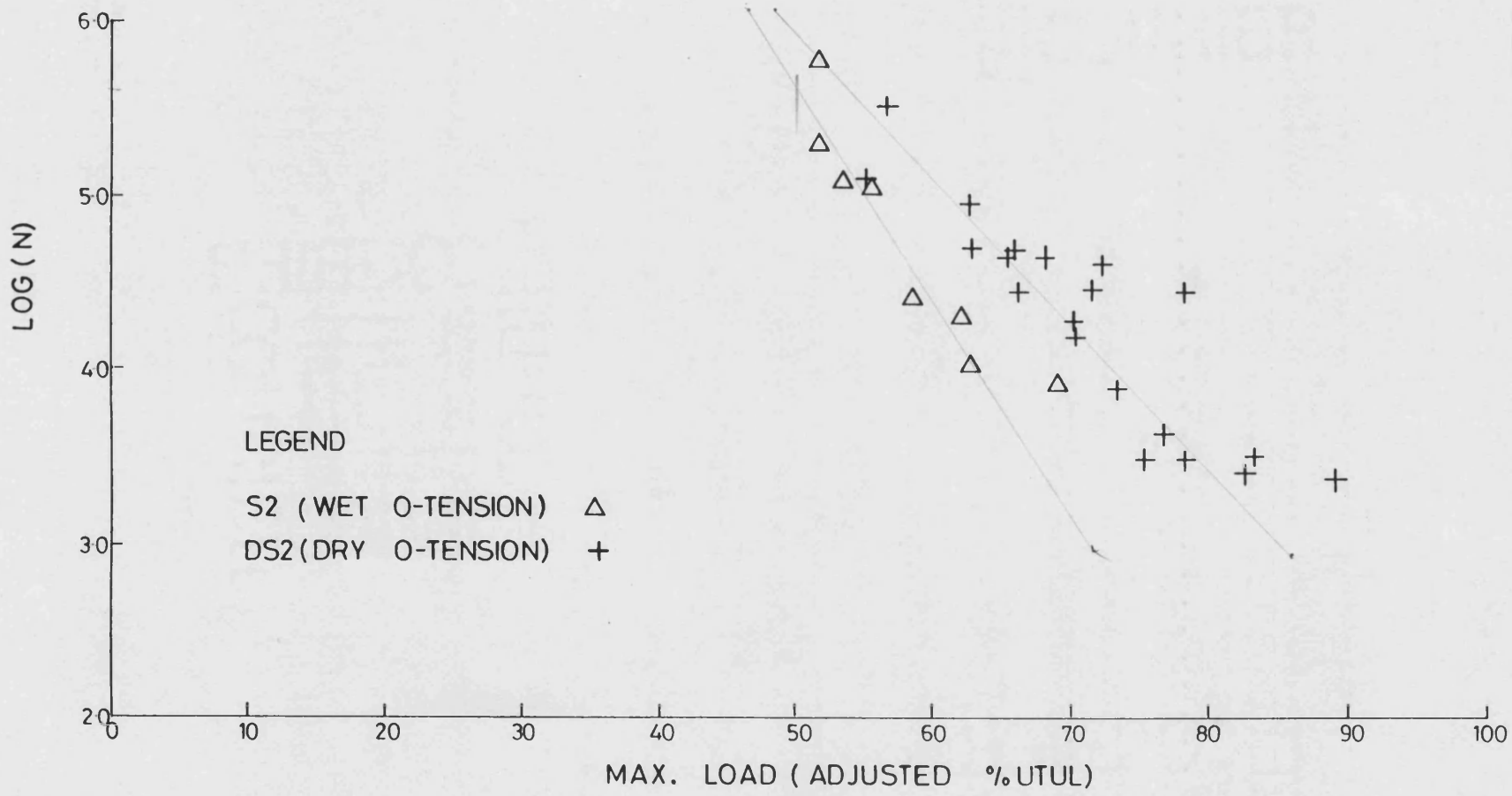

Fig. 4.1 Arrangement for endoscope photography

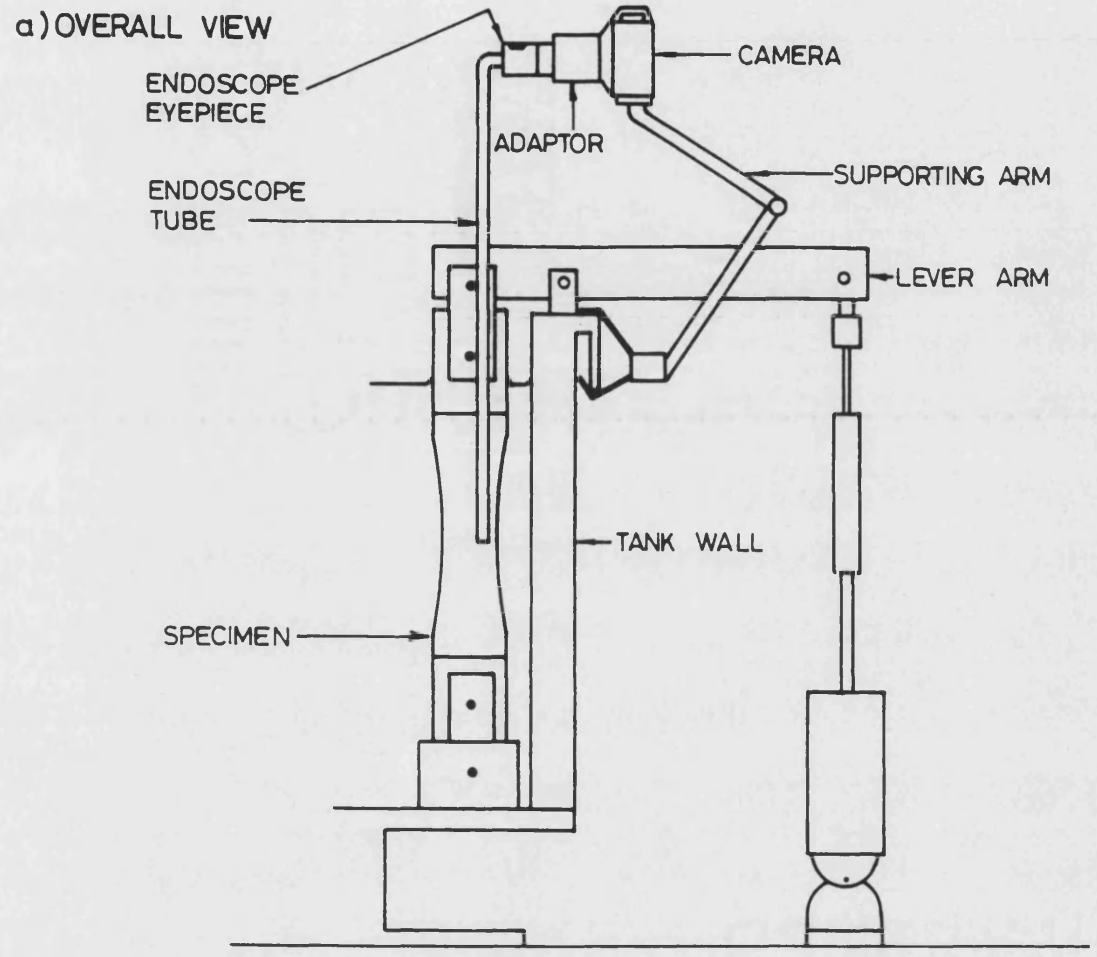

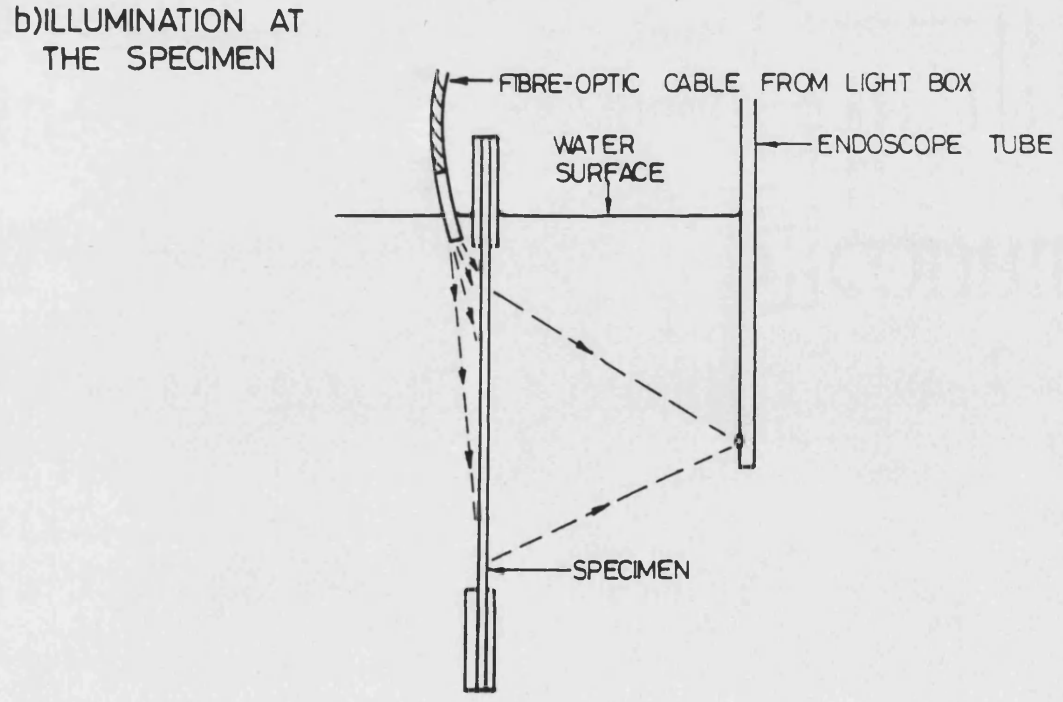

Figure 4.2 Endoscope micrographs during a static test

Crack visible

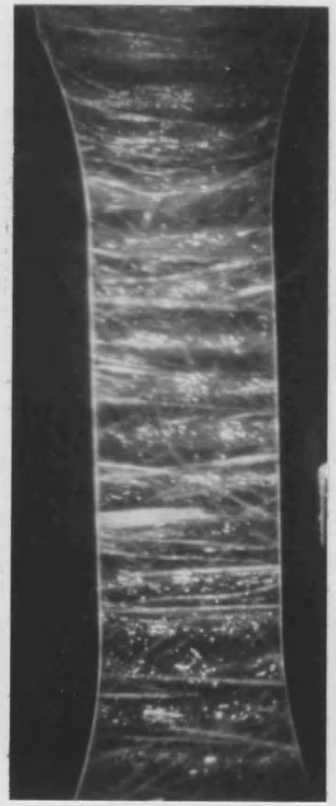
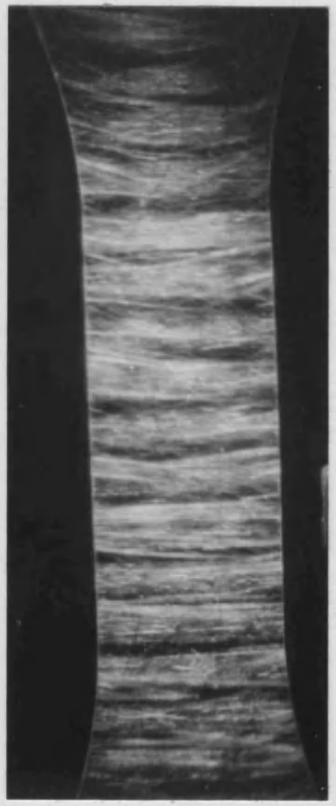
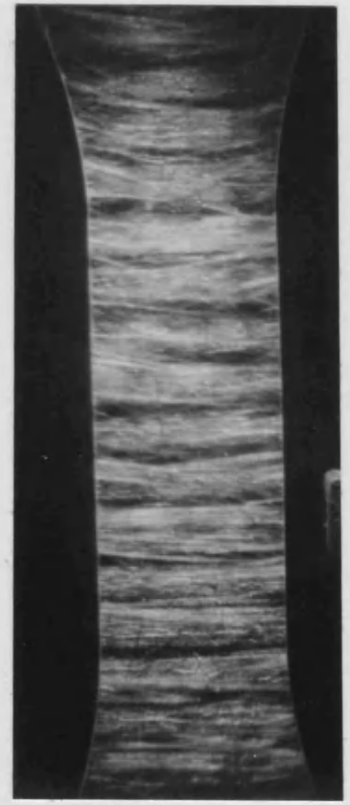
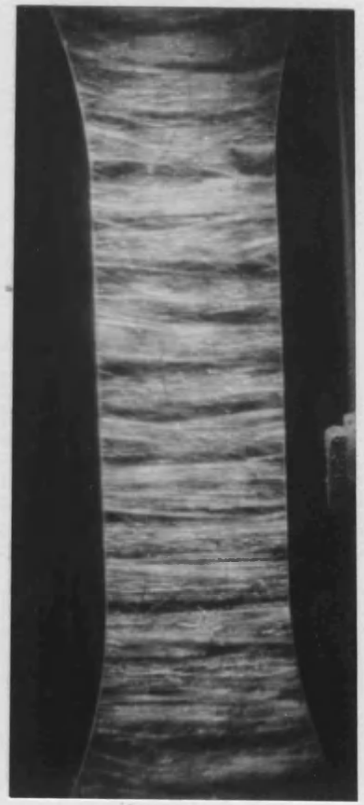

	Pre-start under no load	1 min	5 mins	20 mins
% Life	0	2.1	10.4	41.7

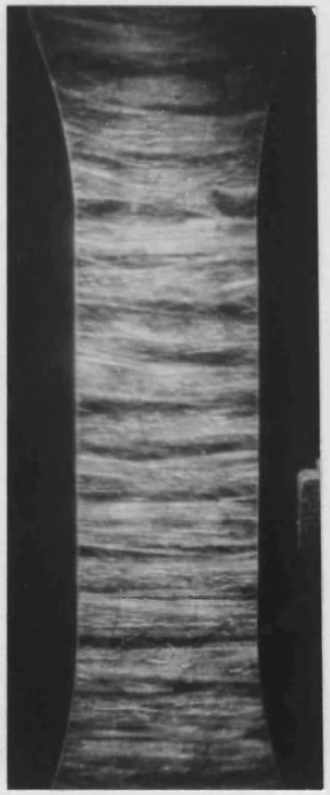

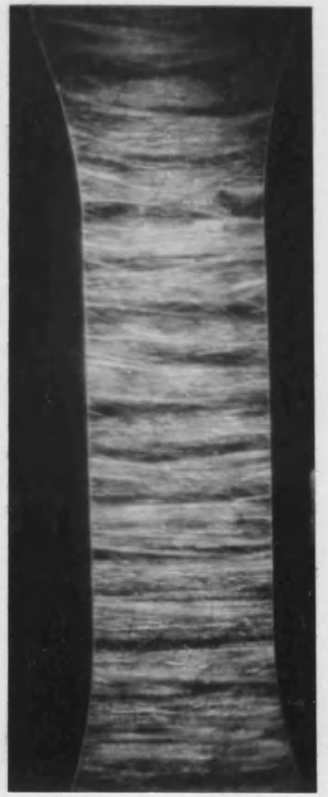

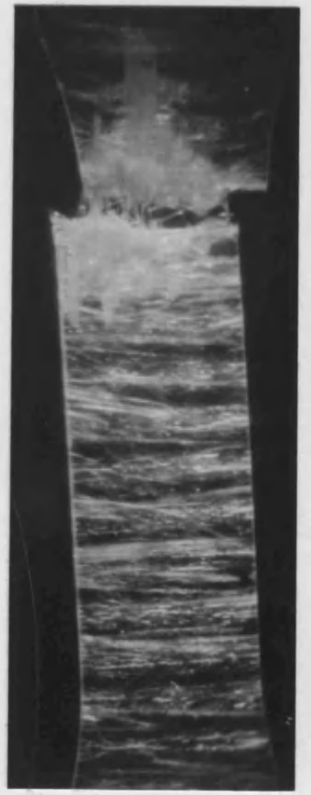

Time	31 mins	41 mins	48 mins
% Life	64.6	85.5	failure

Figure 4.3 Endoscope micrographs during a rectangular wave test

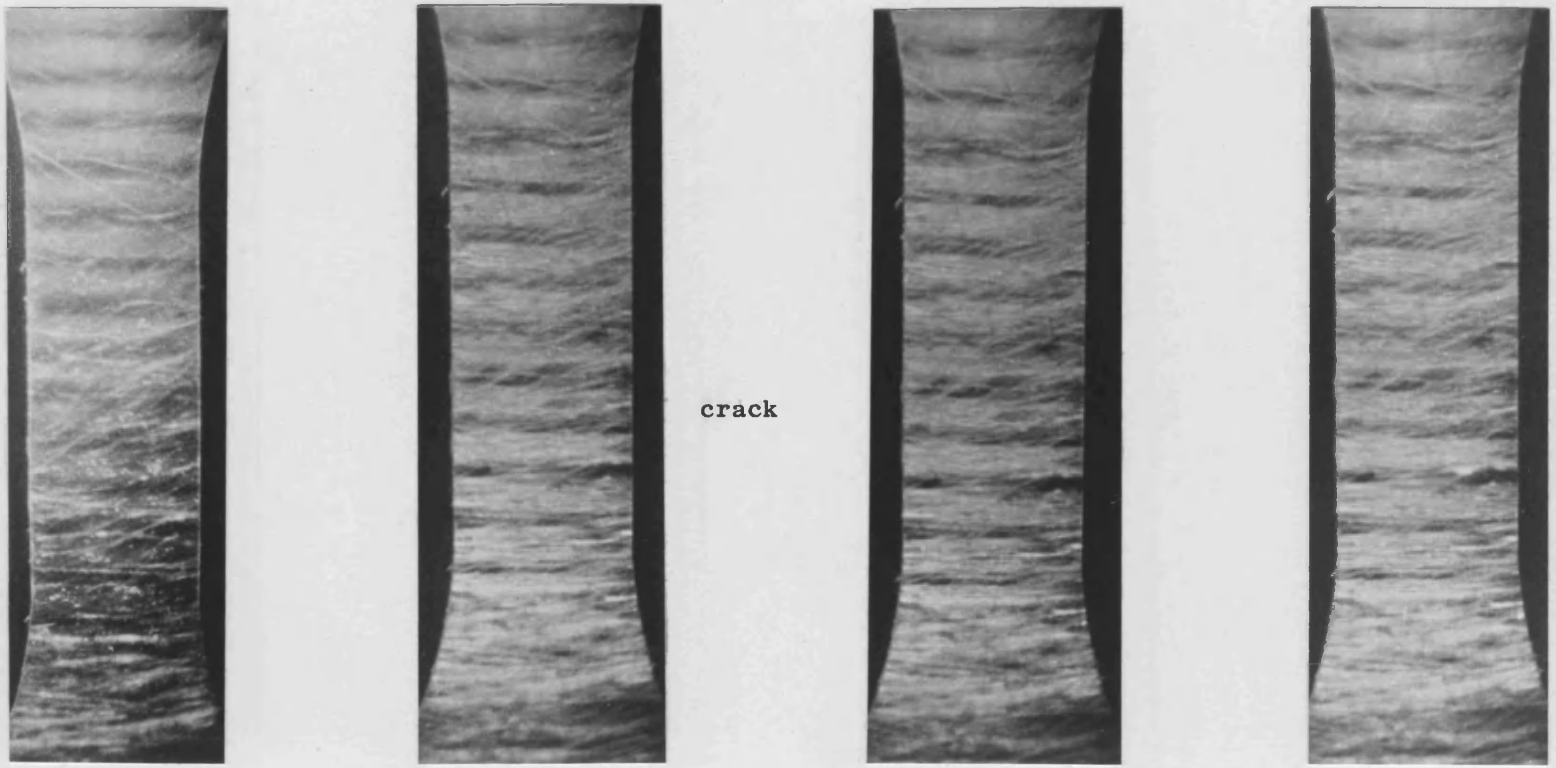

	Pre-start under no load	9 cycles	58 cycles	90 cycles
%Life	0	4.6	15.3	29.6

secondary cracks

debonding of weft roving

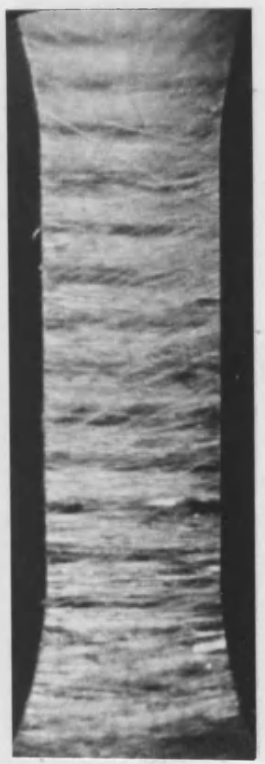

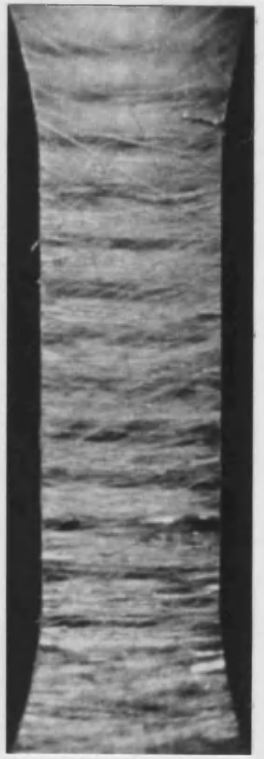

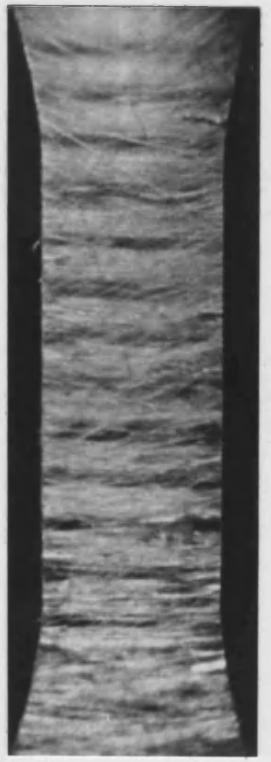

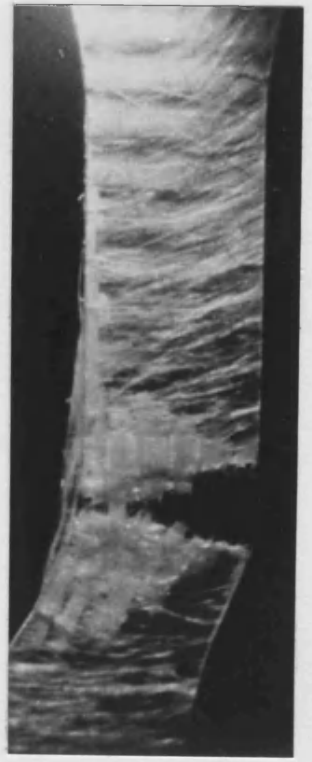

	131 cycles	155 cycles	192 cycles	196 cycles
%Life	66.8	79.1	98.0	failure

Figure 4.4 Micrographs during 0-tension dry fatigue test (DS2)

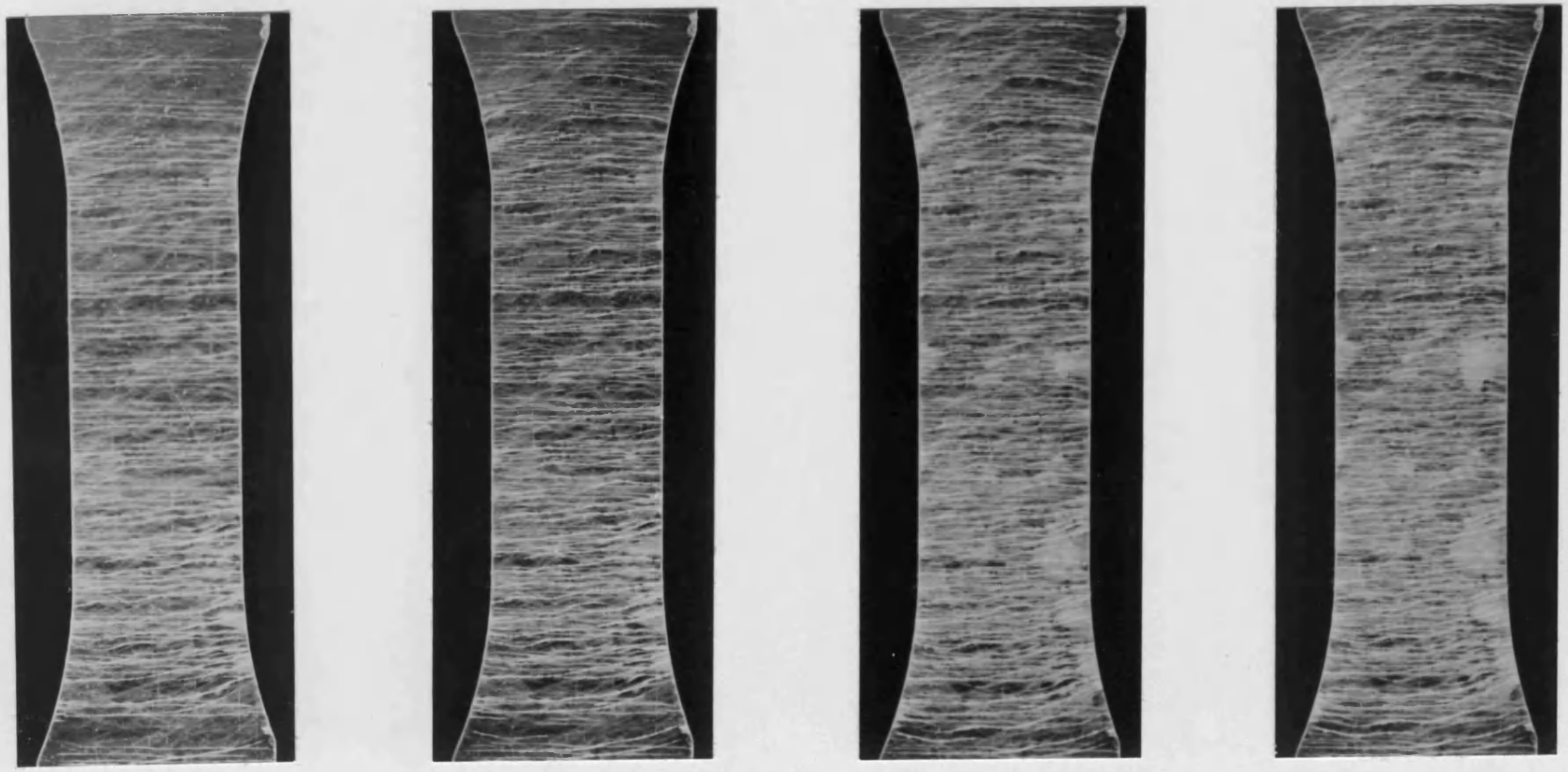

Cycles	90	620	3800	6330
%Life	0.7	5.0	30.6	51.0

crack becomes visible in
largest white area

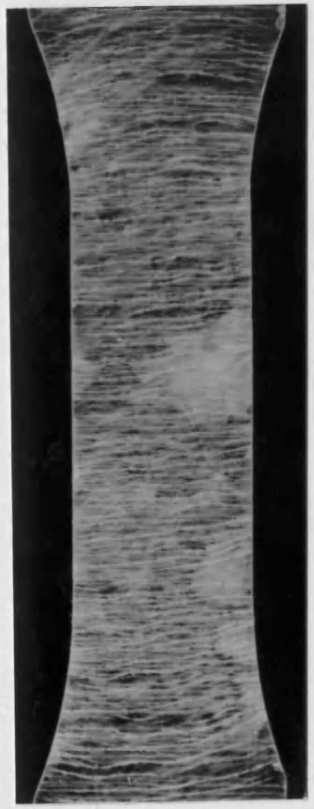

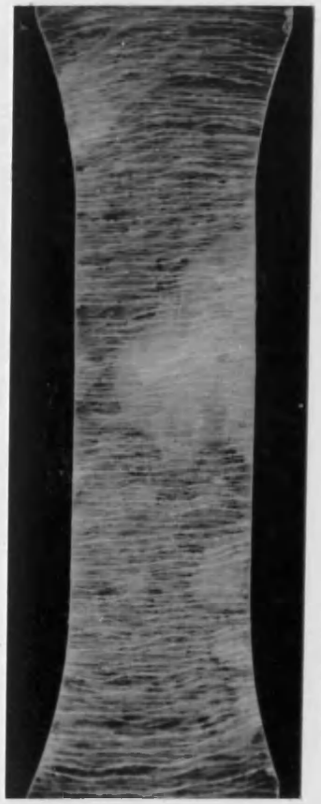

12412
failure

Cycles	8800	11800	12380
%Life	70.9	95.1	99.7

Figure 4.5 Micrographs during mean load ±20% dry fatigue tests (DS1)

Cycles	1300	2800	10500	12450
%Life	6.3	13.6	50.9	60.4

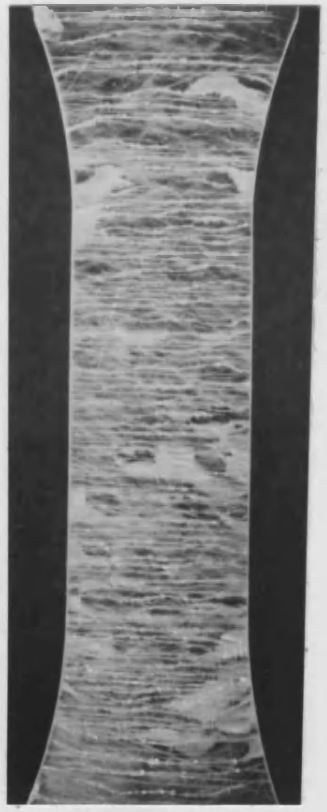

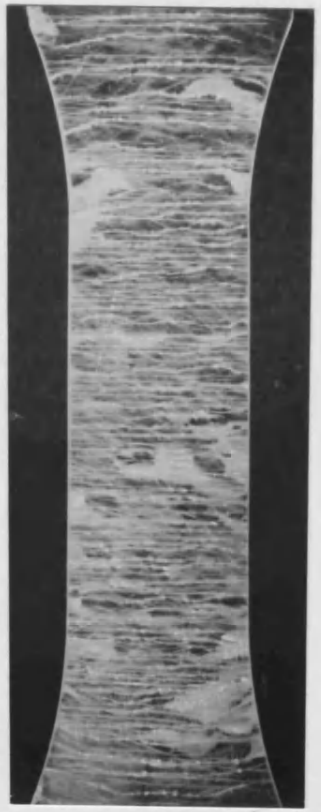

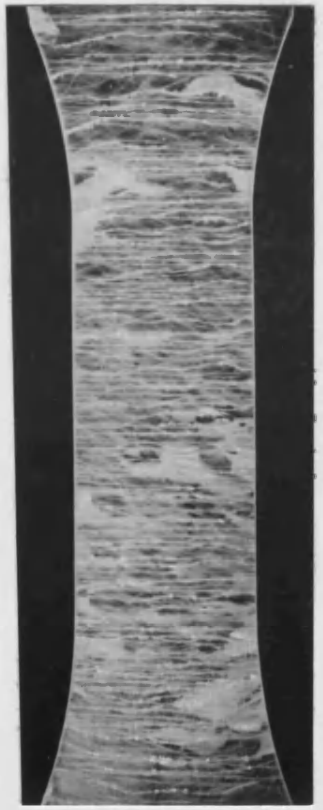

Cycles	1480	16700	18200	20611
%Life	71.8	81.0	88.3	failure

Figure 4.6 Micrographs during O-tension wet fatigue tests (S2)

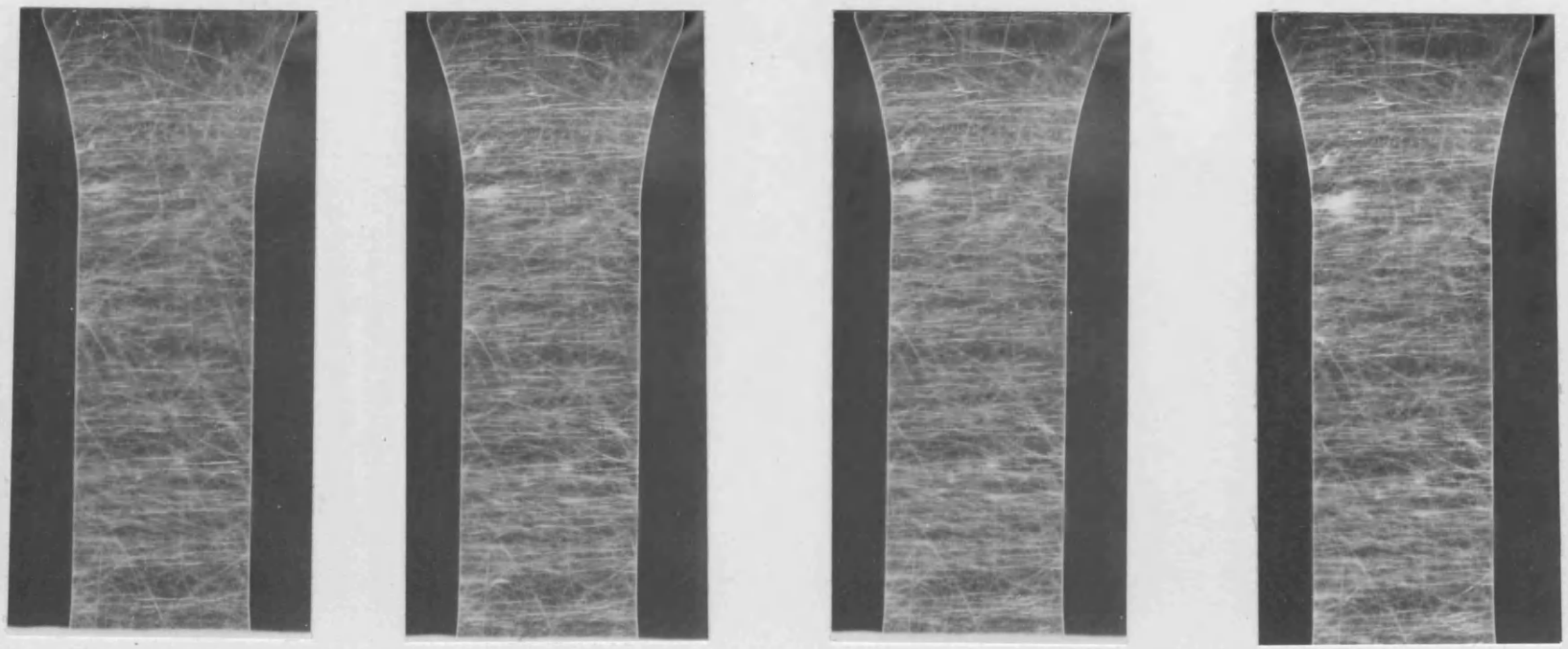

Cycles	1600	10500	15800	30500
%Life	1.6	10.8	16.2	31.3

clear crack becomes visible

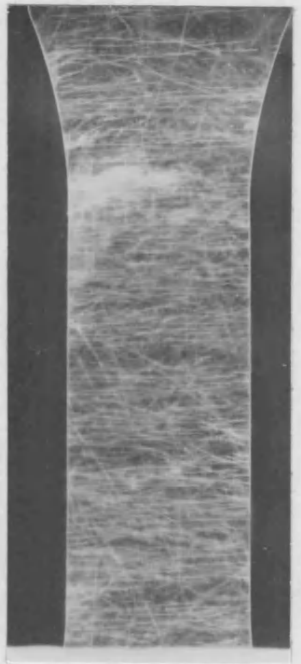

Cycles	78800	82600	90300	97417
%Life	80.7	84.8	92.7	failure

Fig. 4.7 Graphs of log(debonded area) vs. adjusted load

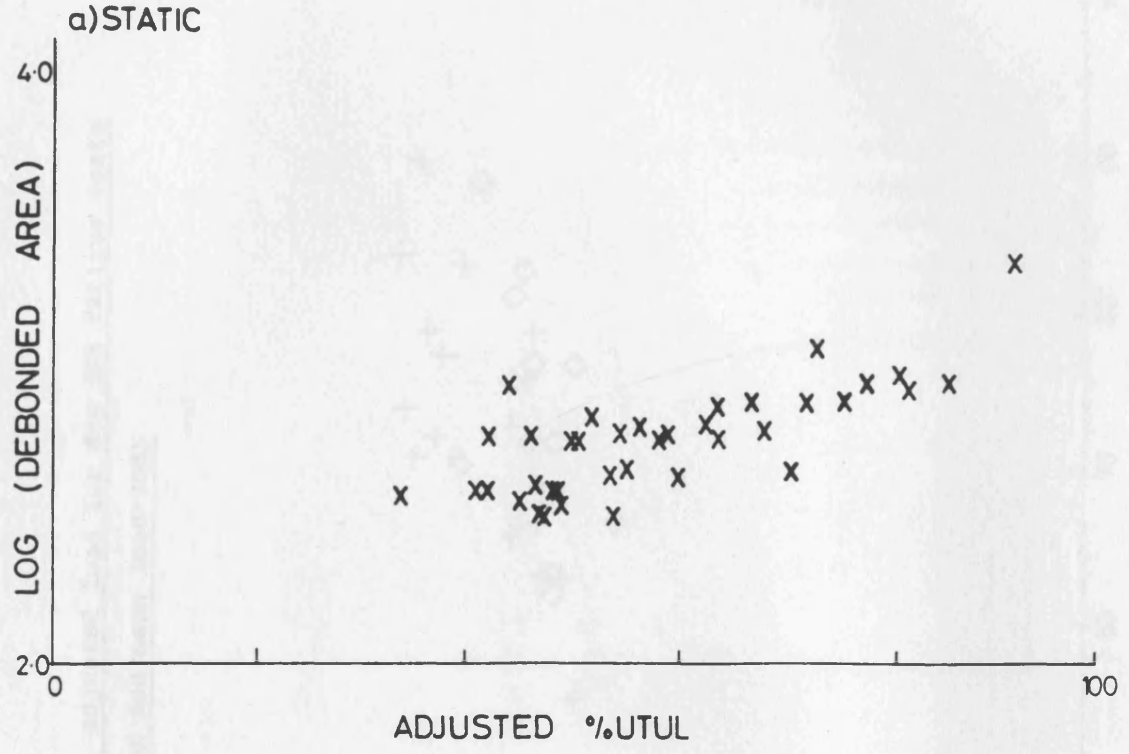

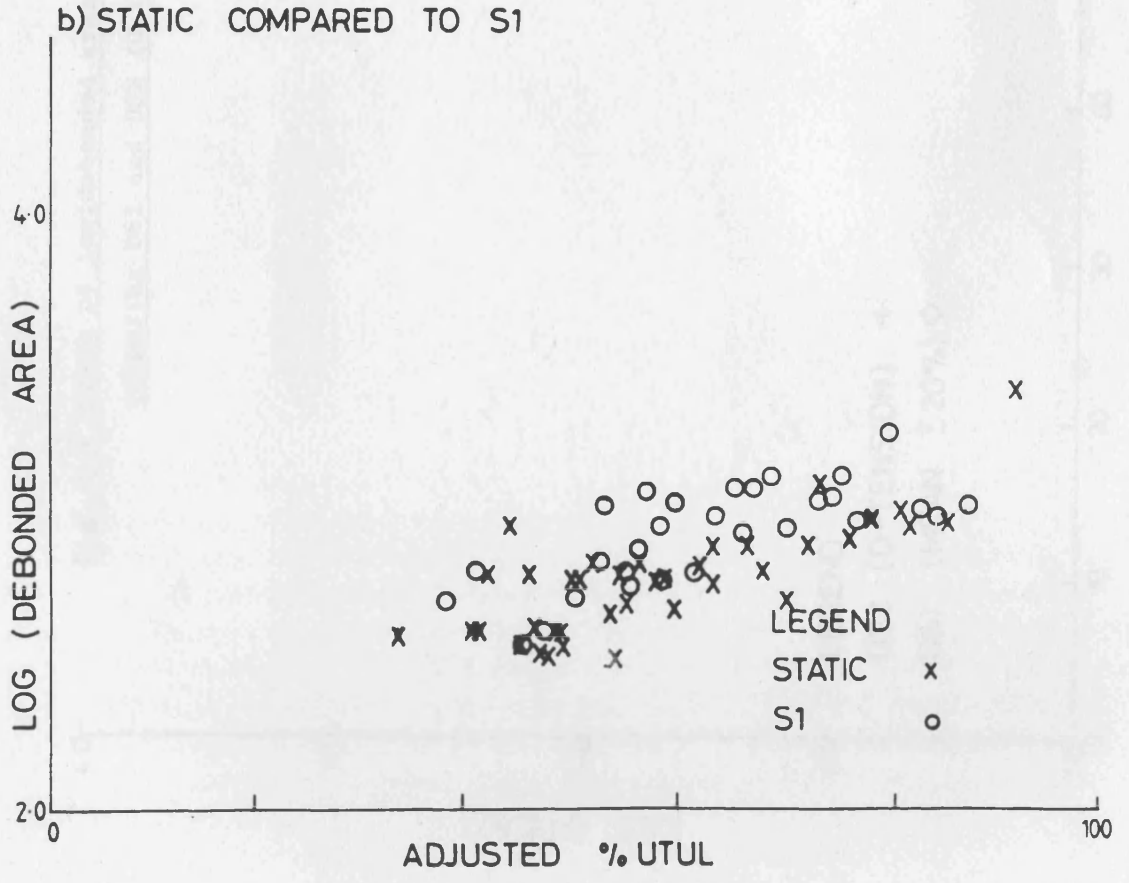

Fig. 4.8 Graph of log(debonded area) vs. adjusted load for dry 1Hz fatigue tests comparing DS1 and DS2 (0-tension and mean load±20%)

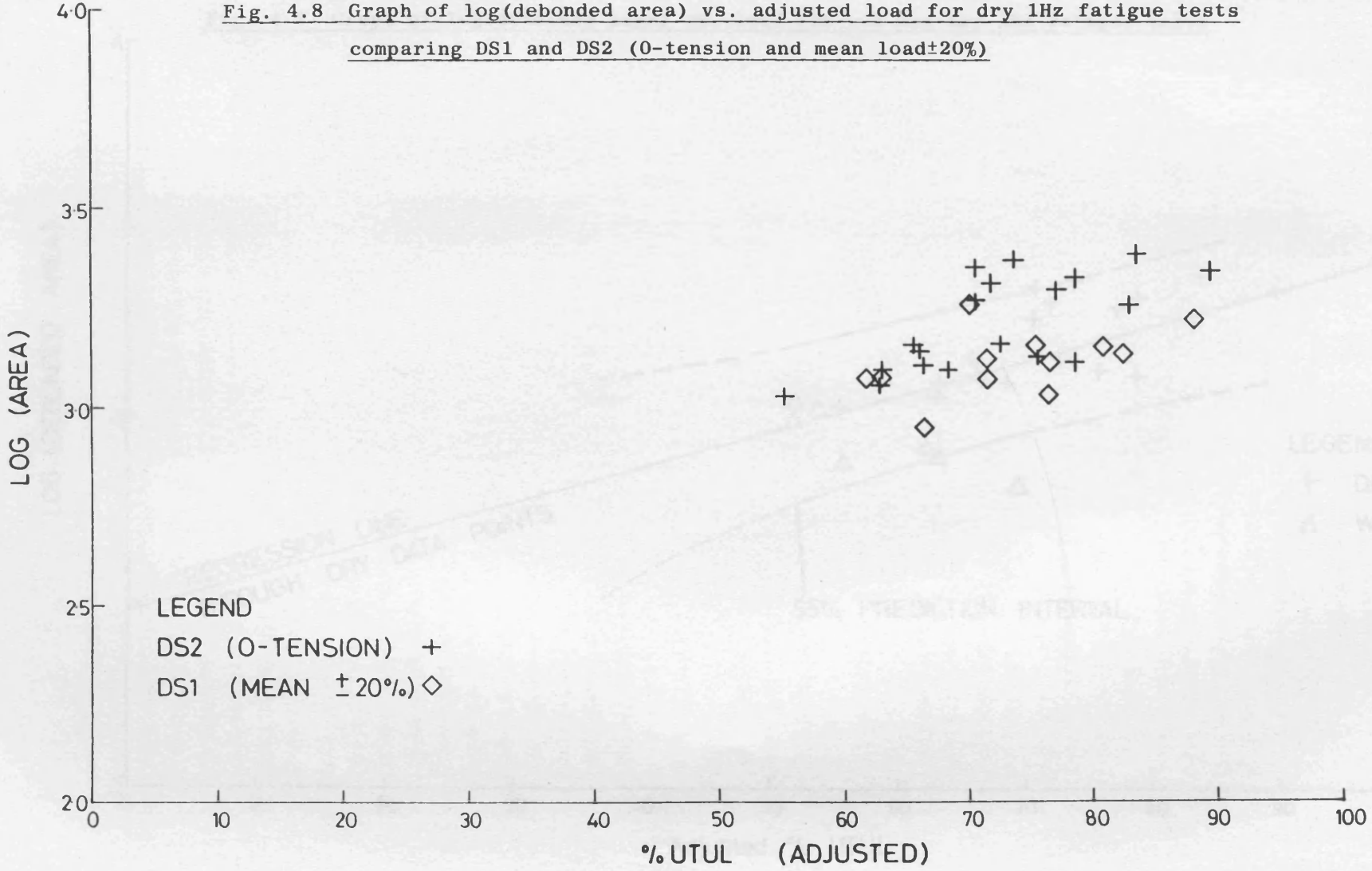

Fig. 4.9 Graph of log(debonded area) vs. load for wet and dry 1Hz fatigue tests

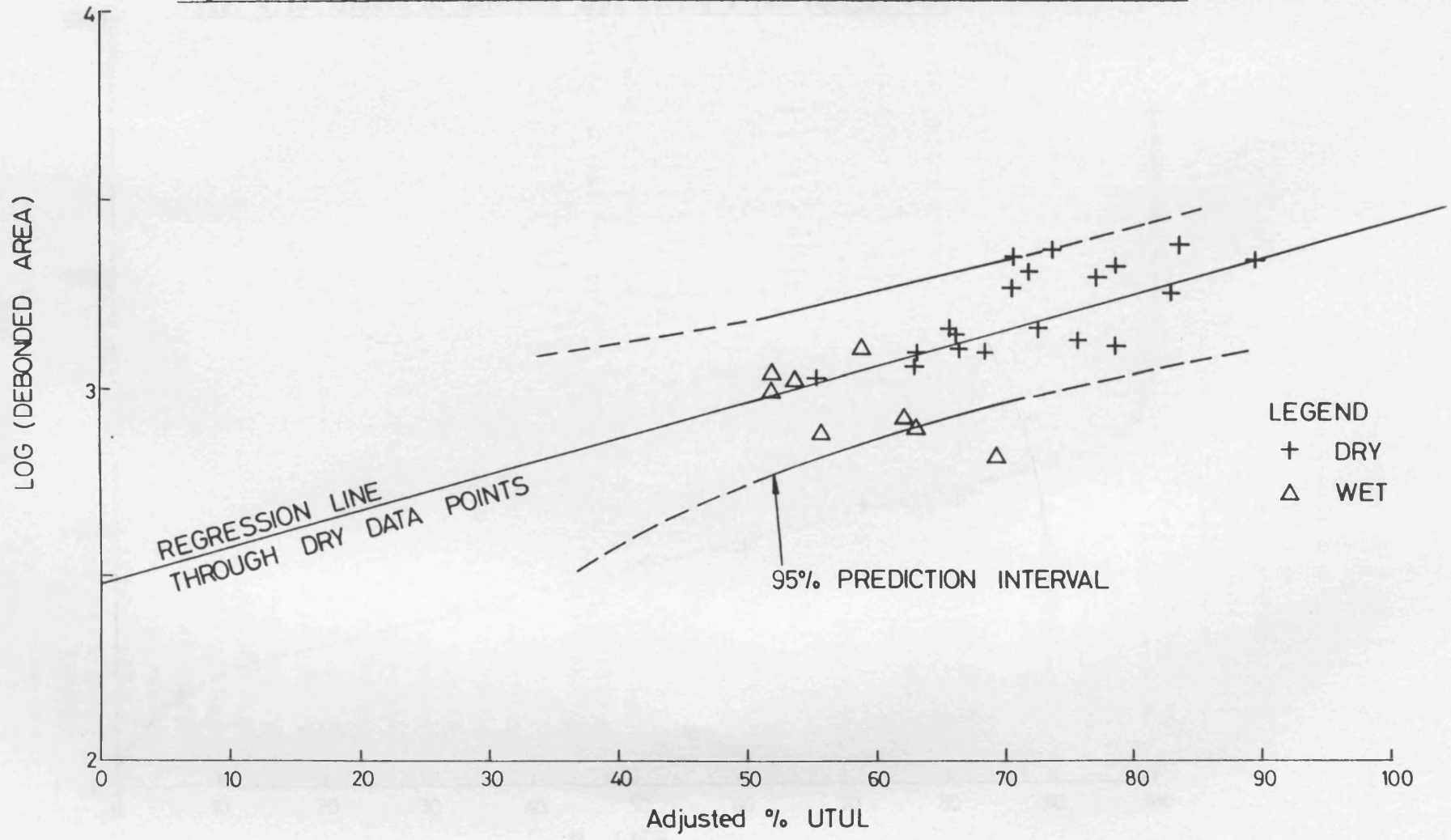

Fig. 4.10 Growth of debonded area during a 1Hz fatigue test

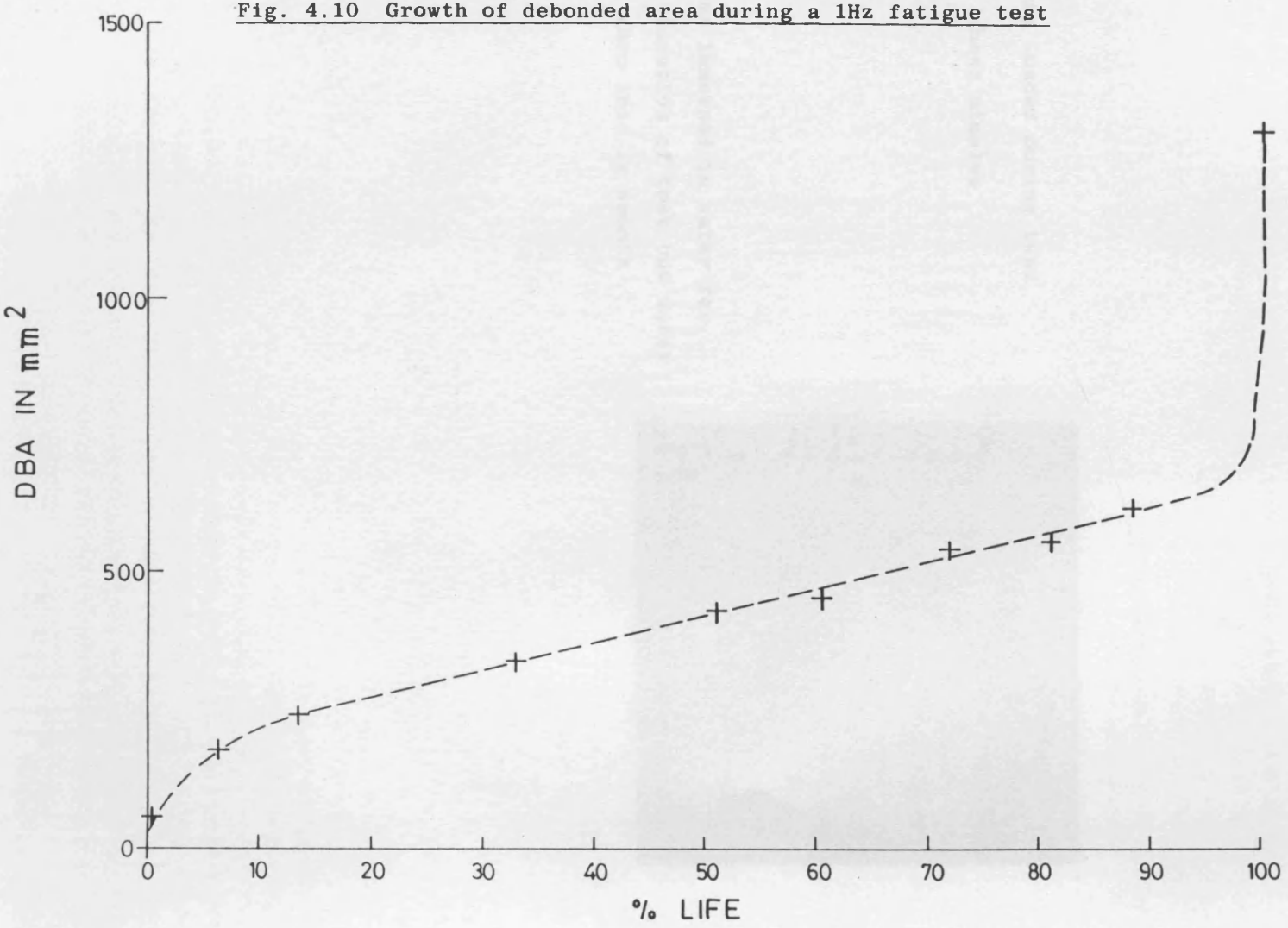

Figure 4.11 An example of permanent dimpling on a static test specimen

Area loaded during test shows dimples

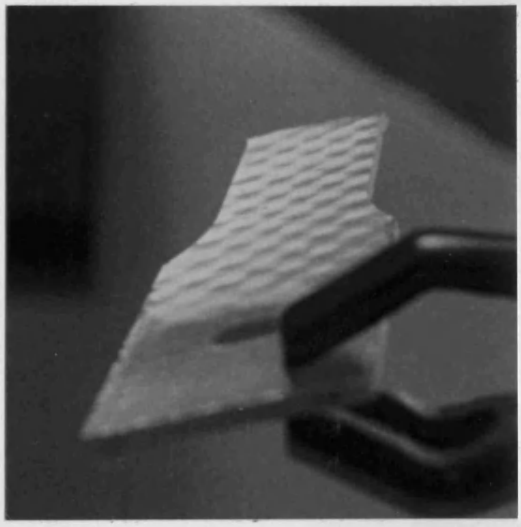

Area immersed in water for duration of test but under zero load is smooth

Fig. 4.12 Loci of failure of warp rovings with respect to weft

a) FAILURE IN CENTRAL 1/3 OF LENGTH OF CROSSOVER.

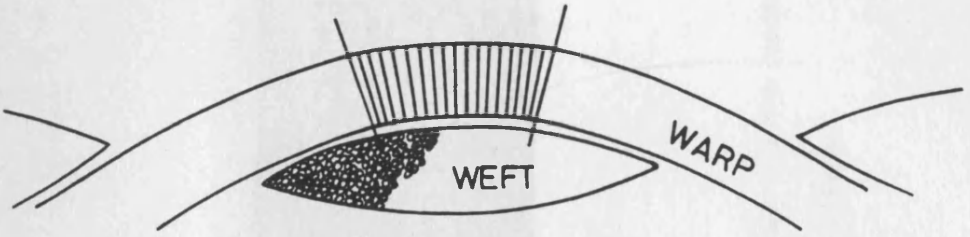

b) FAILURE IN OUTER 2/3 OF LENGTH OF CROSSOVER.

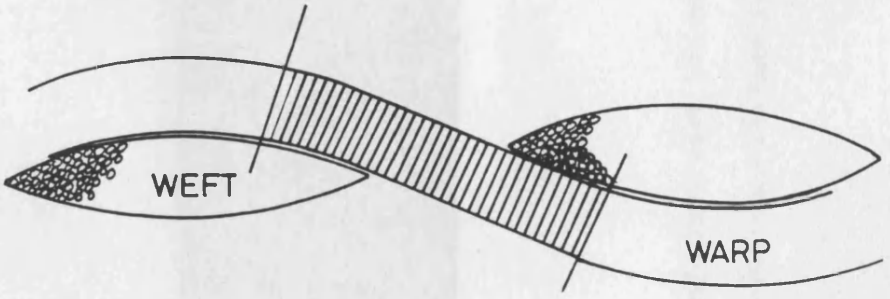

Figure 4.13 An example of failure in dry O-tension 1Hz fatigue test (DS2) showing warp roving failure in central third of successive warp-weft crossovers

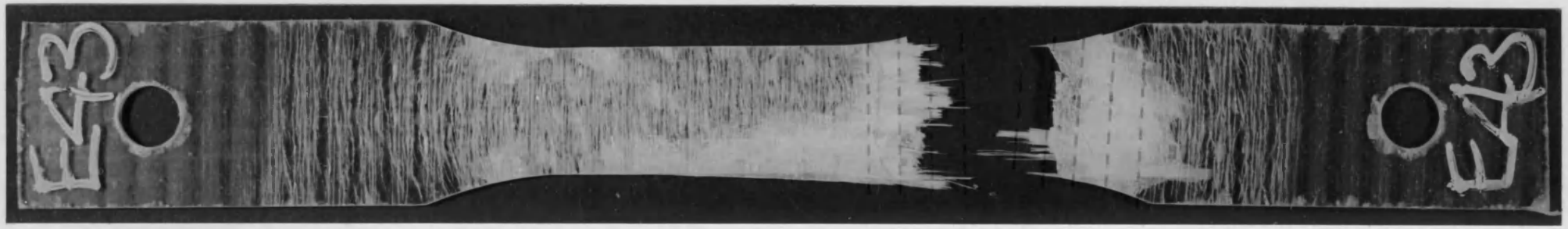

The vertical red dotted lines mark the boundary between one weft roving and the next.

The failure of pulled-out warp rovings is clearly exactly between the lines.

Fig. 4.14 SEM Micrograph showing crack propagation in outer CSM and gel coat layers

Figure 4.15 SEM micrograph showing origin of roving failure in area of low fibre pull-out

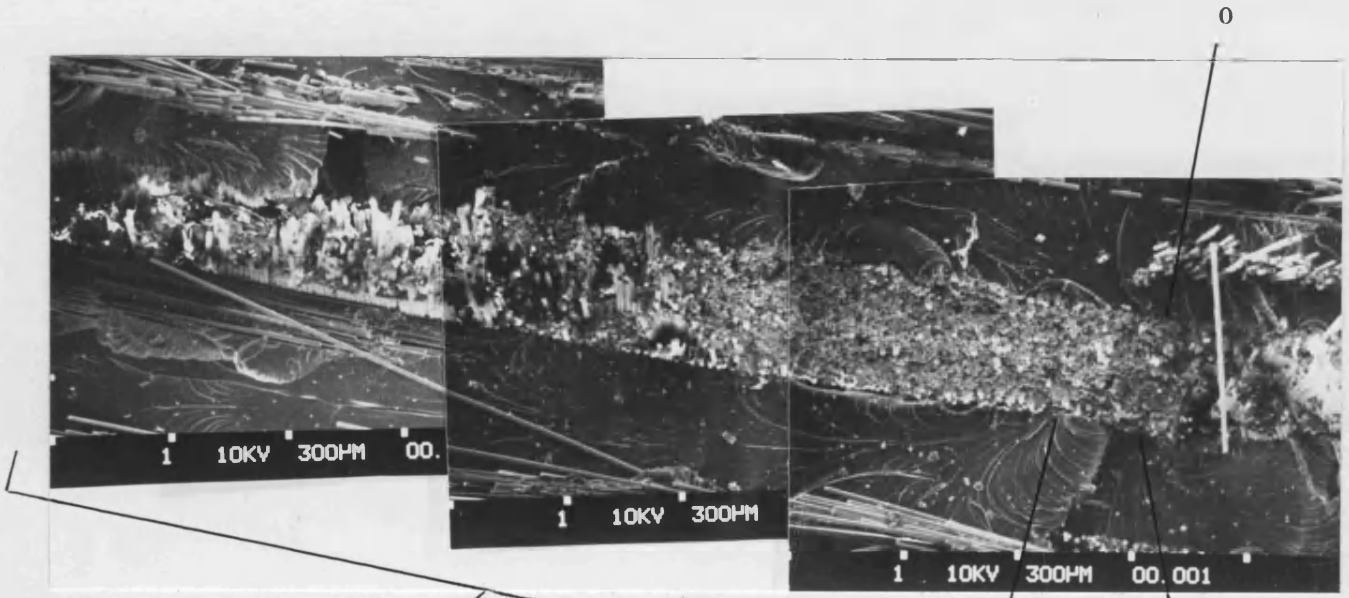

Figure 4.16 Planar fibre fractures

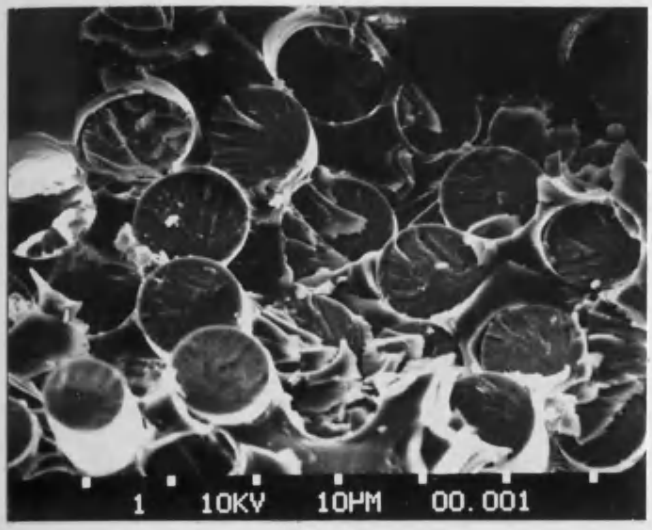

1150

a) An example of large hackle zones

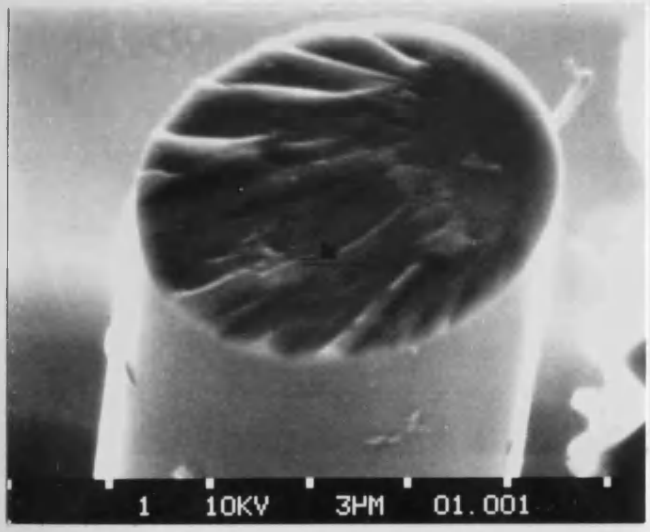

1151

b) Planar fracture with small mirror zone

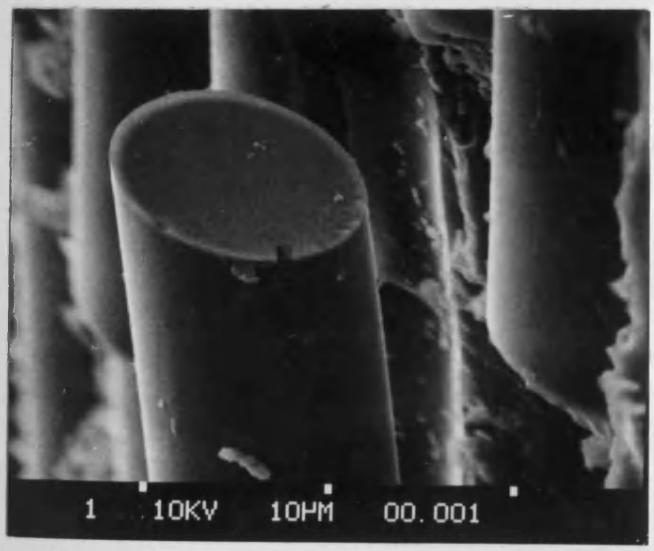

1152

c) Planar fracture with very large mirror zone

Figure 4.17 Examples of irregular fibre fractures

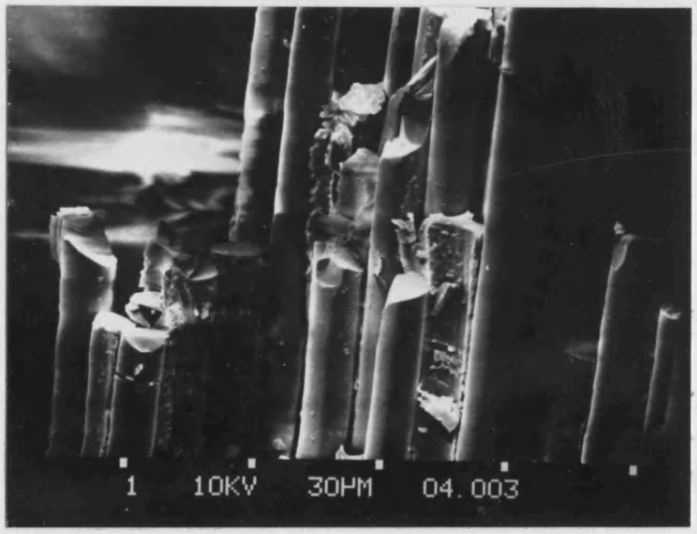

Figure 4.18 Fibre breaks away from the fibre end

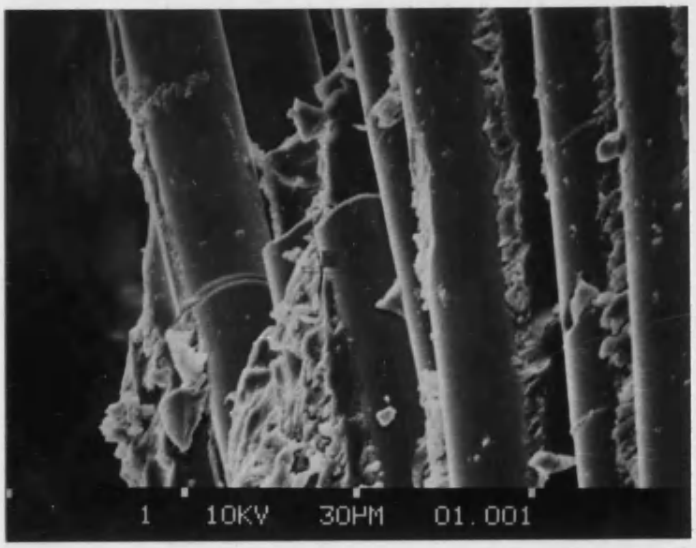

1148

a) A single smooth fibre break from an R3 specimen

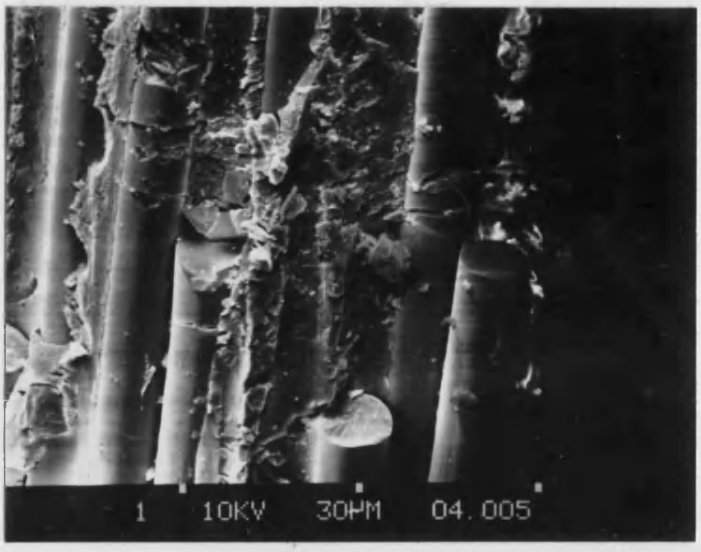

1149

b) Multiple irregular breaks from an R4 specimen

Figure 4.19 Lipped fibre fracture ends

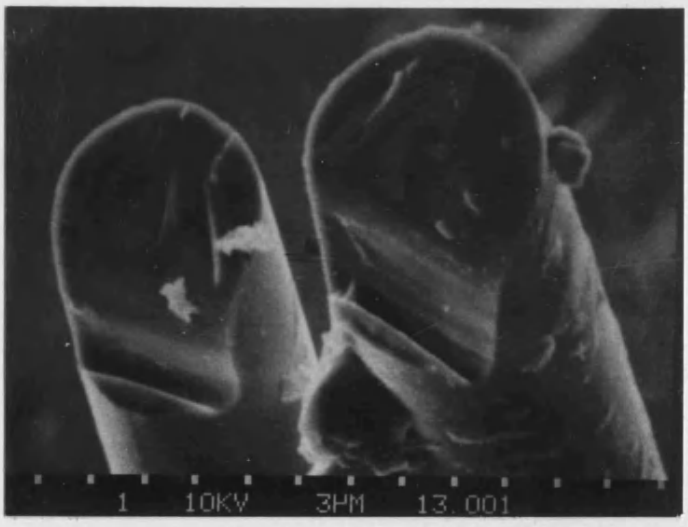

1145

a)

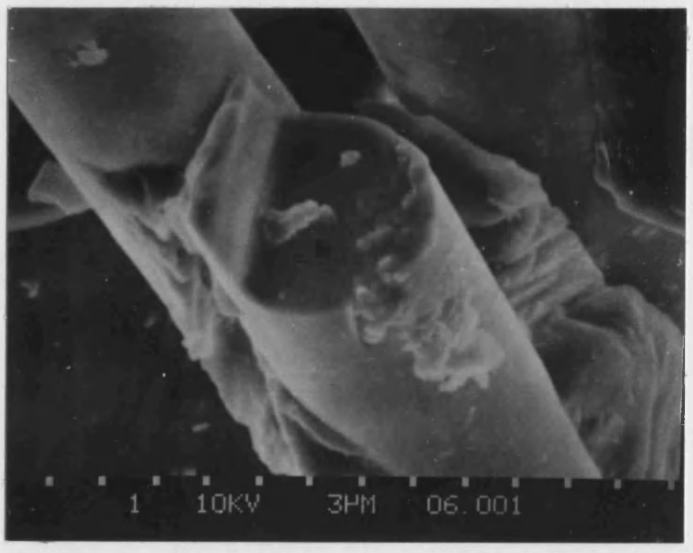

1146

b)

Fig. 5.1 Initial configuration of WR composite

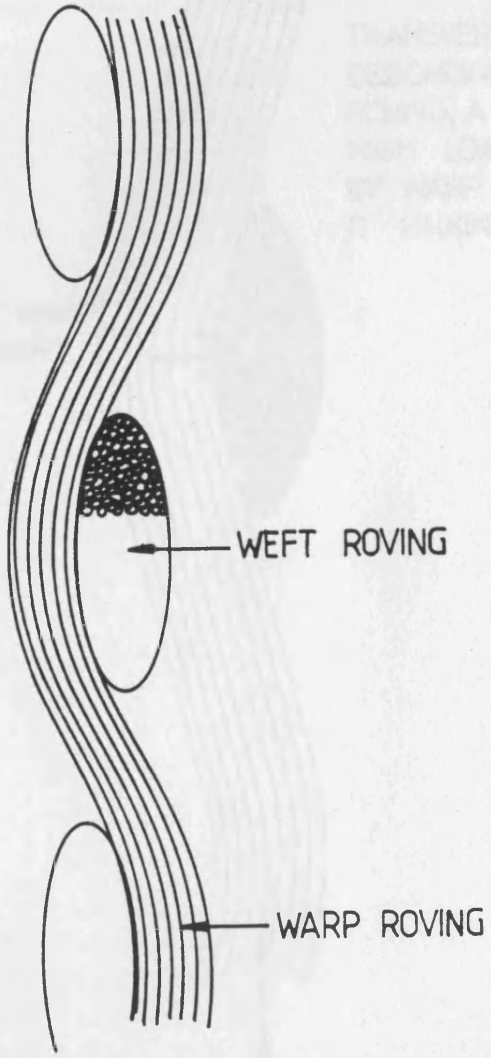

Fig. 5.2 Effect of applied load on WR composite

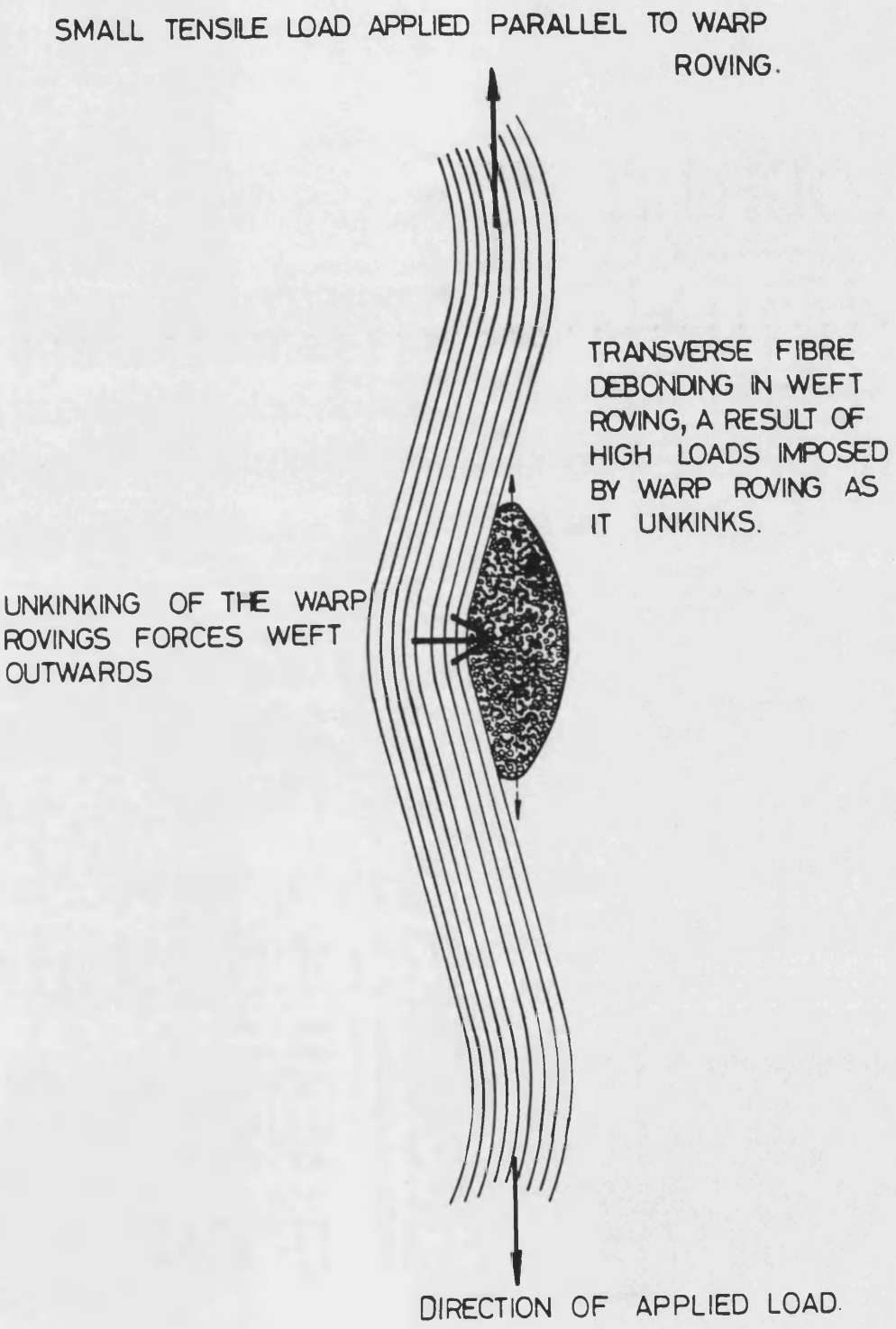

Fig. 5.3 Modelling the vertical deflection of a section of warp roving

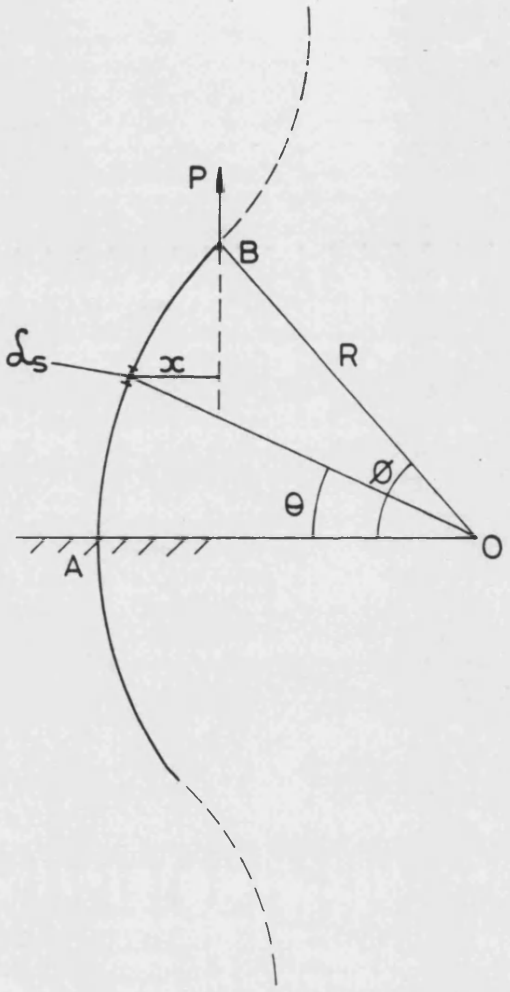

Fig. 5.4 Diagram showing shear stresses which give rise to debonding between warp and weft

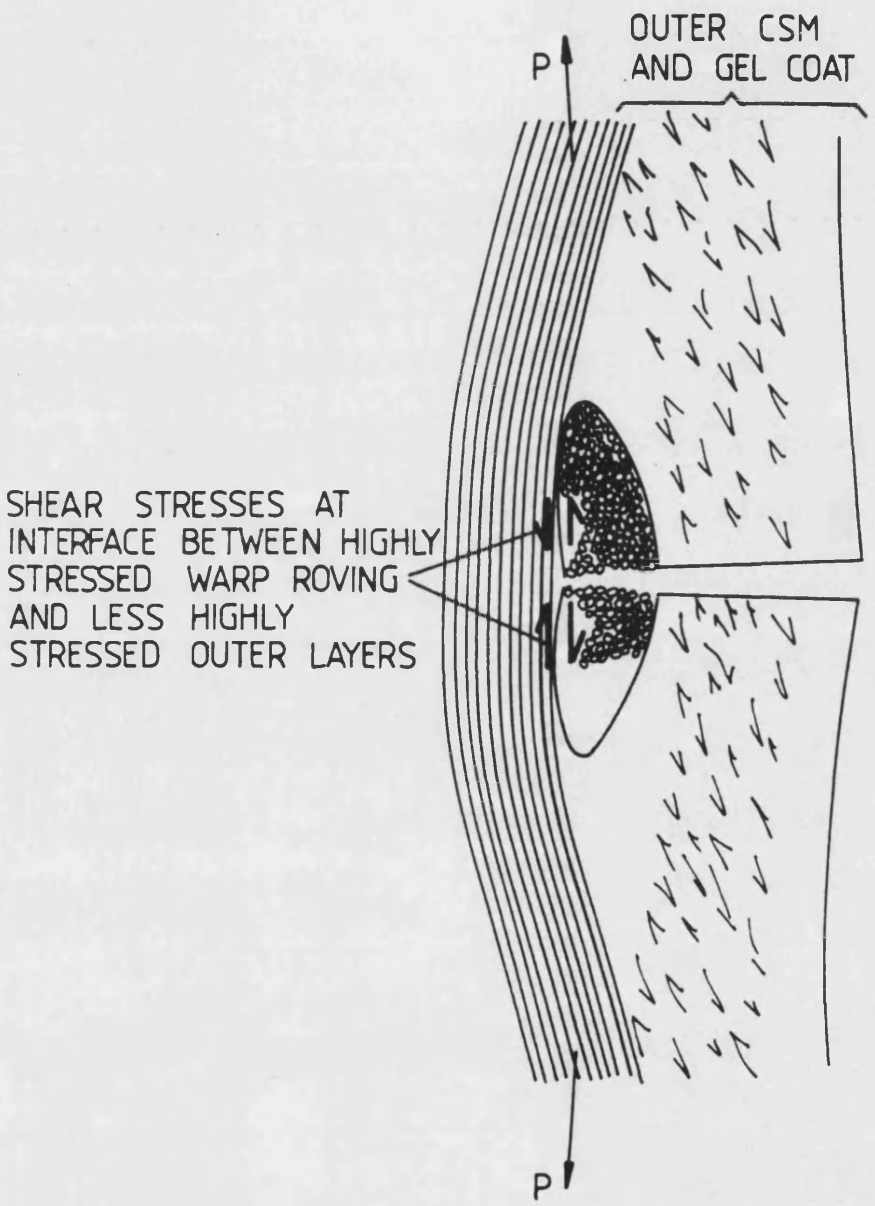

Fig. 5.5 Schematic diagram of possible resin stress ranges during unloading cycles at two frequencies

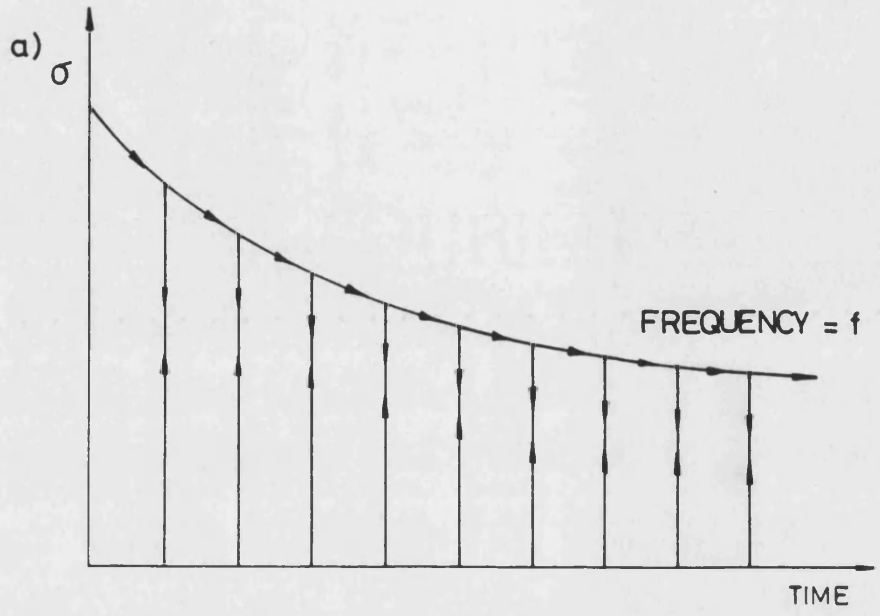

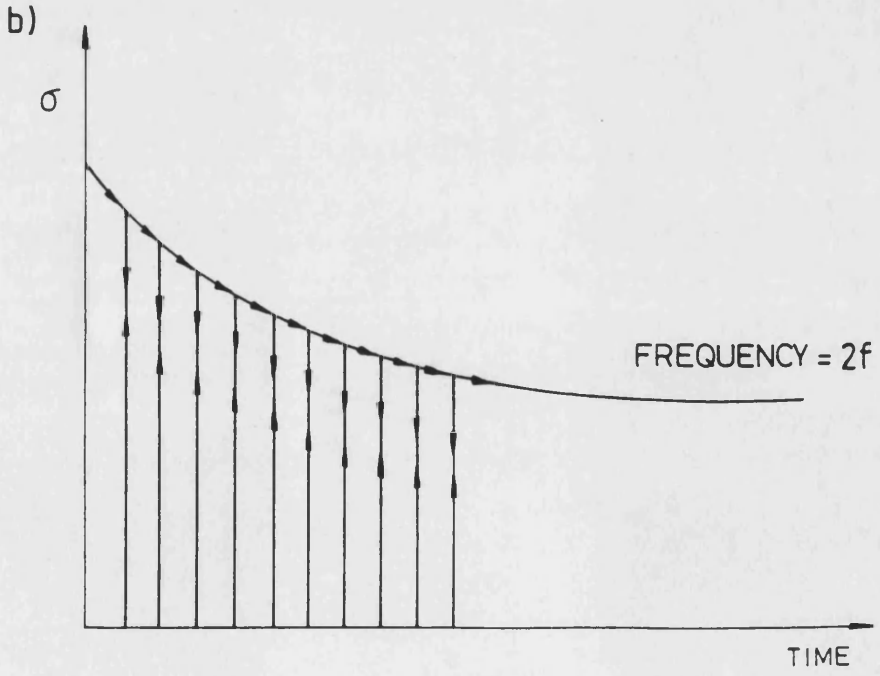

Fig 5.6 Schematic diagram showing how volume of warp roving exposed to the environment might vary with increasing fatigue cycles

a) STATIC REGIME

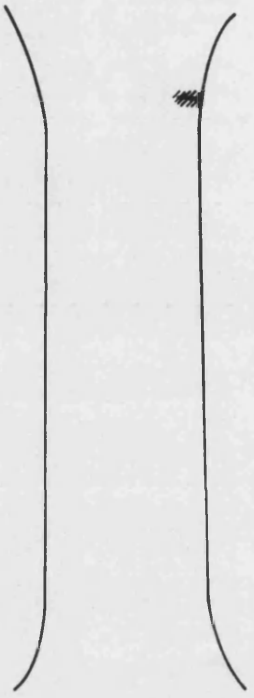

SMALL RESIN CRACK IN SINGLE LOCATION SMALL DAMAGE ZONE WHERE WARP FIBRES EXPOSED TO ENVIROMENTAL ATTACK AND UNSUPPORTED BY RESIN.

//////DENOTES DAMAGE AREA

b) HIGH CYCLE ELEMENT REGIME

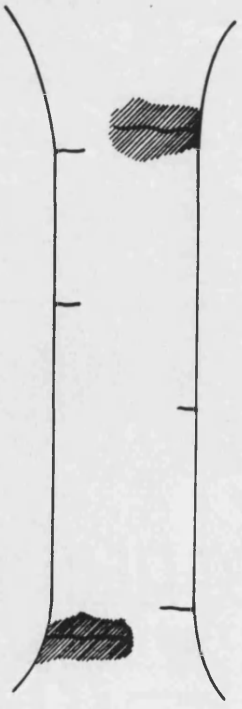

RESIN CRACKS IN MANY LOCATIONS. LARGE WHITENED AREAS INDICATIVE OF DAMAGE. LARGE AREAS WHERE WARP ROVINGS ARE UNSUPPORTED AND OPEN TO ATTACK BY THE ENVIRONMENT.

Fig. 5.7 Schematic diagram of processes contributing to failure

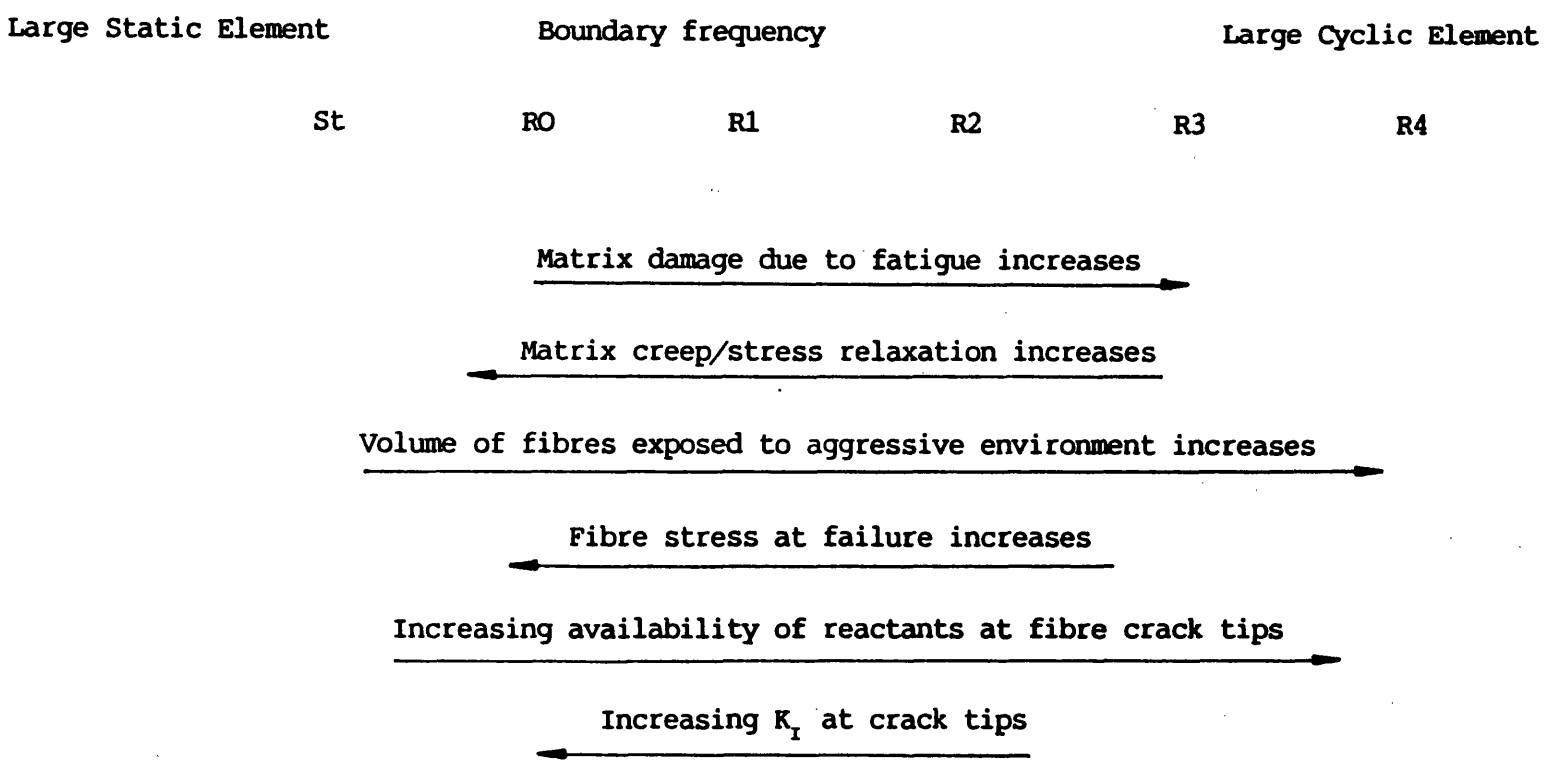

Fig. 6.1 Sketch of revised constant life diagram

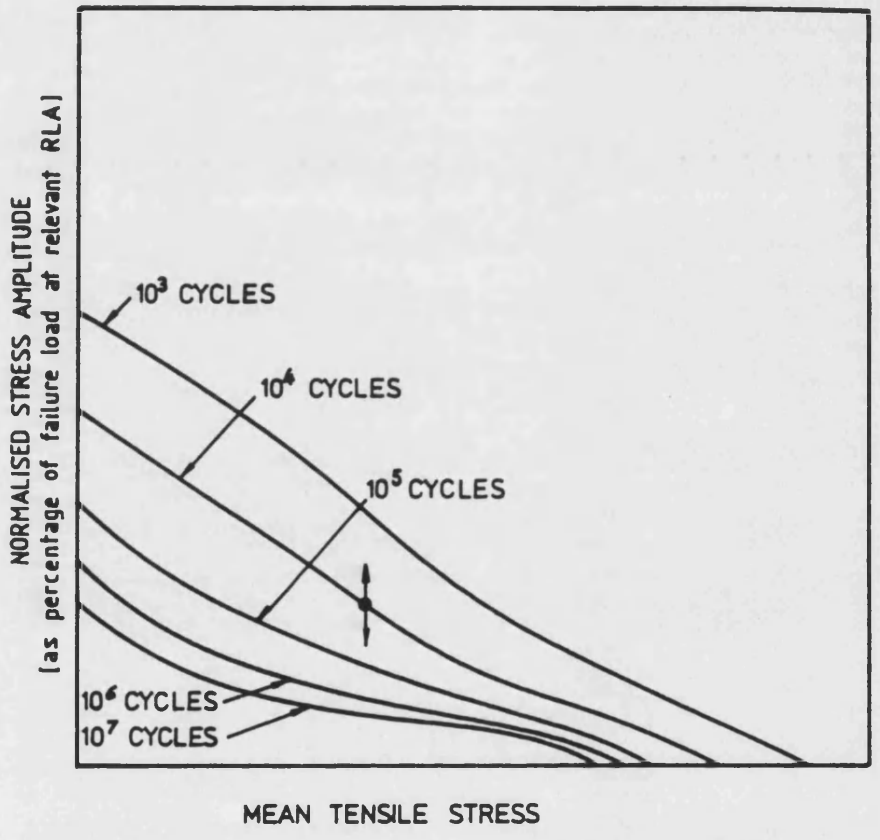

Fig. 6.2a) Effect of varying load amplitude at constant RLA

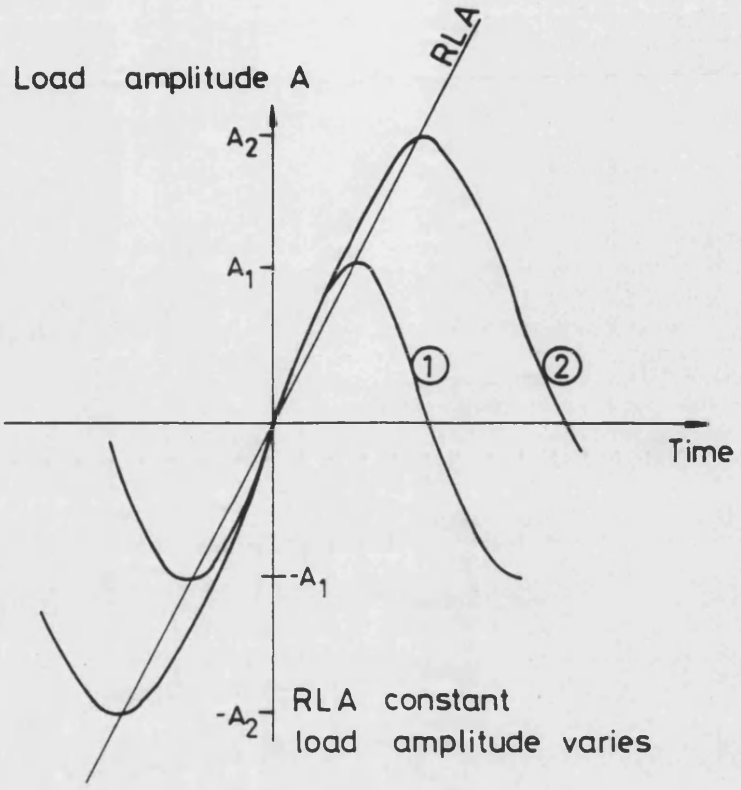

Fig. 6.2b) Effect of varying RLA at constant load amplitude

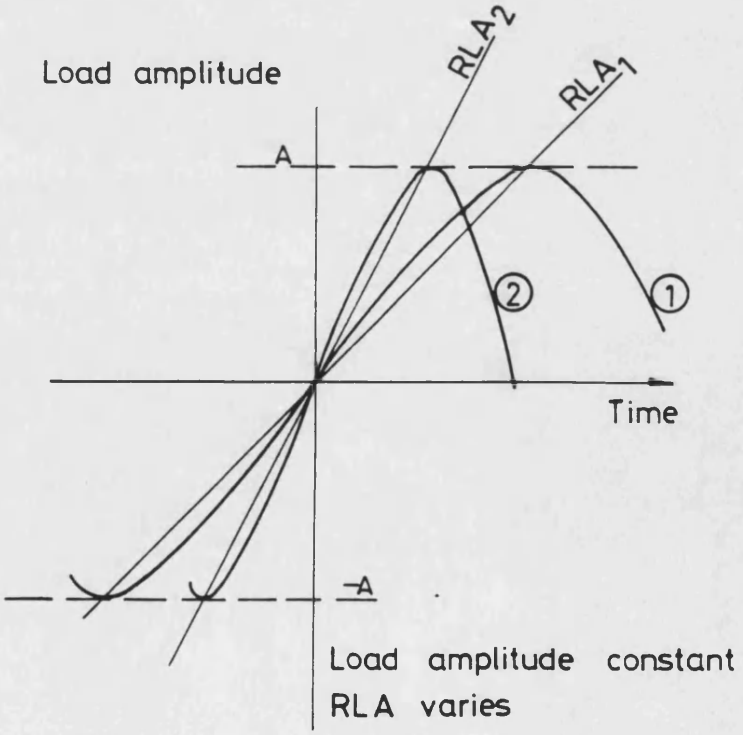

Fig. 6.3 Load-time variation for spike overloads

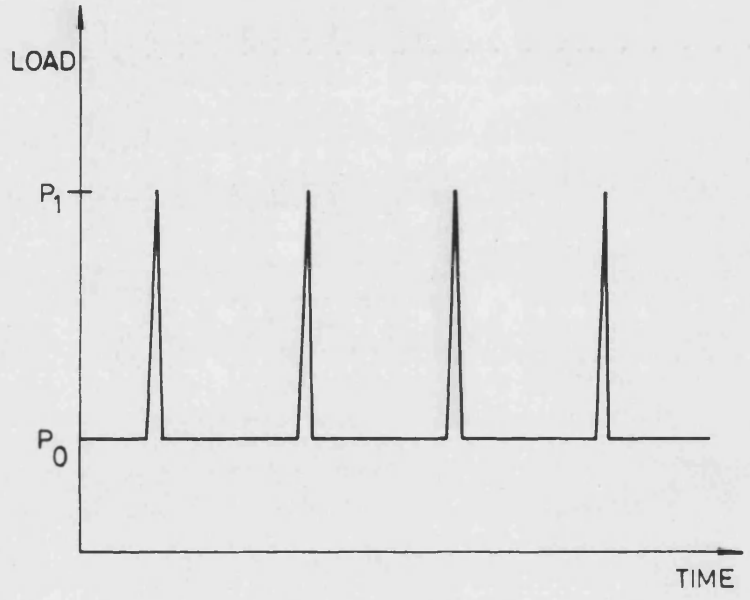

Appendix

Analysis of Variance

In order to determine with which case (shown in Fig. 3.4) the sets of data conform, it is necessary first to evaluate the sum of the squares of deviations of the data points from each of the candidate lines. Whether one line through the data gives a more significant correlation than another is determined by evaluating the ratio of the sums of squares for the two lines, taking into account the degrees of freedom available. This ratio can be tested for significance using an F-test (or "variance ratio" test).

For instance to determine whether drawing lines with individual slopes or lines with a single slope (the pooled slope) through each data set is appropriate, the sums of squares of deviations from each of the 2 possible lines is calculated. The sum of the squares about the individual lines is the smallest, indicating that the lines with a unique slope give the best correlation. The sum of squares about the lines with the pooled slope will always be larger. If the difference between these sums of squares is not significantly larger than might be expected by chance for the number of degrees of freedom available, then the use of individual slopes cannot be justified.

The calculation of the sums of squares to evaluate whether drawing individual lines, separate but equally sloped lines or one single line is correct is possible by constructing a table of the type shown below.

				Sums of Squares	
$\Sigma' x^2$	$\Sigma' y^2$	$\Sigma' xy$	$\Sigma' c^2$	$\Sigma' \hat{y}^2$	for one line through all data
$\Sigma' \bar{x}^2$	$\Sigma' \bar{y}^2$	$\Sigma' \bar{x}\bar{y}$	$\Sigma' \bar{c}^2$	$\Sigma' \hat{y}_m^2$	for one line through the means of the data sets
$\Sigma' x_w^2$	$\Sigma' y_w^2$	$\Sigma' x_w y_w$	$\Sigma' c_w^2$	$\Sigma' \hat{y}_w^2$	for separate lines with pooled slope
$\Sigma' x_1^2$ $\Sigma' x_2^2$	$\Sigma' y_1^2$ $\Sigma' y_2^2$	$\Sigma' x_1 y_1$ $\Sigma' x_2 y_2$	$\Sigma' c_1^2$ $\Sigma' c_2^2$	$\Sigma' \hat{y}_1^2$) $\Sigma' \hat{y}_2^2$)	for each individual line
$\Sigma\Sigma' x^2$	$\Sigma\Sigma' y^2$	$\Sigma\Sigma' xy$	$\Sigma\Sigma' c^2$	$\Sigma\Sigma' \hat{y}^2$	sum for all individual lines.

where $\Sigma' x^2 = \Sigma x^2 - \frac{(\Sigma x)^2}{n}$

$\Sigma' y^2 = \Sigma y^2 - \frac{(\Sigma y)^2}{n}$

$\Sigma' xy = \Sigma xy - \frac{\Sigma x \Sigma y}{n}$

$\Sigma' c^2 = \frac{(\Sigma' xy)^2}{\Sigma' x^2}$

$\Sigma' \hat{y}^2 = \Sigma' y^2 - \Sigma' c^2$

$\Sigma' \bar{x}^2 = \frac{(\Sigma x_1)^2}{n_1} + \frac{(\Sigma x_2)^2}{n_2} - \frac{(\Sigma x)^2}{N}$ $\qquad N = \Sigma n$

$\Sigma' \bar{y}^2 = \frac{(\Sigma y_1)^2}{n_1} + \frac{(\Sigma y_2)^2}{n_2} - \frac{(\Sigma y)^2}{N}$

$\Sigma' \bar{x}\bar{y} = \frac{\Sigma x_1 \Sigma y_1}{n_1} + \frac{\Sigma x_2 \Sigma y_2}{n_2} - \frac{\Sigma x \Sigma y}{N}$

$\Sigma' x_w^2 = \Sigma' x^2 - \Sigma' x^2 = \Sigma\Sigma' x^2$

The previous equation and similar ones for $\Sigma' y_w^2$ and $\Sigma' x_w y_w$ can be used to check the calculations in the first three columns.

Whether separate lines with their own slope or the pooled slope should be drawn was determined first.

$$\text{Test statistic} = \frac{(\Sigma'\hat{y}_w^2 - \Sigma\Sigma'\hat{y}^2) \div \text{D of f}}{\Sigma\Sigma'\hat{y}^2 \div \text{D of f}}$$

The number of degrees of freedom (D of f) are (k-1) for the numerator and $\Sigma(n_i-2)$ for the denominator. (k is the number of data sets and n_i is the points per data set.) This test statistic was compared to critical values taken from F-tables in the usual way. If the improvement in correlation obtained by drawing uniquely sloped lines was not significant, only lines whose slopes were equal to the pooled slope $\Sigma\Sigma'x_w y_w \div \Sigma\Sigma'x_w^2$, could be drawn implying that the individual slopes were not significantly different.

A second F-test was then carried out if no significant difference in slopes was found. This test was to find if the data sets could only be represented by one single line, i.e. the displacement in the y-direction was insignificant.

The test statistic in this case was $\dfrac{\Sigma'\hat{y}^2 - \Sigma'\hat{y}_m^2 - \Sigma'\hat{y}_w^2}{\Sigma'\hat{y}_w^2 \div \text{D of f}}$

The numerator has only 1 D of f and the denominator has N-k-1. This is tested against critical values as before. If there was no significance only one line could be drawn. This implies the slopes and intercepts of regression lines through individual data sets are effectively equal, so the 2 data sets must be assumed to be part of the same population.